Regular Polygon Surfaces and Renormalizable Rectangle Exchange Maps

by

Ian M. Alevy

B.S., University of Chicago; Chicago, IL, 2013

M.S., Brown University; Providence, RI, 2014

A dissertation submitted in partial fulfillment of the

requirements for the degree of Doctor of Philosophy

in The Division of Applied Mathematics at Brown University

PROVIDENCE, RHODE ISLAND

May 2018

This dissertation by Ian M. Alevy is accepted in its present form
by The Division of Applied Mathematics as satisfying the
dissertation requirement for the degree of Doctor of Philosophy.

Date________________ ____

Richard Kenyon, Ph.D., Advisor

Recommended to the Graduate Council

Date________________ ____

Govind Menon, Ph.D., Reader

Date________________ ____

Richard E. Schwartz, Ph.D., Reader

Approved by the Graduate Council

Date________________ ____

Andrew G. Campbell, Dean of the Graduate School

Curriculum Vitae

Ian M. Alevy received both a Bachelor of Science in Mathematics with honors and a Bachelor of Arts in Physics from the University of Chicago in 2013. He received a Master of Science in Applied Mathematics from Brown University in 2014. As a Ph.D. candidate in the Division of Applied Mathematics at Brown University, Ian has been advised and mentored by Richard Kenyon. In July 2018 he will be a Visiting Assistant Professor at the University of Rochester.

While at Brown University Ian has served as a teaching assistant for Topics in Information Theory and Coding Theory, Statistical Inference, Operations Research, Essential Statistics, and Methods of Applied Mathematics. He was the primary instructor for How Big is Infinity? and Fundamentals for Calculus.

Publications

1. I. M. Alevy, *Regular Polygon Surfaces*, ArXiv e-prints (April 2018), 1804.05452

2. I. Alevy, R. Kenyon and R. Yi, *A Family of Minimal and Renormalizable Rectangle Exchange Maps*, ArXiv e-prints (March 2018), 1803.06369

3. I. Alevy and E. Tsukerman, *Polygonal bicycle paths and the Darboux transformation*, Involve **9**(1), 57–66 (2016)

4. T. Nagylaki, L. Su, I. Alevy and T. F. Dupont, *Clines with partial panmixia in an environmental pocket*, Theoretical Population Biology **95**, 24 – 32 (2014)

Preface and Acknowledgments

I would like to thank my advisor, Richard Kenyon, for his support and guidance during my doctoral studies. He originally suggested the study of surfaces built with polygonal tiles and has been a constant source of inspiration and guidance throughout my studies. I would also like to thank Richard Schwartz who has been a mathematical inspiration for me since my first visit to ICERM as an undergraduate.

The work on domain exchange maps had its genesis in an attempt to answer a question posed by Ren Yi. Ren, it has been a joy to collaborate with you and I hope that our collaboration continues into the future.

There are many faculty at Brown in both the Division of Applied Mathematics and the Department of Mathematics that have been instrumental in my development as a mathematician. I would like to thank Govind Menon for serving on my committee and for always pushing me to delve deeply into analysis.

This project would not have been possible without my fellow students. Special thanks to Sanjay Ramassamy for always being willing to answer my questions. You taught me countless things about discrete mathematics. My office mates Sameer Iyer, Michael Burkhart, and Michael Snarski have been great friends. Sharing ideas and working on problems with the three of you has been a great experience and taught me about far-reaching areas in mathematics I would not otherwise have investigated.

I would also like to thank the members of the Discrete math group at Brown including Wai-Yeung Lam, Terrence George, Xufan Zhang, and Olya Mandelshtam.

The software packages Wolfram Mathematica and LaTeX were used extensively. Wolfram Mathematica greatly simplified many of the computations in this thesis and was used to generate many of the figures. The excellent typesetting system LaTeX was used to create and format this document.

The support of many excellent professors during my undergraduate years inspired me to pursue a Ph.D. in applied mathematics. Todd Dupont and L. Ridgway Scott taught me many things about science and how to use mathematics to solve interesting problems. I would also like to thank Sergei Tabachnikov and W. Patrick Hooper for organizing the 2012 Summer at ICERM program. This intensive boot camp helped me develop as a mathematician. I would especially like to thank Patrick for the many helpful conversations we've had since then.

Finally, none of this would have been possible with the support of my parents and my sister. From the earliest age they encouraged me to develop my mathematical skills.

Contents

List of Tables

List of Figures

Chapter One

Introduction

We investigate two different topics in discrete mathematics: the geometry of piecewise-linear surfaces and the long-term behavior of discrete dynamical systems.

Interest in the geometry of piecewise-linear surfaces is motivated in part by the myriad examples in nature of highly organized and complex structures which assemble themselves from identical constituent units in a process known as self-assembly. The tobacco mosaic virus provides one such example [CK62]. Engineers have proposed using self-assembly as a practical means for the fabrication of nanostructures. The December 2017 issue of the journal *Nature* featured four different papers in which self-assembly was used to design nanostructures. In one of these papers, [TPQ17], square tiles (constructed from strands of DNA) are used to build self-assembled nanostructures which render images. We propose a mathematical model for surfaces built from a small set of constituent tiles, which we take to be regular and rigid Euclidean polygons, which can be glued together along their edges. While convex or regular polyhedra are examples of these surfaces, there are many surfaces which have polygonal faces but are neither convex nor symmetrical. Very little is known about these surfaces.

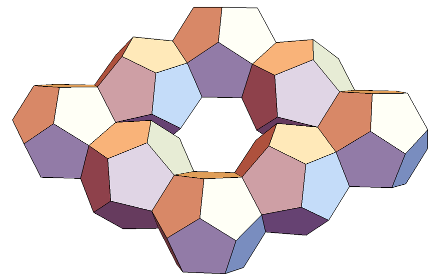

Figure 1.1: A (5)-RPS of genus 1. Notice how this surface can be realized as a union of dodecahedra glued together along common facets.

Definition (2.1.2)**.** Let (Σ, Γ) be a *finite, regular, and proper surface graph*[1] in which Σ is a genus g surface. A genus g *regular polygon surface* (RPS) is a triple (Σ, Γ, ψ) whose *geometric realization* $\psi : \Sigma \to \mathbb{R}^3$ is continuous and maps a face of degree[2] k to a regular Euclidean k-gon with unit edge lengths. To rule out degenerate RPSs,

[1] See definition 2.1.1

[2] The *degree* of a face is the number of incident edges.

we assume that the intersection of the image under ψ of adjacent faces in the graph is either one vertex or one edge and its two incident vertices. If all of the face degrees are contained in the set $\{k_1, \ldots, k_n\}$, then we call the surface a $(k_1, \ldots, k_n)$-RPS.

Figure 1.1 shows a (5)-RPS of genus 1. In chapter 2 we prove the following three theorems characterizing RPSs by their genus and the degrees of their faces.

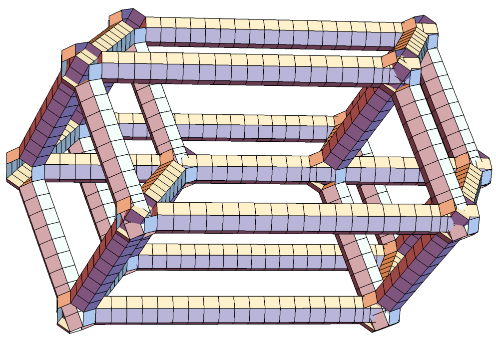

(a) A (4)-RPS of genus 49

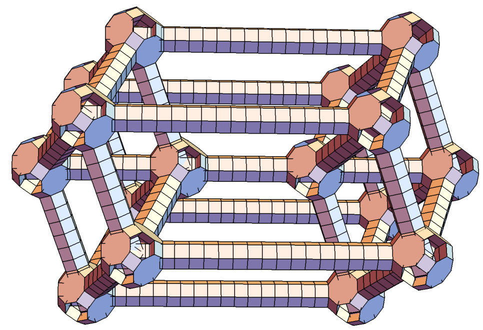

(b) A $(4, 8)$-RPS of genus 49

Figure 1.2: Examples of RPSs

Theorem (2.1.3)**.** *Every oriented genus* 0 *or* 1*,* (5)*-RPS can be realized as the boundary of a union of dodecahedra glued together along common facets.*

Theorem (2.1.4)**.** *The only possible oriented genus* 0*,* $(5, 7, 8, 9, 10)$*-RPSs are those which can be realized as the boundary of a union of dodecahedra glued together along common facets.*

Theorem (2.1.5)**.** *Every oriented genus* 0*,* $(4, 8)$*-RPS can be realized as the boundary of a union of cubes and octagonal prisms glued together along common facets.*

Not all RPSs can be constructed by gluing together convex polyhedra along common facets. The Kepler-Poinsot great dodecahedron shown in figures 2.1a and

2.3 provides one such example. A depiction of this surface first appeared during the Renaissance. There are no classical examples of high genus $(4, 8)$-RPSs which cannot be realized as the boundary of a union of cubes and prisms glued together along common facets. Figure 1.2 shows two such surfaces. In section 2.5 we explain how these surfaces are constructed and present a third example of a high genus RPS which cannot be realized as a union of cubes and prisms glued together (see figure 2.9). The surfaces described in section 2.5 cannot be embedded $\mathbb{R}^3$.

The second topic we investigate in this thesis is the long-term behavior of discrete dynamical systems. In chapter 3 we study a dynamical system known as a *domain exchange map (DEM)*. This chapter was written jointly with Richard Kenyon and Ren Yi. A DEM is an example of a dynamical system which is a *piecewise isometry.* Figure 1.3 shows an example of a DEM defined on a disk.

Definition (3.1.1)**.** Let X be a Jordan domain partitioned into smaller Jordan domains, with disjoint interiors, in two different ways

$$X = \bigcup_{k=0}^{N} A_k = \bigcup_{k=0}^{N} B_k$$

such that for each k, A_k and B_k are translation equivalent, i.e., there exists $v_k \in \mathbb{R}^2$ such that $A_k = B_k + v_k$. A *domain exchange map (DEM)* is the piecewise translation on X defined for $x \in \mathring{A}_k$ by

$$T(x) = x + v_k.$$

The map is not defined for points $x \in \bigcup_{k=0}^{N} \partial A_k$.

A DEM is a generalization of the extensively studied *interval exchange transformation (IET)* to 2-dimensions. An *IET* is a 1-dimensional piecewise isometry. In terms of definition 3.1.1, an IET is a DEM whose domain X is an interval on the

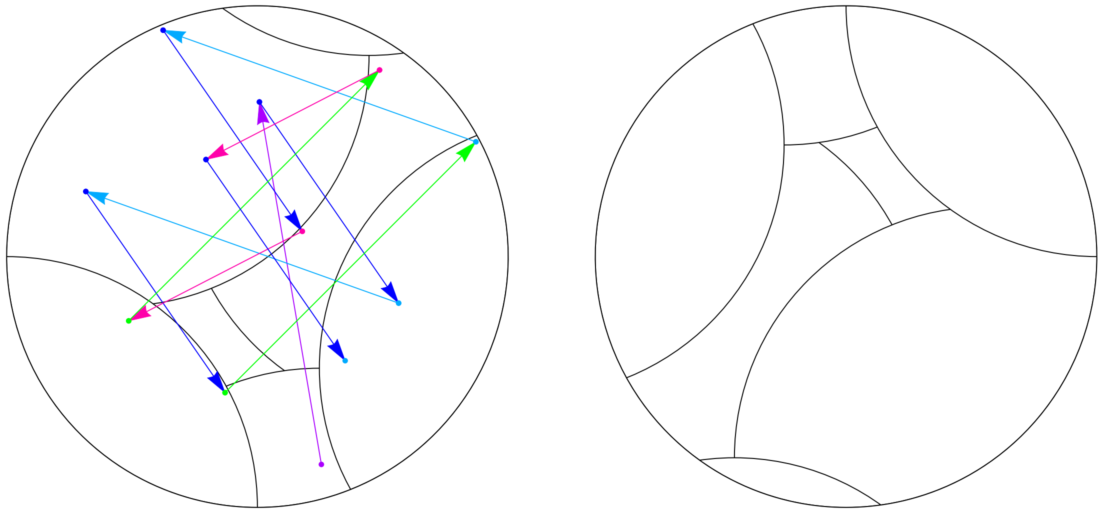

Figure 1.3: The two partitions associated to a DEM in which the domain is a disk and a few iterates of the forward orbit of one point

real line and whose translation vectors are real numbers. IETs first appeared in the literature in [Kea75], although Keane mentions that they had already appeared in a series of lectures in Russian given by Ja. G. Sinai in 1973. Originally IETs were of interest as examples of dynamical systems which are *minimal*, i.e., the orbit of every point with a well-defined orbit is dense, but have multiple ergodic invariant probability measures[3] that are not multiples of Lebesgue measure. In 1982 it was proved independently by Masur [Mas82] and Veech [Vee82] that for almost every minimal IET whose permutation is irreducible the only invariant measures are those which are multiples of Lebesgue measure.

The discovery by Rauzy of a general *renormalization scheme* for IETs, known as *Rauzy induction*, in [Rau79] has been a crucial tool in the study of IETs. For (2)-dimensional piecewise isometries there are no general methods for finding a renor-

[3]Let (X, Σ, μ) be a probability space and $T : X \to X$ a measurable function. The probability measure μ is *invariant* with respect to T if $\mu(T^{-1}(A)) = \mu(A)$ for all $A \in \Sigma$. An invariant measure μ is *ergodic* with respect to T if for all $A \in \Sigma$ with $T^{-1}(A) = A$ either $\mu(A) = 0$ or $\mu(A) = 1$.

malization scheme (unless the system is a trivial product of IETs).

Definition (3.1.6)**.** A dynamical system $T_1 : X_1 \to X_1$ has a *renormalization scheme* if there exists a proper subset $X_2 \subset X_1$, a dynamical system $T_2 : X_2 \to X_2$, and a homeomorphism $\phi : X_1 \to X_2$ such that the *first return map*[4] to Y_1, $\widehat{T_1}|_{Y_1}$, satisfies

$$\widehat{T_1}|_{Y_1} = \phi^{-1} \circ T_2 \circ \phi.$$

A dynamical system is called *renormalizable* or *self-induced* if $T_2 = T_1$.

A few families of piecewise isometries with renormalization schemes are known. Hooper discovered a 2-dimensional family of renormalizable *rectangle exchange maps (REMs)* (see [Hoo13]). A *REM* is a DEM in which each tile in the partition is a rectilinear polygon. Schwartz developed a renormalization scheme for a family of piecewise-isometries he calls *Octagonal PETs* in [Sch14]. These maps arise as an invariant 2-dimensional slice of the *square turning map* he introduced in [Sch18]. We find a new family of REMs which are renormalizable.

In chapter 3 we develop a method for constructing a minimal DEM on any *Jordan domain* X, i.e., a non-empty closed bounded set in $\mathbb{R}^2$ whose boundary is a piecewise smooth Jordan curve. Our DEMs are constructed by projecting a lattice walk in $\mathbb{R}^3$ onto X. Figure 1.4 shows a lattice walk and the tiling associated to the DEM whose translation vectors are the projection of the steps in this lattice walk onto the plane containing X. When the lattice arises from a *cut-and-project set* (see definition 3.1.2) we prove the following theorem:

Theorem (3.1.3)**.** *Every DEM associated to a cut-and-project set is* minimal*, i.e., the orbit of every point, whose orbit is well-defined, is dense.*

[4] See definition 3.1.5

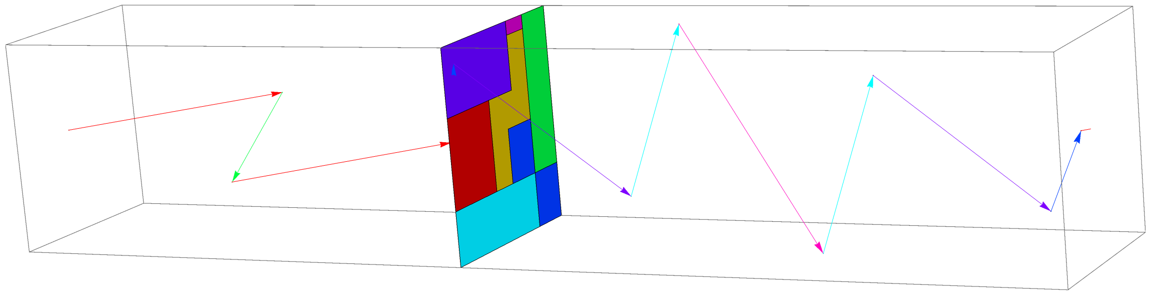

Figure 1.4: A lattice walk and the partition associated to the DEM induced by this lattice walk. Each colored region in the partition is translated by the projection of the step in the lattice walk, with the same color, onto the plane containing the domain X.

When X is a square our method produces REMs because the tiles inherit their shapes from the boundary of the domain. If the lattice has a certain algebraic structure and the domain is a square our construction produces REMs which are renormalizable. We specialize to *PV REMs* in which the lattice is determined by a *PV number*. A *Pisot-Vijayaraghavan number*, more simply called a *PV number*, is a real algebraic integer with modulus larger than 1 whose Galois conjugates have modulus strictly less than one.

Each PV REM is associated to a *Pisot matrix* whose eigenvalues are all real. A *Pisot matrix* is an integer matrix with one eigenvalue greater than 1 in modulus and the remaining eigenvalues strictly less than 1 in modulus (in particular, its leading eigenvalue is a PV number). Define $\mathcal{S}$ to be the set of matrices

$$\mathcal{S} = \left\{ M_n = \begin{bmatrix} 0 & 1 & 0 \\ 0 & 0 & 1 \\ 1 & -n & n+1 \end{bmatrix} : n \geq 6 \right\}.$$

We show in section 3.5.2 that every matrix in $\mathcal{S}$ is a Pisot matrix. For $M_n \in \mathcal{S}$, let

λ be the leading eigenvalue of M_n.

The *Galois embedding* of $\mathbb{Z}[\lambda]$ gives rise to a PV REM (see section 3.2.1). Let T_M denote the PV REM associated to the Galois embedding of the eigenvalues of M. We prove that the set of PV REMs determined by matrices in $\mathcal{S}$ all have the same *combinatorics*. In figure 1.5 we show two PV REMs associated to matrices in $\mathcal{S}$. We prove the following theorem about this family of PV REMs.

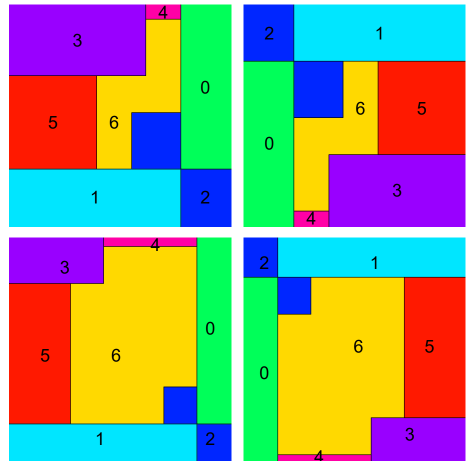

Figure 1.5: The REM described by the top panels has the same *combinatorics* as the REM described by the lower two panels.

Theorem (3.1.7)**.** *Let $M \in \mathcal{S}$ be a matrix and T_M the PV REM associated to the Galois lattice L_λ where λ is the leading eigenvalue of M. Label the eigenvalues of M by λ_1, λ_2 and λ_3 in increasing order. Let $Y \subset X$ be the tile in the partition corresponding to the rectangle* $[1-\lambda_1, 1] \times [1-\lambda_2, 1]$. *The REM T_M is renormalizable, i.e.,*

$$\widehat{T}_M|_Y = \phi^{-1} \circ T_M \circ \phi$$

where $\phi : X \to Y$ is the affine map

$$\phi : (x, y) \mapsto \left(\frac{x + \lambda_1 - 1}{\lambda_1}, \frac{y + \lambda_2 - 1}{\lambda_2} \right).$$

We extend the family $\{T_{M_n} :\ M_n \in \mathcal{S}\}$ of PV REMs to a larger family of REMs via the monoid of matrices $\mathcal{M}$ consisting of nonempty products of matrices in $\mathcal{S}$. Lemma 3.1.4 establishes that $\mathcal{M}$ is in fact a monoid of Pisot matrices.

Lemma (3.1.4)**.** *If $W \in \mathcal{M}$ then its eigenvalues λ_1, λ_2 and λ_3 are real and satisfy the inequalities*

$$0 < \lambda_1 < \lambda_2 < 1 < \lambda_3.$$

There is a subset of matrices $\mathcal{M}_R \subset \mathcal{M}$, containing $\mathcal{S}$ as a proper subset, for which the associated REMs all have the same combinatorics. In section 3.5 we construct a *multistage REM* associated to each matrix in $\mathcal{M}_R$. We prove that multistage REMs are minimal and have a renormalization scheme with multiple steps. In figure 1.6 we show a multistage REM and the REM in each step of its renormalization scheme. Notice that only the first and last REMs in the figure are affinely conjugate to each other. We prove two theorems about multistage REMs.

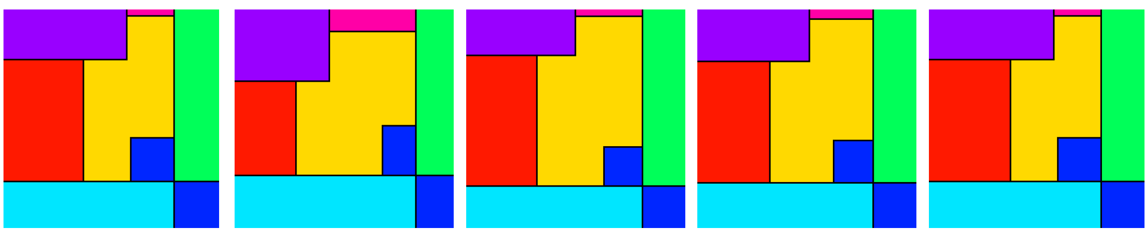

Figure 1.6: The multistage REM T_W and associated REMs $T_{W_1}, T_{W_2}, T_{W_3}$ and $T_{W_4} = T_W$ with $W = M_7 M_7 M_8 M_6$.

Theorem (3.1.8)**.** *Multistage REMs are minimal.*

Theorem (3.1.9)**.** *Let $W = M_{n_L} \cdots M_{n_2} M_{n_1} \in \mathcal{M}_R$ and define $W_k = M_{n_k} \cdots M_{n_2} M_{n_1}$ for $1 \leq k \leq L$. The associated multistage REM is renormalizable, i.e., for each k there exists $Y_k \subset X$ and an affine map $\phi_k : Y_k \to X$ such that*

$$\widehat{T}_{W_{k+1}}|_{Y_{k+1}} = \phi_k^{-1} \circ T_{W_k} \circ \phi_k.$$

Each affine map has the form

$$\phi_k : (x, y) \mapsto \left(\frac{x + x_k - 1}{x_k}, \frac{y + y_k - 1}{y_k} \right)$$

where x_k and y_k are the dimensions of the tile in the partition corresponding to the rectangle $[1 - x_k, 1] \times [1 - y_k, 1]$.

Figure 1.7 shows the parameter space of renormalizable multistage REMs. We conjecture its closure is topologically a Cantor set.

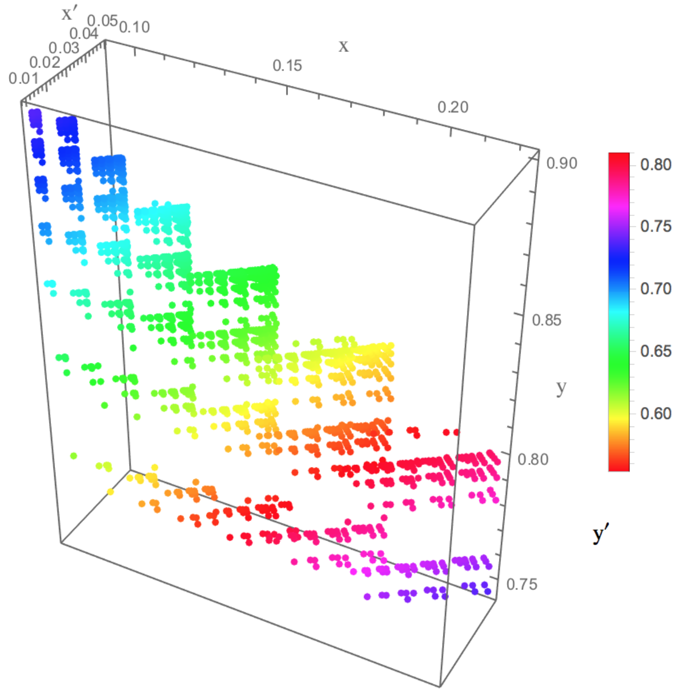

Figure 1.7: The 4-dimensional parameter space of multi-stage REMs. Each point in coordinates (x, x', y, y') corresponds to a pair of eigenvectors $(1, x, x')$ and $(1, y, y')$ of a matrix determining a multistage REM. Points are colored by the coordinate y'.

When a REM is induced by a lattice walk in a 3-dimensional lattice, the dynamical system on the lattice consists of a single bi-infinite lattice walk. One consequence of this fact is that the resulting REM has no periodic points. To produce REMs with more complicated behavior, in chapter 4 we generalize our method for constructing REMs using cut-and-project sets to 4-dimensional lattices. This chapter discusses joint work with Richard Kenyon and Ren Yi. In this case the subspace orthogonal to the domain is 2-dimensional and supports multiple bi-infinite lattice walks. In figure 1.8 we show the projection of the Galois embedding of the lattice $\mathbb{Z}[\lambda]$ where

λ is a root of the polynomial $p(x) = x^4 - 4x^2 + x + 1$ and two possible choices of bi-infinite lattice paths. Figure 1.9 shows the two partitions associated to the two different REMs arising from these two different choices of bi-infinite lattice paths.

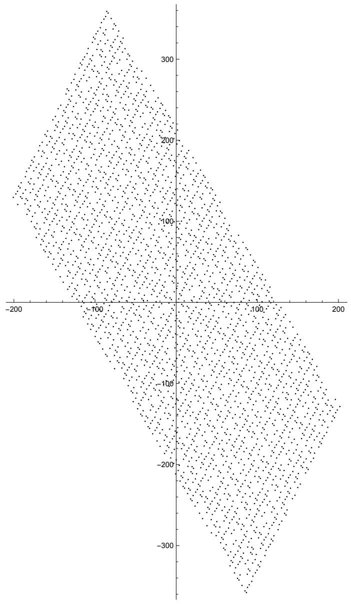

(a) Projection of the lattice onto the plane orthogonal to X

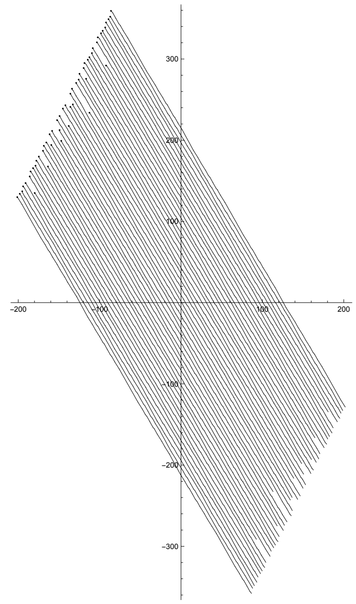

(b) Bi-infinite lattice paths

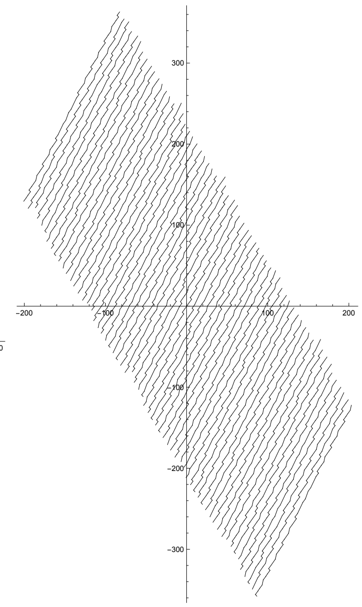

(c) A second set of bi-infinite lattice paths

Figure 1.8: Constructing the REM associated to a root of $x^4 - 4x^2 + x + 1$

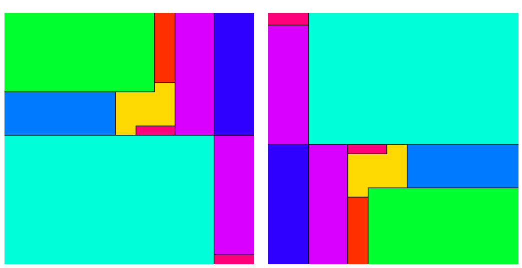

(a) REM induced by paths in fig. 1.8b

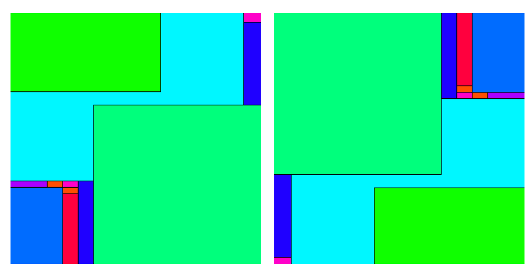

(b) REM induced by paths in fig. 1.8c

Figure 1.9: Two different REMs arising from the lattice in figure 1.8

In chapter 5 we develop a model for random surfaces using the framework developed in chapter 2. We find two different infinite surface graphs which support non-trivial probability measures. There is a natural translation-invariant probability measure which can be parametrized by a local measure on the dihedral angles incident to each vertex, subject to a feasibility constraint. In one case the measure is preserved by a transformation which is surprisingly similar to the Ising Y-Delta transformation.

Chapter Two

Regular Polygon Surfaces

2.1 Introduction

We study surfaces built by gluing regular and rigid Euclidean polygons together along their edges. Recently surfaces built out of regular polygons with boundary have been used to build flexible metamaterials that can be deformed into various configurations [OWHB17]. Very little is known about the space of shapes of these generalized polyhedra, called *regular polygon surfaces* (RPSs) (see definition 2.1.2), which are neither convex nor symmetric. We prove that under certain assumptions on the genus and face degrees, RPSs can be realized as a union of Platonic solids glued along common facets. Before giving a rigorous definition of a RPS, we introduce some terminology from graph theory.

Definition 2.1.1. A *surface graph* (Σ, Γ) is a graph Γ embedded on a closed surface Σ in such a way that $\Sigma \setminus \Gamma$ is a union of connected complementary components called *faces* with each face homeomorphic to the 2-cell. If in addition the closure of each face is homeomorphic to the closed 2-cell, we call the surface graph a *regular surface graph*. When the intersection of the closure of any two faces is either empty, a vertex in Γ, or an edge in Γ we say that the surface graph is *proper*.

The *degree* of a face in a surface graph is the number of edges incident to that face.

Definition 2.1.2. Let (Σ, Γ) be a finite, regular, and proper surface graph in which Σ is a genus g surface. A genus g *regular polygon surface* (RPS) is a triple (Σ, Γ, ψ) whose *geometric realization* $\psi : \Sigma \to \mathbb{R}^3$ is continuous and maps a face of degree k to a regular Euclidean k-gon with unit edge lengths. To rule out degenerate RPSs, we assume that the intersection of the image under ψ of adjacent faces in the graph is either one vertex or one edge and its two incident vertices. If all of the face degrees are contained in the set $\{k_1, \ldots, k_n\}$, then we call the surface a $(k_1, \ldots, k_n)$-RPS.

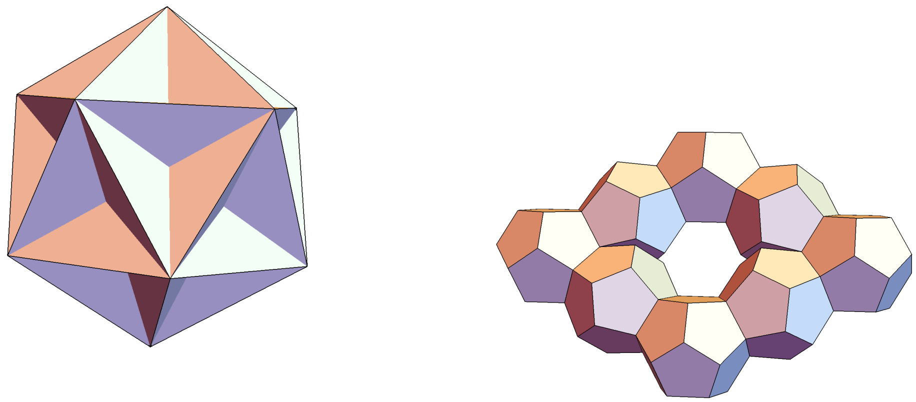

(a) Great dodecahedron (b) Dodecahedral torus

Figure 2.1: Regular polygon surfaces with degree five faces

We allow geometric realizations which are not *embeddings*, i.e., ψ may not be injective and the geometric realization of the surface may have self-intersections.

In figure 2.1 we show two examples of RPSs. The familiar Platonic solids as well as the Kepler-Poinsot polyhedra [Cox63] are all examples of RPSs. One way to build more complicated RPSs is to *glue* two RPSs together along a common facet when both surfaces have facets with the same number of incident edges. To be precise, suppose P and Q are RPSs which both have a face of degree n and let f_p and f_q denote the respective faces. After cutting out the interior of f_p from P and the interior of f_q from Q we can glue the two surface graphs together along their boundaries (in an orientation-reversing way). The new RPS inherits a geometric realization in the obvious way from the geometric realizations of the original two RPSs. An example of a RPS constructed in this fashion is the *dodecahedral torus* shown in figure 2.1b.

When the genus is low enough the space of RPSs is constrained and we are able to prove the following three theorems.

Theorem 2.1.3. *Every oriented genus* 0 *or* 1*,* (5)*-RPS can be realized as the bound-*

ary of a union of dodecahedra glued together along common facets.

Theorem 2.1.4. *The only possible oriented genus* 0*,* $(5, 7, 8, 9, 10)$*-RPSs are those which can be realized as the boundary of a union of dodecahedra glued together along common facets.*

Theorem 2.1.5. *Every oriented genus* 0*,* $(4, 8)$*-RPS can be realized as the boundary of a union of cubes and octagonal prisms glued together along common facets.*

Not all RPSs can be constructed by gluing together convex polyhedra. Figure 2.2 shows a (4)-RPS with genus 49 which cannot be realized as a union of cubes and prisms glued together. In section 2.5 we explain how this surface is constructed and present two other examples of high genus RPSs which are not unions of cubes and prisms (figs. 2.8 and 2.9). Note that the surfaces described in section 2.5 cannot be embedded $\mathbb{R}^3$.

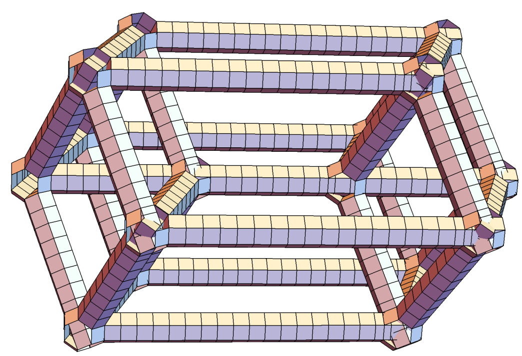

Figure 2.2: A (4)-RPS of genus 49

The RPSs studied in this paper are examples of generalized polyhedra. While the five convex regular polyhedra known as *Platonic solids* were described in Euclid's *Elements*, there is no characterization of generalized polyhedra. New examples of polyhedra (in $\mathbb{R}^3$) are still being discovered (see [GSW14] for examples of regular polyhedra and [GS09] for examples of *toroidal polyhedra*). Moreover, mathematicians have not reached a consensus on the definition of a generalized polyhedron. See [Gru03a] for a historical account of the study of polyhedra and a proposed definition of a generalized polyhedron. Although it is generally known that there are 13 convex *Archimedean polyhedra*, whether regularity is a "local" or "global" condition has resulted in a mathematical error in many enumerations of these objects [Gru09].

A few examples of generalized polyhedra were known classically. The Kepler-Poinsot great dodecahedron (figure 2.1a) is a genus four RPS with faces of degree five which is not a union of convex polyhedra since its vertex figures are the nonconvex star polygons known as pentagrams. It can be constructed in two steps by first *stellating* (extending the faces symmetrically to form a new polyhedron) the dodecahedron to obtain the small stellated dodecahedron, then dualizing the polyhedron [Cox63]. The great dodecahedron was first depicted in a 1568 etching by Amman (see figure 2.3) of an engraving made by Jamnitzer [JA68].

There has been some recent work on low genus polyhedra with rectangular faces. Donoso and O'Rourke [DO01] proved that a polyhedron, of genus at most one with rectangular faces, has dihedral angles which are all integer multiples of $\pi/2$. In addition they constructed a genus seven polyhedron with rectangular faces whose dihedral angles are not integer multiples of $\pi/2$. Their result was later extended to genus two polyhedra with rectangular faces by Biedl et al. [BCD$^+$02]. Thurston developed a global theory that describes triangulations of the sphere with at most 6 triangles around a vertex [Thu98]. He found a natural bijection between these triangulations and a quotient space of a discrete lattice

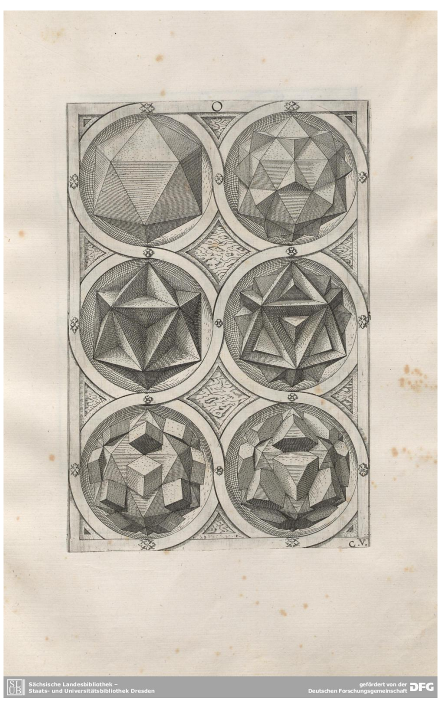

Figure 2.3: The Renaissance etching showing the earliest known depiction of the great dodecahedron [JA68]

in $\mathbb{C}^{1,9}$. See [Sch15] for a readable introduction to Thurston's paper which provides alternative proofs of the main theorems in [Thu98].

RPSs also have applications to statistical mechanics. In the lattice formulation of quantum gravity, physicists are naturally led to an infinite dimensional integral over the space of Riemannian metrics. By approximating a manifold by piecewise linear manifolds, such as RPSs, with fixed edge lengths, one can replace the integral by a discrete sum, vastly simplifying the problem [Dav92]. Sampling large random piecewise linear manifolds is an important aspect of this theory [AB14]. It is conjectured that the associated metric space converges to the Brownian map. See [LGM12] for a definition of the Brownian map and a survey of results about large random planar maps. Surface graphs which support a family of different geometric realizations can be used as a model for random surfaces. Our results imply that certain surface graphs do not have a non-trivial space of geometric realizations.

Although much is known about convex polyhedra in $\mathbb{R}^n$ (see [Ale05] or [Gru03b]) and convex ideal polyhedra in $\mathbb{H}^3$ (see [Riv96]), their techniques do not apply to the inherently nonconvex surfaces we study in this paper.

In order to prove the three main theorems we use inductive arguments that rely on a procedure for simplifying RPSs by removing certain subgraphs. Just as we can build more complicated RPSs by gluing two RPSs together, there is an inverse process where we can simplify a RPS by removing certain subgraphs and replacing them by others. We call the process *polyhedral surgery* and it is defined as follows. Let P be a RPS with data $(\Sigma_1, \mathcal{G}_1, \psi_1)$ and Q a RPS with data $(\Sigma_2, \mathcal{G}_2, \psi_2)$. Suppose both RPSs contain cycles of length n, call them C_1 and C_2 respectively. Label the vertices in P along C_1 by $v_1, \ldots, v_n$ and the vertices in C_2 by $w_1, \ldots, w_n$. In addition, suppose there exists an isometry G of $\mathbb{R}^3$ such that $G \circ \psi_1(v_i) = \psi_2(w_i)$. Cutting Σ_1 along the cycle disconnects it into two hemispheres, H_P^1 and H_P^2 and likewise for Σ_2 with hemispheres H_Q^1 and H_Q^2. Now we can glue H_P^1 to H_Q^1 along their respective boundaries to form a new RPS with geometric realization defined by

$$\psi(x) = \begin{cases} G \circ \psi_1(x) & \text{if } x \in H_P^1 \\ \psi_2(x) & \text{if } x \in H_Q^1 \end{cases}.$$

It is possible that there is a face f in H_P^1 and a face g in H_Q^1 that are adjacent in the surface graph of the new RPS and $\psi(f)$ and $\psi(g)$ intersect in more than just one edge. When two faces intersect in this manner we call them *dangling faces*. However, a slight modification of C_1 to include f prevents this from occurring.

Polyhedral surgery can always be performed when the geometric realization of the RPS formed by gluing the hemispheres H_P^2 and H_Q^1 forms a convex polyhedron. As an example we consider a case when the two hemispheres form a cube. Let P be a RPS containing the subgraph as shown on the left-hand side of figure 2.4 and Q a RPS containing the subgraph shown on the right-hand side of the same figure. We can cut P along the cycle in green, remove the hemisphere containing v_1 and glue in the hemisphere of Q which contains the subgraph shown in the right-hand side of figure 2.4. The resulting RPS has the same genus as P but has two fewer faces.

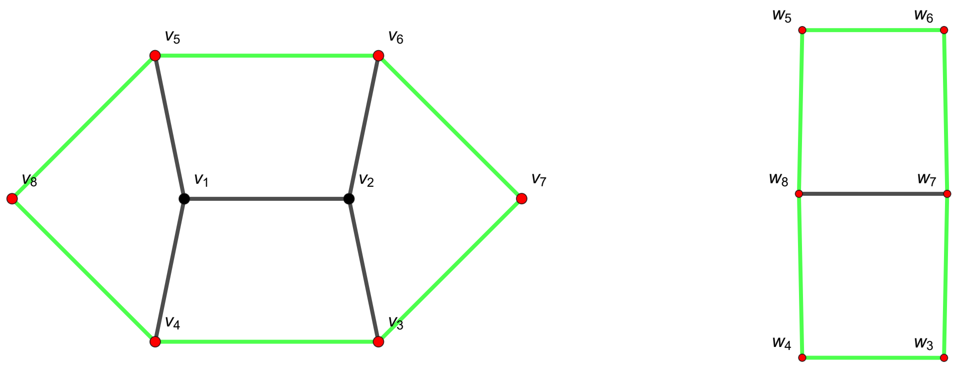

Figure 2.4: Surgery on a cube

2.2 (5)-RPSs

When the degree of each face in a RPS is large and the genus is low, geometric constraints impose some rigidity on the structure of the geometric realization of the surface. In this section we use a discrete form of the Gauss-Bonnet theorem to prove theorem 2.1.3.

Theorem 2.2.1 (Discrete Gauss-Bonnet Theorem)**.** *For a RPS P with Euler characteristic χ and curvature k_v at each vertex v of P we have*

$$\sum_{v \in P}^{n} k_v = 2\pi\chi$$

where the vertex curvature k_v *is* 2π *minus the sum over all faces containing* v *of the interior angle at* v *in the geometric realization of the face.*

A proof of this theorem can be found in many places including [Sch11]. While the Gauss-Bonnet theorem is not normally proved for the RPSs we study in this paper, the extension to our case is straightforward. One way to prove the theorem is by triangulating the RPS, counting the contribution to the curvature from each face π, and applying Euler's formula for a graph on a surface with Euler characteristic χ.

We will find it more useful to assign curvature to faces instead of vertices. The *facial curvature* k_f associated to face f is given by

$$k_f = \sum_{v \in f}^{n} \frac{k_v}{d_v}$$

where the sum is over all vertices incident to f and d_v is the degree of vertex v.

For the remainder of this section we restrict our attention to pentagonal RPSs, those with all faces of degree five. Before proving theorem 2.1.3 we first prove a useful lemma.

Lemma 2.2.2. *Let f be a face of a RPS with all faces of degree five. If f has positive facial curvature then each vertex is of degree three. Moreover, if f has one negative curvature vertex then f has non-positive facial curvature.*

Proof. Since f has positive facial curvature there must be a vertex incident to f with positive vertex curvature. The curvature at a vertex of degree d is $\pi/5(10-3d)$ which is only positive if the vertex has degree three. This vertex contributes $\pi/5(10/d-3)$ to the facial curvature of each face containing it. If vertices with degrees $d_1, \ldots d_5$ are incident to a face then its facial curvature is

$$\frac{\pi}{5} \sum_{i=1}^{5} \left(\frac{10}{d_i} - 3 \right) = -3\pi + \pi \sum_{i=1}^{5} \frac{2}{d_i}.$$

This function is monotonically decreasing as a function of the degrees. If one vertex has degree 6 then it is non-positive. Checking the finitely many cases in which each vertex has degree less than or equal to 6 we find that the facial curvature is only positive when the face has at least 4 degree three vertices and a fifth vertex with degree at most 5.

Next assume that the face f has four vertices of degree three and a fifth vertex v with degree either four or five. Let g and h be the two faces incident to v which share an edge with f. Since g shares an edge with f it must also share two vertices with f and since f only has one vertex with degree more than three, g and f must also share a degree three vertex. Thus the dihedral angle between g and f in the geometric realization is fixed to be that of the dodecahedron, and likewise for the dihedral angle between f and h in the geometric realization. This implies that the geometric realizations of g and h intersect along an edge. Therefore three is the maximum degree of v. From this proof we find that when f has one negative curvature vertex it must have a second and any face with at least two negative curvature vertices has facial curvature of at most zero. $\square$

Proof of theorem 2.1.3. First we prove theorem 2.1.3 for genus zero RPSs. Suppose that the set of counterexamples to the theorem is nonempty. Our RPSs are assumed to be finite thus there exists a lower bound on the number of faces in a surface which is an element of the set of counterexamples. Let n be this lower bound and P a member of the set of counterexamples with n faces. Let (Σ, Γ, ψ) denote the data of P. We use polyhedral removal surgery to construct a RPS with fewer than n faces whose realization is not a union of dodecahedra, therefore contradicting the assumption of minimality.

By assumption, P has genus zero and total curvature 4π thus contains a face with positive facial curvature. Lemma 2.2.2 states that the degree of every vertex incident to a face with positive facial curvature is three. Let f be a face with positive facial curvature. To simplify notation, we label faces that share an edge with f as *first-generation* faces and faces that share an edge with first-generation faces as *second-generation* faces. If a first-generation face had positive curvature, then it would have to share a degree three vertex with some second-generation face. Let C_1 be the cycle in Γ bounding the seven faces consisting of f, the first-generation faces and the face in the second-generation which shares a degree three vertex with a first generation face. Cut the surface along C into two hemispheres H_P^1 and H_P^2, where H_P^1 is the hemisphere with seven faces. Since all faces in H_P^1 are connected by the same type of degree three vertices it can be realized as a hemisphere of a dodecahedron.

Let Q be a genus zero RPS with twelve faces. As can be seen from counting the curvature at every vertex, its geometric realization is a dodecahedron. Cut it along a curve C_2 into two hemispheres such that one hemisphere has five faces and the other has seven. Label the hemisphere with five faces H_Q^1 and the other H_Q^2. Using polyhedral removal surgery we can glue H_Q^1 and H_P^2 along their boundaries to form a genus zero RPS P' with $n-2$ faces. Since P cannot be realized as a union of dodecahedra and the faces we removed can be realized as a part of a dodecahedra, the new surface P' cannot be realized as a union of dodecahedra. However, P' has $n-2$ faces which contradicts the assumption that n was the lower bound on the number of faces in a RPS which cannot be realized as a union of dodecahedra. It is possible that after gluing the hemispheres together, two adjacent faces have the same geometric realization. However, we can resolve this issue by changing C_1 so that one of these faces is in H_P^1. Likewise we modify C_2 so that the boundaries of H_Q^1 and H_P^2 agree.

Now we argue by contradiction to establish that the surface must contain a face with positive facial curvature with an adjacent face that also has positive facial curvature. Assume that no face in the first-generation has positive facial curvature.

No face in the second-generation can have positive facial curvature either. Otherwise it would have all degree three vertices thus share a degree three vertex with a first-generation face and we could apply the same argument as in the preceding paragraph to construct a counterexample to the theorem with $n-2$ faces. Since each first generation face has two degree three vertices and the facial curvature is a monotonic function of the degrees, the facial curvature can be maximized by maximizing the number of degree three vertices. Each face has negative curvature so there are at most three degree three vertices. The only geometrically realizable configuration with three degree three vertices, subject to the constraint that the face has negative facial curvature, is the configuration with three vertices of degree three that are in different orientations. However in this case the remaining two vertices must have degree at least five giving this configuration curvature $-\pi/5$, otherwise the surface would not have a valid geometric realization. If the face has two degree three vertices then its facial curvature is maximized with three degree four vertices and this configuration has facial curvature $-\pi/6$. Since facial curvature is a monotonic function, any configuration with less than two degree three vertices will have less curvature than the configuration with two degree three vertices and three degree four vertices.

The central face f has facial curvature $\pi/3$ which gives the region including f and the first generation faces, total facial curvature $-2\pi/3$. Every positive curvature face must be contained in a region with total facial curvature at most $-2\pi/3$, and these regions must be disjoint because second generation faces also have negative facial curvature. Thus, $-2\pi s/3$ is an upper bound on the total curvature of the surface where s is the number of positive curvature faces. This contradicts our assumption that the surface has genus zero and positive total curvature. Therefore the RPS must have at least one face with positive facial curvature which is adjacent to a face with positive facial curvature. Using polyhedral removal surgery we can always build a counterexample to the theorem with fewer than n faces.

Finally, we extend the result to genus one RPSs. Arguing in the same manner as the genus zero case, suppose the set of genus one counterexamples to theorem 2.1.3 is non-empty and let n be a lower bound on the number of faces of a RPS in this set. Let P be an element of the set of counterexamples with n faces. Since the total curvature of P is zero, we divide the proof into two cases. In the first case, P has at least one face with positive facial curvature. The same argument in the preceding paragraph shows that P must have a region of seven contiguous faces on which we can use polyhedral surgery to build a counterexample with $n-2$ faces, thus contradicting the assumption that n is a lower bound on the number of faces in a counterexample. In the second case, every face of P has zero facial curvature. Recall that the curvature of a face with vertices of degrees $d_1, \ldots, d_5$ is

$$-3\pi + \pi \sum_{i=1}^{5} \frac{2}{d_i}.$$

This sum is negative when at least one of the vertices has degree greater than six. Checking the (finitely many) cases with each $d_i \leq 6$ we find that the sum is zero either when the face has four degree three vertices and one degree six vertex or when the face has three degree three vertices and two degree four vertices. A RPS cannot have a face with four vertices of degree three and one vertex of degree six. Two adjacent faces incident to such a vertex would have 2-dimensional intersection in the surface's realization thus violating one of the conditions in the definition of a RPS. For the remainder of the proof we assume that every face has three degree three vertices and two degree four vertices.

In each face the two degree four vertices must be adjacent in order for the surface to have a geometric realization. This condition severely restricts the combinatorics

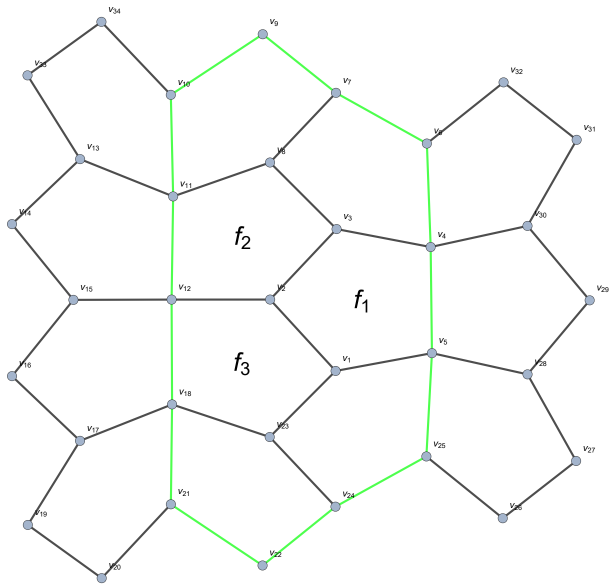

Figure 2.5: Subgraph of the surface graph of a RPS in which every face has zero facial curvature

of the underlying surface graph. In figure 2.5 we show a subgraph of a surface graph for which the three faces f_1, f_2 and f_3 satisfy this requirement on the degrees. Notice that there are three degree three vertices in the interior of the cycle shown in green, thus we can apply polyhedral removal surgery on the green cycle to reduce the number of faces in the surface. The hemisphere we glue in has five faces and comes from a hemisphere of a dodecahedron.

$\square$

2.3 $(5, 7, 8, 9, 10)$-RPSs

In this section we restrict our attention to $(5, 7, 8, 9, 10)$-RPSs and prove theorem 2.1.4. Our assumption that a RPS has a geometric realization in $\mathbb{R}^3$ places a restriction on the types of degree three vertices that may be present. A degree three vertex is only geometrically realizable when it has non-negative curvature. The curvature of a vertex at which two degree five faces and one degree n face meet is $(n-10)\pi/5n$ so the configuration is only realizable if $n \leq 10$, justifying our restriction on the maximum degree of a face. Moreover, if two degree seven (or higher) faces meet at a vertex then the curvature is negative. Thus every degree three vertex is formed by the intersection of at least two degree five faces and one other face which may degree larger than five.

We exclude degree six faces because the existence of large combinatorial spheres with regular pentagonal and hexagonal faces, such as the truncated icosahedron, present an obstacle to our methods. Our methods are local arguments and these large combinatorial spheres imply that we must examine neighborhoods with many faces. Furthermore, vertices at which three degree six faces meet have zero vertex curvature which implies that the surface may have large regions of faces with zero facial curvature in between positive curvature faces. Nevertheless we conjecture that any genus zero RPS with faces of degree five or higher can be realized as a union of dodecahedra and truncated icosahedra glued together along common facets.

Before proving theorem 2.1.4 we introduce notation for the different types of vertices a face may have. A vertex at which k faces of degree m and l faces of degree n meet is denoted by m^k, n^l. For a face with vertices $v_1, \ldots v_n$ we use the product notation $({m_1}^{k_1}, {n_1}^{l_1}) \cdots ({m_t}^{k_t}, {n_t}^{l_t})$ to indicate that vertex v_i is of the form $({m_i}^{k_i}, {n_i}^{l_i})$. We always assume the vertices are ordered cyclically.

In order for a RPS to have a geometric realization only certain vertex combinations on a face are allowed. For example, a vertex of the form $(5^2, 7)$ cannot be adjacent to a vertex of the form (5^3). At a degree three vertex the degree of the faces incident to the vertex determine the dihedral angles between the images of the faces

Vertex type	$5-5$ Dihedral angle	$5-n$ Dihedral angle.
(5^3)	116.57°	116.57°
$(5^2, 7)$	142.65	132.43
$(5^2, 8)$	152.54	141.67
$(5^2, 9)$	162.27	153.22
$(5^2, 10)$	180	180

Table 2.1: Dihedral angles between faces incident to a $(5^2, n)$ vertex

under the geometric realization. In table 2.1 we record the dihedral angles between faces incident to vertices with non-negative vertex curvature. Since the dihedral angles are different for different type vertices, we find that two degree three vertices can only be adjacent if both vertices have the same type.

Suppose a face f is incident to two degree three vertices v and w, both of which are adjacent to a third vertex u. The dihedral angles between any two of the three faces incident to a degree three vertex are determined by the vertex type (see table 2.1). Let g be the face incident to both u and v (which isn't f) and h the face incident to both u and w (which isn't f). If v and w do not have the same vertex type then the dihedral angle between g and h will not be one of those listed in table 2.1, implying that the degree of u is at least 4. However, the vertex cannot have degree 4 because a regular polygon cannot be adjacent to both g and h. Therefore the vertex must have degree at least 5.

Now we prove two lemmas which we use to prove theorem 2.1.4.

Lemma 2.3.1. *Let f be a face of a RPS of degree n with $n \geq 7$. If f has positive facial curvature then every vertex incident to f has the form $(5^2, n)$. Moreover, if f has one vertex with negative vertex curvature then f has negative facial curvature.*

Proof. The only positive curvature vertices are those of the form $(5^2, n)$ with vertex curvature $\pi\,(2/n - 1/5)$. The curvature of a degree four vertex incident to f is at most $\pi\,(2/n - 1/5)$ where the vertex has configuration $(5^3, n)$. If a face has k vertices of degree greater than 3 and $n-k$ vertices of degree 3 then its facial curvature is $-\pi(2n^2 + 4kn - 20n + 5k)/30n$ which is negative when $k > 1$ for $n \geq 7$.

Assume that f has $n-1$ vertices of type $(5^2, n)$ and one vertex v which may have degree greater than 3. Let g and h be the two faces adjacent to f which are also incident to v. Under the geometric realization of the surface, g and h intersect along an edge because the degree 3 vertices determine the dihedral angle between these two faces. If v had degree 4 then a face would be adjacent to both g and h but then the realization of this face could not be a regular polygon because two of its edges have the same geometric realization. This implies that v has degree at least five. However, if v had degree 5 then the geometric realization of two of the faces incident to v would overlap which is a contradiction. We find that v has degree at least 6.

A vertex of degree 6 has the largest vertex curvature in configuration $(5^5 - n)$ with vertex curvature $2\pi(-1 + 1/n)$. If a face has $n-1$ vertices of type $(5^2 - n)$ and one vertex of degree 6 then its facial curvature is at most $-(n-1)(n-5)\pi/15n$ which is negative for $n > 5$. Therefore when f has positive facial curvature every vertex must be of type $(5^2, n)$. Furthermore, this argument implies that a face with one negative curvature vertex must have a second vertex with negative vertex curvature and thus have negative facial curvature. $\square$

Lemma 2.3.2. *In a* $(5, 7, 8, 9, 10)$*-RPS of genus zero, there exists a face of degree five with positive facial curvature.*

Proof. Suppose every face of degree five has non-positive curvature and let f be a degree n face with positive facial curvature. By lemma 2.3.1, each vertex incident to f has configuration $(5^2, n)$ and so f is adjacent to n degree five faces, all of which have non-positive facial curvature. Each face in the first generation has at least two adjacent vertices of type $(5^2, n)$. As previously discussed, degree 3 vertices with different types cannot be adjacent and are separated by a vertex of degree at least 5. A configuration with two different types of degree three vertices has facial curvature at most $\pi(160 - 47n)/75n$ when it is of type $(5^2, n)^2(5^4, n)(5^3)(5^4, n)$. Each first generation has at most 4 degree three vertices since the remaining vertex is incident to two degree n faces. The configuration with only one type of degree three vertex with the largest facial curvature is $(5^2, n)^4(5^2, n^2)$ with facial curvature $\pi(110/n - 17)/30$. Any other facial configuration has less facial curvature and we find that the most curvature a face in the first generation can have is in the configuration $(5^2, n)^4(5^2, n^2)$.

The sum of the facial curvature from f and its n first generation faces is $13\pi/3 - 19\pi n/30$ which is negative for $n \geq 7$. None of the faces in f's second generation can have positive curvature because each either has degree five or is a degree n face incident to a vertex of degree 4 of the form $(5^2, n)^4(5^2, n^2)$ and as a result has negative facial curvature.

Thus, by summing the curvature over all faces with positive facial curvature and their first generation faces we find that the surface has negative total curvature. This contradicts the assumption that the surface has genus zero and we conclude that there exists a degree five face with positive facial curvature. □

Proof of theorem 2.1.4. The proof is similar to the proof of theorem 2.1.3. Suppose that the set of counterexamples to the theorem is non-empty and let n be the lower bound on the number of faces of an element in the set. Let P be a counterexample with n faces. By lemma 2.3.2 there exists a degree five face f with positive facial curvature. Since f has positive curvature, every vertex incident to f has positive vertex curvature. Moreover, f is incident to an odd number of vertices, implying that all vertices incident to f have the form 5^3. Thus all faces in the f's first generation have degree five. If the second-generation faces were all degree five, then we could use the argument from the proof of theorem 2.1.3 to construct a counterexample with $n-2$ faces. Thus, there exists a face with positive curvature such that a face in its second generation has degree larger than 5. Without loss of generality, assume that f is this face. If a face in f's first generation had positive curvature then we could use polyhedral surgery, as in the proof of theorem 2.1.3, to construct a counterexample to theorem 2.1.4 with $n-2$ faces. The same argument implies that no degree five face in the second generation can have positive curvature.

Let g be a face with degree greater than five in the second-generation. This face shares two vertices with a face h in the first generation. Since h has degree five and two vertices of the form 5^3, the two vertices it shares with g must have degree at least four. Since g has two degree four vertices its facial curvature is $-\frac{\pi(n-5)(n-1)}{15n}$ which is negative for $n \geq 6$. The vertex configuration of a first-generation face which maximizes the facial curvature of the face is the one with the fewest degree n vertices. The first generation faces contribute the most curvature with three of type $(5^3)^2(5^4)^3$, one of type $(5^3)^2(5^3,n)(5^2,n)(5^4)$, and one of type $(5^3)^2(5^4)(5^3,n)(5^4)$. The sum of the facial curvature of f and its first generation faces is $(5-2n)\pi/(3n)$ which is negative for $n \geq 4$. Since no second-generation face has positive curvature, the sum over all positive curvature faces, of the facial curvature of a face and its first-generation neighbors, gives an upper bound on the total curvature of the surface. However, this upper bound is negative which contradicts our assumption that the surface has genus zero. □

2.4 $(4,8)$-RPSs

RPSs with faces of degree four or eight have both vertices with zero curvature and faces with zero facial curvature. Since positive curvature and negative curvature faces can be separated by large regions of zero curvature faces, we cannot use the curvature of local regions to rule out certain configurations as in the previous sections. However, these surfaces have additional structure which is not present in RPSs with faces of degree five. Let P be a RPS with data (Γ, Σ, ψ). The geometric realization of each face in the graph is composed of pairs of parallel edges.

Definition 2.4.1. A *band* $B_{e,f}$ is a simple cycle in the dual graph $\bar{\mathcal{G}}$ of $\mathcal{G}$ starting at edge e and face f of $\mathcal{G}$ with the property that the geometric realizations of the primal edges associated to consecutive edges in the cycle are parallel translates (in R^3) of each other.

The *dual graph* $\hat{\mathcal{G}}$ of $\mathcal{G}$ is the graph whose vertices correspond to faces of $\mathcal{G}$ and where two vertices in $\hat{\mathcal{G}}$ are adjacent exactly when the corresponding faces in the primal graph $\mathcal{G}$ share an edge.

We can cut Σ along the edges in $\mathcal{G}$ bounding a band $B_{e,f}$. When the RPS has genus zero the cut disconnects Σ into two hemispheres H_1 and H_2, and an annulus. If every face in the band has degree four, then we can glue the two hemispheres together by identifying pairs of boundary edges, and their incident vertices, which were incident to the same face in the band $B_{e,f}$ to form a new surface P'. The geometric realization ψ' of P' is

$$\psi'(x) = \begin{cases} \psi(x) - e & \text{if } x \in H_1, \\ \psi(x) & \text{if } x \in H_2 \end{cases}$$

where ψ is the realization of the original surface. We call the process of removing a band and gluing two hemispheres together *band surgery*. The new surface P' satisfies all conditions of being a RPS except for one: two adjacent faces may have the same image under ψ. Removing every such pair of dangling faces forms an actual RPS with the same genus as P. If every face in a genus zero RPS has degree four then we can use band surgery to prove the following theorem.

Theorem 2.4.2. *Every genus zero RPS with faces of degree four can be realized as a union of cubes glued together along common facets.*

Proof. We use complete induction on the number of faces in the surface to prove the theorem. Since the total curvature is 4π and the most curvature a vertex can have is $\pi/2$, there are at least eight vertices in the surface. Likewise, the facial curvature can be as large as $2\pi/3$ when all vertices are degree three. Thus there are at least six faces in the surface. The only possible geometric realization of a RPS with six faces is that of a cube. This proves the base case of the theorem. For our inductive hypothesis we assume the theorem is true for all surfaces with fewer than n faces with $n \geq 6$. Let P be a RPS with n faces. Let $B_{e,f}$ be a band in the surface through face f with edges that are parallel transports of e (in their geometric realizations). Since all faces in the surface have degree four we can use band surgery to remove $B_{e,f}$ and form a new surface with fewer than n faces. Remove all pairs of dangling faces until what remains is a RPS which we call P'. By induction it is a union of cubes. Let γ_1 and γ_2 denote the boundary edges of $B_{e,f}$ in P which are identified to form P'. Since P' is a union of cubes, the arc γ_1 can be realized by a *cycle* in a surface built by gluing cubes together along common facets. A *cycle* is a sequence of alternating edges and vertices starting and ending at the same vertex such that each edge is incident to the two vertices preceding and succeeding it in the sequence and without repeated edges. Splitting P' along γ_1 and inserting a new layer of cubes forms a surface $\tilde{P}$. For each pair of dangling faces that was removed we glue in a cube, possibly identifying faces of neighboring cubes. The resulting RPS Q can be realized as a union of cubes. Since Q has the same genus as P and the surface graphs of the two surfaces are isomorphic, we conclude that P can be realized as a union of cubes. $\square$

When faces of degree eight are also present in the surface, the surface may not have a band in which every face has degree four. Band surgery doesn't work on bands with degree eight faces because after cutting the band out and gluing the two hemispheres together, the resulting surface may not have a valid geometric realization. However, we can still use bands to help us characterize the structure of these surfaces. A path in the dual graph has a *turning point* at a primal face f if the two faces adjacent to f in the path intersect f along edges which are not parallel translates of each other in the geometric realization of the surface. A *band bigon* is a simple cycle in the dual graph with exactly two turning points. Every band bigon is formed by two intersecting bands which intersect at the primal faces corresponding to the two turning points. The faces of the bigon are the primal faces corresponding to the dual vertices of the bigon. The geometric realization of the two turning points are faces in the RPS which lie in parallel planes in $\mathbb{R}^3$ since both faces contain parallel transports of the edges determining the bands. At a turning point the dot product between the two unit vectors determining the bigon is either $0, 1/\sqrt{2}$ or $-1/\sqrt{2}$. Since the geometric realization of the RPS sends every edge of the graph to a unit vector in $\mathbb{R}^3$, we will often abuse notation and identify an edge with its corresponding unit vector in $\mathbb{R}^3$.

Cutting Σ along the boundary of a bigon disconnects the surface into two disks and an annulus. If one of the disks does not contain any bigons then the bigon is said to be *minimal*. We call the subset of Σ corresponding to the union of the annulus and the disk which doesn't contain any bigons, the *interior* of the bigon. The *strict interior* of the bigon is just the disk which contains no bigons. It is an easy consequence of the Jordan curve theorem that on a genus zero RPS, the bands forming a minimal bigon pass through adjacent edges of the faces corresponding to the turning points of the bigon (see lemma 2.4.3).

After a careful analysis of all minimal bigons, we show that the there are only a few possible geometric realizations of the interior of a minimal bigon. For any minimal bigon, the arc γ bounding the interior can be realized as a cycle on a surface built out of a union of cubes and octagonal prisms glued together along common facets. This result is established in a sequence of lemmas and is crucial in the proof of theorem 2.1.5. The first lemma in the sequence states that the turning points of a minimal bigon are either both squares or both octagons. To prove this we use the elementary fact that any band which passes through the interior of a minimal bigon must cross both bands forming the bigon. This is an easy corollary of the Jordan curve theorem combined with the assumption of minimality. A genus zero RPS cannot have a simple cycle in the dual graph with exactly one turning point (a *monogon*) because no band can pass through two edges of a face which are not parallel to each other.

Lemma 2.4.3. *On a genus zero RPS, no minimal bigon can have a square at one turning point and an octagon at the other.*

Proof. Suppose two distinct bands B_v and B_h form a minimal bigon with one turning point a degree four face and the other a degree eight face. Label the faces S and O respectively. Since the two bands cross in a degree four face the dot product of their corresponding unit vectors must satisfy $|v \cdot h| = 1$. Thus the geometric realizations of S and O are parallel to the plane spanned by v and h. The edges on O which are parallel transports of v and h cannot be adjacent which implies that there must be an edge between them and a band through this edge which passes through the interior of the minimal bigon. However, the RPS is topologically a sphere so by the Jordan curve theorem this band must exit the bigon and in the process cross either B_v or B_h. In either case this contradicts the assumption of minimality. □

We are now able to classify bigons based on the types of their turning points. A minimal square bigon has squares at each of its two turning points and similarly a minimal octagon bigon has octagons at each of its two turning points.

Lemma 2.4.4. *Suppose B_v and B_h are two bands forming a minimal octagon bigon on a genus zero RPS. Two bands, neither of which are part of the bands forming the bigon, cannot cross in the interior of this minimal bigon.*

Proof. Let B_h and B_v be the two bands forming the minimal octagon bigon and let O_1 and O_2 be the two octagons at the turning points of the bigon. As previously noted, the bands of the bigon must pass through adjacent edges of the octagons at the turning points. Since the geometric realizations of O_1 and O_2 are regular octagons with unit edge lengths, the angle between v and h is fixed so that $|h \cdot v| = 1/\sqrt{2}$. By changing coordinates we may assume $v = (1, 0, 0)$ and $h = 1/\sqrt{2}(1, 1, 0)$. Since any band through the bigon must exit, the dot product of the unit vector associated to any band through the bigon with v or h is either $0, 1/\sqrt{2}$ or $-1/\sqrt{2}$.

First we show that the faces along B_h and B_v in the minimal bigon in between O_1 and O_2 all have degree four. Suppose there were an octagon on the boundary of the minimal bigon and without loss of generality that it's on B_v. Let a, b and c denote the directions of the geometric realizations of the consecutive edges on this octagon with bands through them that enter the bigon. Since the realization of this face is a regular octagon we must have the following relations

$$|a \cdot v| = |c \cdot v| = |a \cdot b| = |b \cdot c| = 1/\sqrt{2} \text{ and } |b \cdot v| = 0.$$

However, one of the edges of the octagon is a parallel transport of v and since the realization of the octagon is a plane these equations cannot all be satisfied. For $|b \cdot v| = 0$ implies $b = (0, b_2, \pm\sqrt{1 - b_2^2})$ but B_b must cross B_h which implies $b_1 = 0$ or ± 1. Then there are six possibilities for a,

$$a = 1/\sqrt{2}(1, \pm 1, 0), 1/\sqrt{2}(1, 0, \pm 1) \text{ or } 1/\sqrt{2}(0, 1 \pm 1)$$

but none of these directions are allowed because B_a must cross B_h.

Now suppose two bands cross in a face in the interior of the bigon. Since this face cannot lie on B_h or B_v, there are two edges e and g on the face with $e \cdot g = 0$. By the assumption of minimality B_e crosses both B_h and B_v. Likewise B_g crosses both B_h and B_v as well. Since there are no octagons along B_h and B_v, these crossings must all occur at degree four faces. Thus,

$$|e \cdot h| = |g \cdot h| = |e \cdot v| = |g \cdot v| = 0$$

but there do not exist vectors in $\mathbb{R}^3$ which satisfy both the above equations and $e \cdot g = 0$.

□

The preceding lemma implies that the geometric realization of a minimal octagon bigon is in fact part of an octagonal prism. In other words, every face in the interior of the minimal bigon has degree four except for the two degree eight turning points. The dihedral angles between degree four faces are either π or $3\pi/4$ and between degree eight and degree four faces the angles are $\pi/2$. Moreover, every face in the interior of the bigon lies on one of the bounding bands and all bands that cross through the bigon are parallel transports of the same unit vector.

A minimal bigon is bounded by two cycles one of which is not adjacent to a face in the interior of the bigon. Let C be this cycle. Cutting Σ along C disconnects the surface into two hemispheres H^1 and H^2. Assume that H^1 is the hemisphere containing the interior of the minimal bigon. As shown in the preceding paragraph, we can glue a hemisphere from a RPS which can be realized as an octagonal prism to H^1 resulting in a RPS whose realization is an octagonal prism. Gluing the other hemisphere to H^2 forms a new RPS with data $(\Sigma', \mathcal{G}', \psi'$ in which $\mathcal{G}'$ has two fewer degree eight faces than the original graph $\mathcal{G}$. By construction, Σ' is homeomorphic to Σ so this operation does not change the genus of the surface. The geometric realization is defined from the original geometric realization ψ as $\psi'(x) = \psi(x)$ for $x \in H^2$ and extended by linearity to the complement $\Sigma' \setminus H^1$. This operation is a special case of polyhedral surgery and we refer to it as *octagon removal surgery*. It is possible that octagon removal surgery creates dangling faces, but after modifying C to include one of these faces there will be no dangling faces in the new surface. For later reference we record the content of this paragraph as the following lemma.

Lemma 2.4.5. *Octagon removal surgery removes two degree eight faces from any genus zero RPS with a minimal octagon bigon.*

Square bigons are potentially more complicated, however in some cases they turn out to be very simple to analyze.

Lemma 2.4.6. *If a genus zero RPS has a minimal square bigon without any degree eight faces on the boundary of the bigon, then the dihedral angle between any two faces in the interior of the bigon, in the realization of the surface, is π. In particular, the realization of a minimal square bigon that does not contain an octagon consists of four faces of a rectangular prism.*

Proof. Let B_a and B_b be the two bands forming the minimal square bigon. Suppose that two adjacent faces have a dihedral angle which is not π and let B_c and B_d be the two bands that pass through these two faces. Since both c and d are orthogonal to a and b, c must be parallel to d which implies that the dihedral angle between the faces is π.

Now, suppose there is a face strictly in the interior of the bigon. Let B_c and B_d be the bands that cross at this face. Since both bands must pass through both sides of the bigon this creates four mutually perpendicular vectors in $\mathbb{R}^3$ which is a contradiction. Thus the bigon consists of two bands that cross at two squares and every face in the interior of the bigon lies on one of the two belts, B_a or B_b. $\square$

When a minimal square bigon satisfies the conditions of 2.4.6, its realization consists of four facets of a prism and we can use polyhedral removal surgery to remove these four facets and replace them by the other two facets of the prism in a manner analogous to octagon removal surgery. Polyhedral removal surgery applied to a prism reduces the number of faces in the surface's surface graph by 2. We call this special case of polyhedral surgery, *prism removal surgery.*

Lemma 2.4.7. *Let f be a face in the interior of a minimal square bigon and let*

e be a unit vector determined by the geometric realization of an edge incident to f. Choose coordinates so that the bigon is formed by two bands, B_v and B_h, with $h = (1,0,0)$ and $v = (0,1,0)$. Then the vector e is a parallel translate of one of eight possible unit vectors:

$$\frac{1}{\sqrt{2}}(1,\pm 1,0),\frac{1}{\sqrt{2}}(1,0,\pm 1)),\frac{1}{\sqrt{2}}(0,1,\pm 1)) \text{ or } (0,0,\pm 1)).$$

Proof. Let B_e be the band through the face f starting at edge e. Since the bigon is minimal, B_e must pass through both B_v and B_h and it must cross at either a square or an octagon. Thus the angle between e and v is either $\pi/2$, $3\pi/4$, $5\pi/4$ or $3\pi/2$. Likewise for the angle between e and h. Therefore e is a parallel translate of the eight directions listed in the statement of the theorem. □

Lemma 2.4.8. *Suppose there is a degree eight face on the boundary of a minimal square bigon on a genus zero RPS and let B_a, B_b and B_c denote the other three bands through this face in cyclic order. Each face on B_a in the interior of the bigon is adjacent to a face on B_b. Similarly, each face on B_c in the interior of the bigon is adjacent to a face on B_b.*

Proof. Choose coordinates so that the square bigon is formed by two bands, B_v and B_h, with $h = (1,0,0)$ and $v = (0,1,0)$. Let O be the degree eight face in the statement of the theorem and without loss of generality assume that it lies on B_v. Since the surface is topologically a sphere, by the Jordan curve theorem B_a, B_b and B_c must cross B_h. Since a, b, c and v are the directions of four consecutive edges of a face whose realization is a regular octagon, we have

$$|a \cdot b| = |b \cdot c| = |c \cdot v| = |a \cdot v| = 1/\sqrt{2}$$

and

$$|a \cdot c| = |b \cdot v| = 0.$$

Moreover B_a, B_b and B_c all pass through B_h, so the dot product of each with h is either 0, $1/\sqrt{2}$ or $-1/\sqrt{2}$. From lemma 2.4.7 we know that there are eight possible choices for the directions of the edges. The only possible directions for a, b, and c that satisfy all of these conditions are

$$a = 1/\sqrt{2}(0,1,-1),\ b = (0,0,1),\ \text{and}\ c = 1/\sqrt{2}(0,1,1).$$

Now suppose that there is a face in the interior of the minimal square bigon between B_b and B_c. This face could have degree four or eight, but in both cases there are two bands through this face determined by unit vectors which are orthogonal to each other. Let B_x and B_y denote these two bands. Since the bigon is minimal, B_x must cross B_c or B_a, and likewise for B_y. Of the eight possible directions for x and y, the only directions consistent with the crossing condition is $x = 1/\sqrt{2}(0,1,-1)$ and $y = 1/\sqrt{2}(0,1,1)$. Computing $x \cdot h$ we find that B_x crosses B_h at a degree eight face. Let O_1 be this face and let the directions of the edges of the realization be a', b', and c'. The fourth direction is a parallel translate of B_h because O_1 is on B_h. A similar calculation to the one determining the directions a, b, and c shows that the unit vectors determining these directions are

$$a' = 1/\sqrt{2}(1,0,-1),\ b' = (0,0,1),\ \text{and}\ \ c' = 1/\sqrt{2}(1,0,1).$$

Likewise B_y also crosses B_h at a degree eight face, which we label O_2. An identical argument shows that the same unit vectors as above determine the directions of the realizations of the edges of O_2. However, computing the dot products we find B_x crosses O_1 along the edge in the direction of b' and B_y crosses O_2 along the edge in the direction of b'. This is a contradiction because x and y are orthogonal directions. $\square$

There are two remaining operations to define before we can prove theorem 2.1.5. In the proof we analyze all minimal bigons and use polyhedral surgery to decrease either the number of faces in the surface or the number of degree eight faces in the surface. When a minimal square bigon has degree eight faces along its boundary, the bigon can be very complex to analyze. The two operations we introduce are the *cube flip* and the *prism flip*. Both allow us to decrease the number of faces in the bigon, thereby reducing the complexity of the bigon.

First, we define the cube flip. Let h be a turning point of a minimal square bigon and let f and g be the two faces in the interior of the bigon which are adjacent to h. If all three faces have degree four, then in their realization they form three faces of a cube. In an operation we call a *cube flip*, we replace these three faces in the RPS by the three faces that form the other half of the cube. Figure 2.6 shows a subgraph of a surface graph and the effect of a cube flip on this subgraph. The geometric realization of the new RPS is defined by extending the geometric realization of the original surface to the three faces f', g' and h' linearly so that the realization of each face is a Euclidean square with unit edge lengths.

Suppose that there exists a minimal bigon and that a cube flip can be performing on one of the turning points. Let B_h and B_v denote the bands determining the bigon and f_1 and f_2 the two faces corresponding to the bigon's turning points. After a cube flip at f_1, the bigon formed by B_h and B_v, which passes through f_2, also passes through one of the new faces formed by the cube flip. The new bigon is still a minimal bigon but it contains fewer bands through its interior than the original minimal bigon.

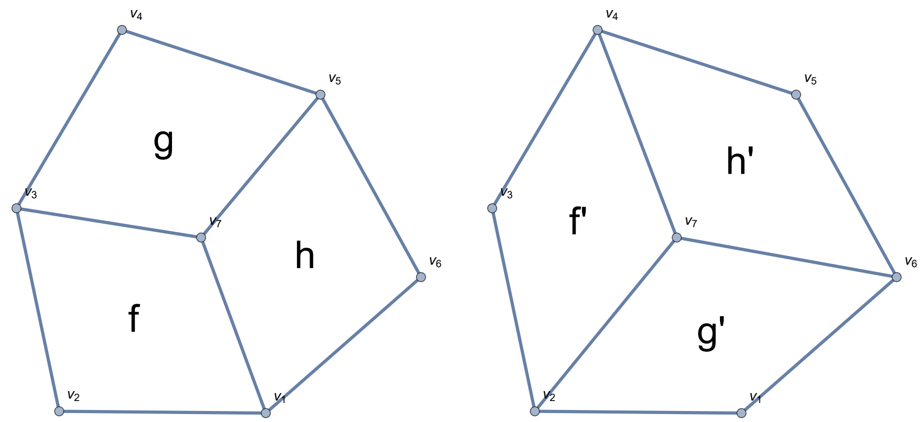

Figure 2.6: Cube flip

The prism flip is defined similarly to the cube flip. In the prism flip we replace five faces in the RPS, whose realization forms part of an octagonal prism, with the five faces that form the other half of the prism. We skip a formal definition of the prism flip because it is so similar to the cube flip. A prism flip that involves the face at the turning point of the bigon reduces the number of bands that cross through the interior of the bigon. Finally, all of the tools are in place to prove theorem 2.1.5.

Proof of theorem 2.1.5. Let P be a RPS with data (Σ, Γ, ψ). We use induction on the number of degree eight faces in the RPS. Let n be the number of degree eight faces in the surface. The base case, $n = 0$, is theorem 2.4.2. Assume that the theorem is true for any RPS with fewer than n faces. Since the surface has a finite number of faces, there is always at least one minimal bigon. There are two cases depending on the type of the bigon. First, assume that the minimal bigon is an octagon bigon. Lemma 2.4.5 explains how octagonal removal surgery applied to this bigon produce a new RPS P' with two fewer degree eight faces than P. By the induction hypothesis this surface can be realized as a union of cubes and prisms. Since the bigon that was removed can be realized as part of an octagonal prism, we can glue an octagonal prism to P' to form a surface which has the same surface graph and genus as P. Thus P can be realized by a union of cubes and prisms.

In the second case, the minimal bigon is a square bigon. Suppose that this bigon is determined by two bands, B_h and B_v, and has a turning point at a face f. Let g and h be the two faces in the interior of the minimal bigon which are adjacent to f. If both g and h have degree four then we can use a cube flip to decrease the number of bands through this bigon. If one of g and h has degree four and the other degree eight, then by lemma 2.4.8 there are five faces, including f, whose realization is a part of an octagonal prism. Thus we can always use a cube flip or a prism flip to decrease the number of bands through the bigon.

Since the bigon has finitely many faces, after finitely many flips the bigon will have one face which is adjacent to both turning points. If this face has degree four then we can remove a cube with polyhedral removal surgery and decrease the number of degree four faces in the surface by 2. If the face has degree eight then we could remove an octagonal prism with polyhedral removal surgery and decrease the number of degree eight faces in the surface by 2. This procedure reduces the number of degree four faces in the surface monotonically. However, we cannot remove all of the degree four faces from the surface. The surface has genus zero and thus has positive curvature vertices. At least two squares meet at every positive curvature vertex. Thus after removing finitely many faces from the surface, we must reach a surface P' in which the only minimal bigons are octagon bigons. Removing this octagon bigon and applying the induction hypothesis we find that the surface can be realized as a union of cubes and prisms. Since at every step we have removed either a part of a cube or a prism, we can glue these cubes and prisms back to P' to form a surface with the same surface graph and genus as P. Therefore P can be realized as a union of cubes and prisms.

□

2.5 Examples of higher genus RPSs

In this section we construct three examples of high genus RPSs which are not unions of convex polyhedra. This can be seen by the absence of certain faces in the surfaces. All of the examples in this section can be constructed in two steps. First, place convex polyhedra at the vertices of a 3-cube or a 4-cube. Second, remove certain faces from each polyhedron and connect the boundary components using prisms with matching boundary components. Whether a 3-cube or a 4-cube is used depends on the structure of the convex polyhedra.

Figure 2.7 shows a genus 49 surface whose faces have degree four. It is constructed out of truncated octahedra placed at the vertices of a 4-cube and connected by hexagonal prisms. All hexagonal faces have been removed from the constituent truncated octahedra and hexagonal prisms. The Euler characteristic of the surface is

$$\chi = 16 \cdot 2 - 16 \cdot 8 - 64 \cdot 6 + 64 \cdot 6 = -96.$$

Figure 2.8 shows a genus 49 surface whose faces have degree four and eight. It is constructed out of truncated cuboctahedra placed at the vertices of a 4-cube and connected by hexagonal prisms. All hexagonal faces have been removed from the constituent truncated cuboctahedra and hexagonal prisms. The Euler characteristic of the surface is

$$\chi = 16 \cdot 2 - 16 \cdot 8 - 64 \cdot 6 + 64 \cdot 6 = -96.$$

Figure 2.9 shows a genus 17 surface whose faces have degree four and eight. It is constructed out of truncated cuboctahedra placed at the vertices of a 3-cube and connected by octagonal prisms. All octagonal faces have been removed from the constituent truncated cuboctahedra and hexagonal prisms. The Euler characteristic of the surface is

$$\chi = 8 \cdot 2 - 8 \cdot 6 - 24 \cdot 8 + 24 \cdot 8 = -32.$$

Acknowledgments

I thank Richard Kenyon for suggesting the study of RPSs and for his advice throughout this project. I thank Sanjay Ramassamy for suggesting a simplification of the proof in Section 2.2. I also thank Ren Yi for many helpful conversations.

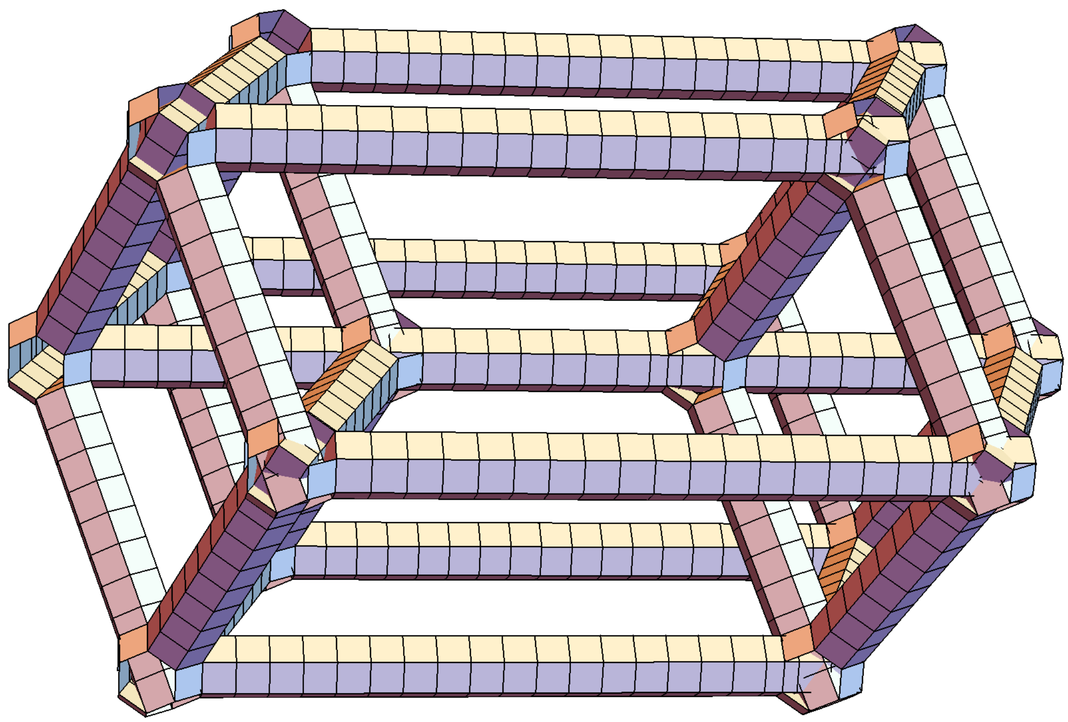

Figure 2.7: A (4)-RPS of genus 49

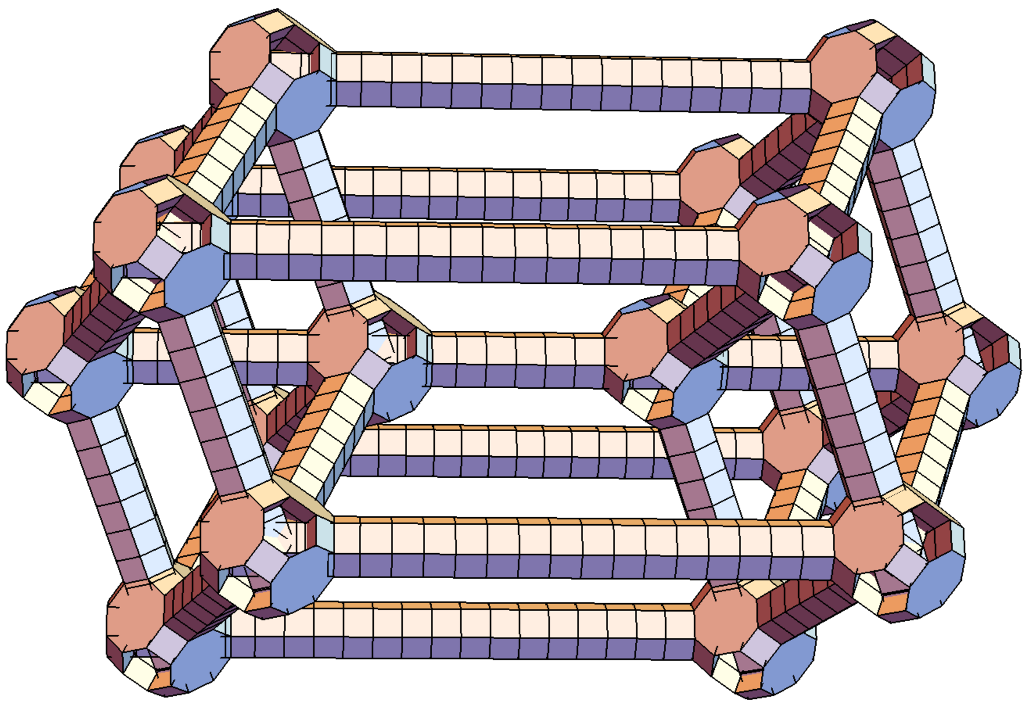

Figure 2.8: A $(4, 8)$-RPS of genus 49

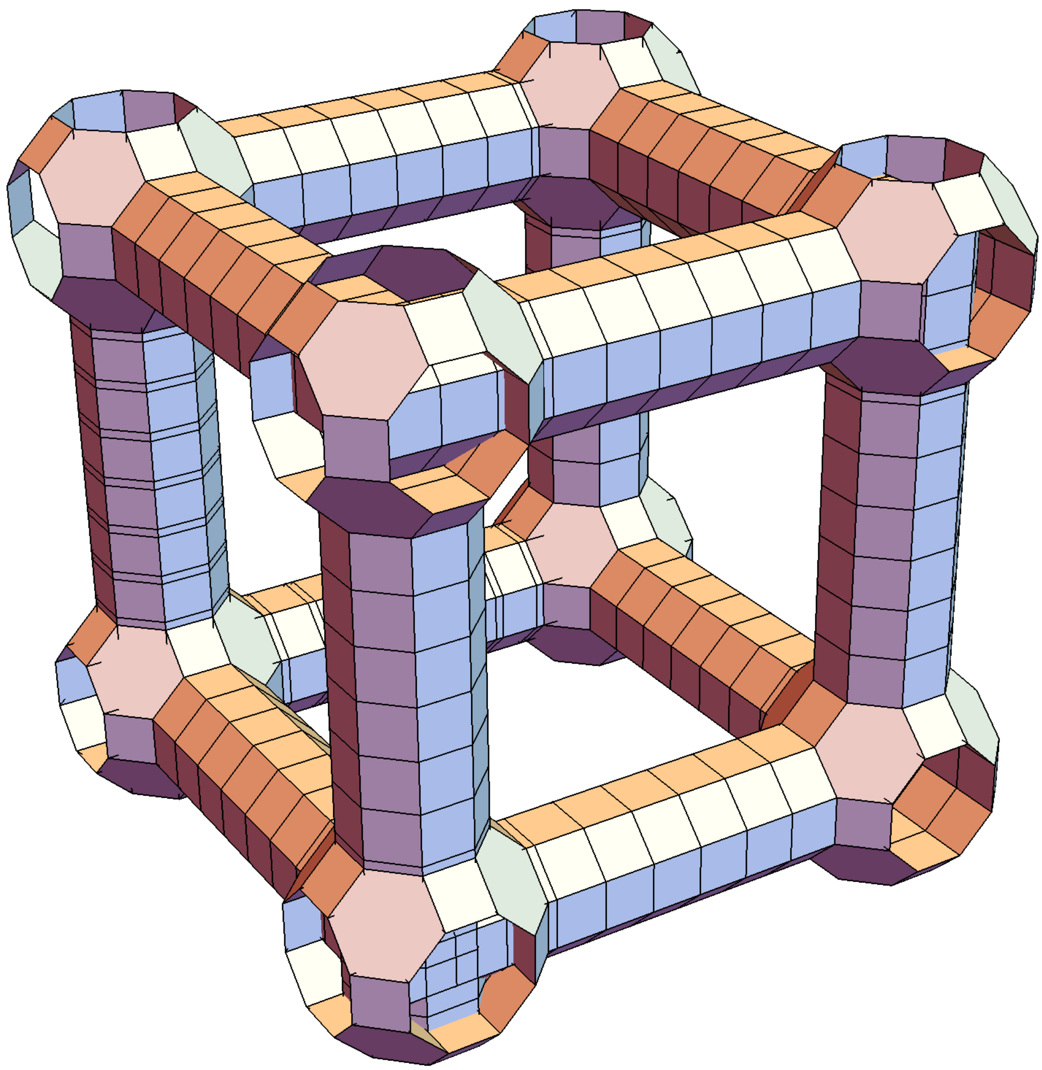

Figure 2.9: A $(4, 6)$-RPS of genus 17

Chapter Three

A Family of Minimal and Renormalizable Rectangle Exchange Maps

This chapter was written jointly with Richard Kenyon and Ren Yi.

3.1 Introduction

A ***smooth Jordan domain*** X is a non-empty closed bounded set in $\mathbb{R}^2$ whose boundary is a piecewise smooth Jordan curve. We construct a dynamical system on X which is a piecewise translation known as a ***domain exchange map (DEM)***. The dynamical system is a 2-dimensional generalization of an interval exchange transformation.

Definition 3.1.1. Let X be a Jordan domain partitioned into smaller Jordan domains, with disjoint interiors, in two different ways

$$X = \bigcup_{k=0}^{N} A_k = \bigcup_{k=0}^{N} B_k$$

such that for each k, A_k and B_k are translation equivalent, i.e., there exists $v_k \in \mathbb{R}^2$ such that $A_k = B_k + v_k$. A ***domain exchange map*** is the piecewise translation on X defined for $x \in \mathring{A}_k$ by

$$T(x) = x + v_k.$$

The map is not defined for points $x \in \bigcup_{k=0}^{N} \partial A_k$.

In section 2 we explain how to use ***cut-and-project sets*** to define a DEM on any smooth Jordan domain X.

Definition 3.1.2. Let L be a full-rank lattice in $\mathbb{R}^3$ and X a domain in the xy-plane in $\mathbb{R}^3$. Define

$$P = \{\pi_z(p) \ : \ p \in L \text{ and } \pi_{xy}(p) \in X\}.$$

where π_z is the projection onto the z axis and π_{xy} is the projection onto the xy-plane. The point set P is a ***cut-and-project set*** if the following two properties are satisfied:

1. $\pi_z|_L$ is injective
2. $\pi_{xy}(L)$ is dense in $\mathbb{R}^2$.

In this setting we define $\Lambda(X, L)$ to be the set of lattice points

$$\Lambda(X, L) = \{\mathbf{x} \in L \ : \ \pi_{xy}(\mathbf{x}) \in X\}.$$

The projection $\pi_{xy}(\Lambda(X, L))$ is dense in X.

The DEM is defined by projecting a dynamical system on $\Lambda(X, L)$ onto X. Figure

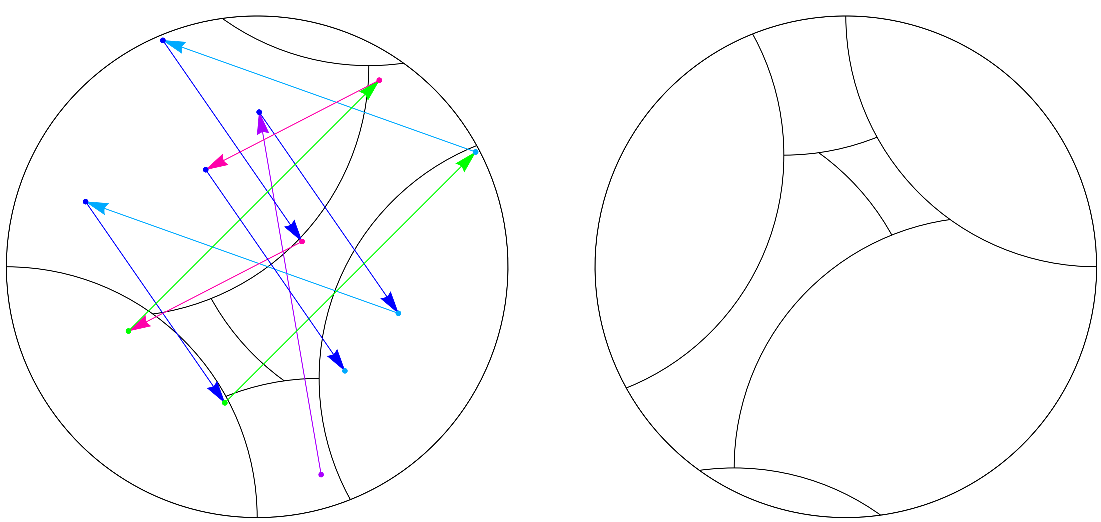

Figure 3.1: Domain exchange map on a disk and the forward orbit of a point

3.1 shows a DEM, in which X is the unit disk, constructed in this manner. The boundary of each tile is an arc of a circle with unit radius. For almost every point x the forwards and backwards orbits of x under the DEM are well-defined. We characterize the orbits of DEMs constructed using cut-and-project sets:

Theorem 3.1.3. *Every DEM associated to a cut-and-project set is* **minimal***, i.e., the orbit of every point, whose orbit is well-defined, is dense.*

The DEMs produced by our construction are amenable to analysis when the lattice and domain have a special algebraic structure. A ***Pisot-Vijayaraghavan number***, more simply called a ***PV number***, is a real algebraic integer with modulus larger than 1 whose Galois conjugates have modulus strictly less than one.

Let $\lambda = \lambda_3$ be a PV number whose Galois conjugates λ_1, λ_2 are real. Then $\mathbb{Q}[\lambda]$ has three embeddings into $\mathbb{R}$, and we can identify $\mathbb{R}^3$ with the product of these three embeddings, with the x-, y- and z-coordinates corresponding to embeddings sending λ to $\lambda_1, \lambda_2, \lambda_3$ respectively. Then $\mathbb{Z}[\lambda]$ is a lattice in $\mathbb{R}^3$ of the above type, and

$$\pi_{xy}(a + b\lambda + c\lambda^2) = (a + b\lambda_1 + c\lambda_1^2, a + b\lambda_2 + c\lambda_2^2).$$

Multiplication by λ is an integer transformation of $\mathbb{Z}[\lambda]$. We call this the ***Galois embedding*** of the lattice $\mathbb{Z}[\lambda]$. Note that $\mathbb{Z}[\lambda]$ can be identified with $\mathbb{Z}^3$ under the map

$$(a, b, c) \mapsto a + b\lambda + c\lambda^2.$$

When X is a smooth Jordan domain and L is the Galois embedding of a PV number whose Galois conjugates are real then the point set $\Lambda(X, L)$ satisfies the conditions of being a cut-and-project set. We call a DEM associated to a Galois lattice a ***PV DEM***. We give a detailed analysis of PV DEMs in the case when the lattice is a Galois lattice and X is the unit square $[0,1]^2$. Since the tiles inherit their shape from the boundary of X, under these assumptions the tiles are rectilinear polygons. We call these DEMs ***rectangle exchange maps (REMs)***.

One way to construct a PV DEM is to find a ***Pisot matrix*** whose eigenvalues are all real. A ***Pisot matrix*** is an integer matrix with one eigenvalue greater than 1 in modulus and the remaining eigenvalues strictly less than 1 in modulus (in particular, its leading eigenvalue is a PV number). Define $\mathcal{S}$ to be the following set of matrices:

$$\mathcal{S} = \left\{ M_n = \begin{bmatrix} 0 & 1 & 0 \\ 0 & 0 & 1 \\ 1 & -n & n+1 \end{bmatrix} : n \geq 6 \right\}$$

We will show in Section 3.5.2 that every matrix $M_n \in \mathcal{S}$ is a Pisot matrix. For $M_n \in \mathcal{S}$, let λ be the leading eigenvalue of M_n. The Galois embedding of $\mathbb{Z}[\lambda]$ gives rise to a PV REM (Section 3.2.1). Let T_M denote the PV REM associated to the Galois embedding of the eigenvalues of M.

We extend the family $\{T_{M_n} : \ M_n \in \mathcal{S}\}$ of PV REMs to a larger family of REMs via the monoid of matrices $\mathcal{M}$ consisting of nonempty products of matrices in $\mathcal{S}$. Lemma 3.1.4 establishes that $\mathcal{M}$ is in fact a monoid of Pisot matrices.

Lemma 3.1.4. *If $W \in \mathcal{M}$ then its eigenvalues λ_1, λ_2 and λ_3 are real and satisfy the inequalities*

$$0 < \lambda_1 < \lambda_2 < 1 < \lambda_3.$$

Admissible REMs are defined by a subset of **admissible matrices** $\mathcal{M}_A \subset \mathcal{M}$ for which the REM T_W associated to the matrix $W \in \mathcal{M}_A$ has the same combinatorics as the REM T_{M_n} (see definition 3.5.1). We say that two REMs, $T, T' : X \to X$

with associated partitions $\mathcal{A} = \{A_i\}_{i=1}^{N}$, $\mathcal{A}' = \{A'_i\}_{i=1}^{N'}$ respectively, have the ***same combinatorics*** if

1. The cardinalities of the partitions $\mathcal{A}, \mathcal{A}'$ are equal.
2. For each i, the polygons $A_i \in \mathcal{A}$ and $A'_i \in \mathcal{A}'$ have the same number of edges and edge directions, that is, they are the same up to changing edge lengths.
3. Two elements A_i and A_j in $\mathcal{A}$ meet along a common edge if and only if A'_i and A'_j share an edge in the corresponding position.

See Figure 3.2 for an example of two REMs with the same combinatorics. The admissibility condition on $\mathcal{M}_A \subset \mathcal{M}$ is a set of linear equations in the eigenvectors of M (see definition 3.5.1).

Let $W \in \mathcal{M}_A$ be written $W = M_{n_L} \dots M_{n_2} M_{n_1}$. Define $W_k = M_{n_k} \dots M_{n_2} M_{n_1}$ for $1 \leq k \leq L$. When each REM T_{W_k} has the same combinatorics as T_W for every $k = 1, \dots, L$ we call T_W a ***multistage REM*** (see Definition 3.5.2). We use $\mathcal{M}_R \subset \mathcal{M}_A$ to denote the subset of admissible matrices which produce multi-stage REMs.

For a multistage REM we study the ***first return map*** to one of the tiles in the partition and prove that it is affinely conjugate to the original map. This is known as a ***renormalization scheme***. Renormalization schemes are an essential tool in the study of long term behavior of dynamical systems.

Definition 3.1.5. Let $T : X \to X$ be a map and $Y \subset X$. The ***first return map*** $\hat{T}|_Y$ maps a point $p \in Y$ to the first point in the forward orbit of p lying in Y, i.e.

$$\widehat{T}|_Y(p) = T^m(p) \quad \text{where } m = \min\{k \in \mathbb{Z}_+ : T^k(p) \in Y\}.$$

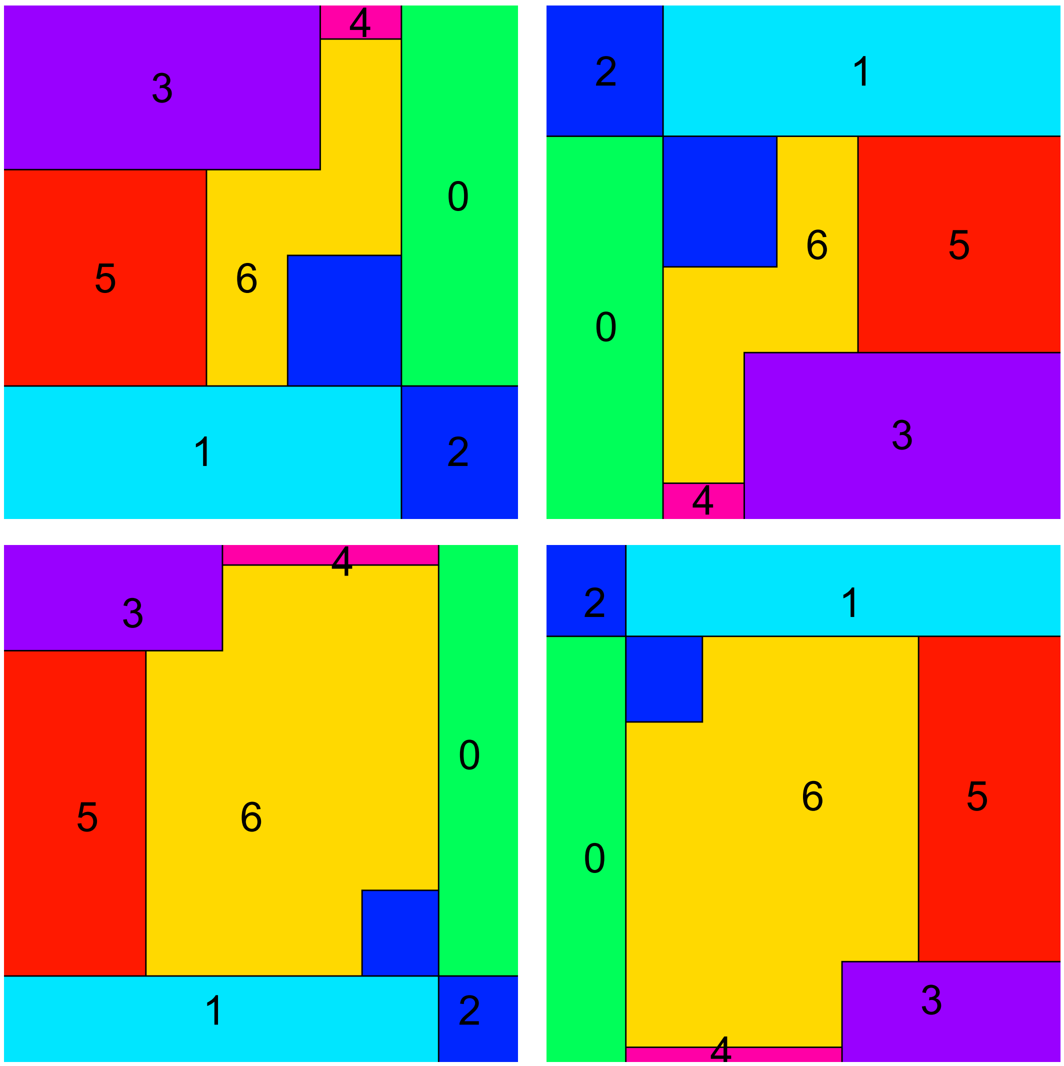

Figure 3.2: The REM described by the top panels has the same combinatorics as the REM described by the lower two panels.

The notation $T|_Y$ means the dynamical system T restricted to Y.

When X is a finite measure space and T a measure-preserving transformation, the Poincaré Recurrence Theorem [Poi17] ensures that the first return map is well-defined for almost every point in the domain.

Definition 3.1.6. A dynamical system $T_1 : X_1 \to X_1$ has a ***renormalization scheme*** if there exists a proper subset $X_2 \subset X_1$, a dynamical system $T_2 : X_2 \to X_2$, and a homeomorphism $\phi : X_1 \to X_2$ such that

$$\widehat{T_1}|_{Y_1} = \phi^{-1} \circ T_2 \circ \phi.$$

A dynamical system is ***renormalizable*** or ***self-induced*** if $T_2 = T_1$.

3.1.1 Main Results

The main focus of our paper is the development of a renormalization scheme for the multistage REM T_M, defined in Section 3.2.1 below, for every $M \in \mathcal{M}_A$.

Theorem 3.1.7. *Let $M \in \mathcal{S}$ be a matrix and T_M the PV REM associated to the Galois lattice L_λ where λ is the leading eigenvalue of M. Label the eigenvalues of M by λ_1, λ_2 and λ_3 in increasing order. Let $Y \subset X$ be the tile in the partition corresponding to the rectangle $[1-\lambda_1, 1] \times [1-\lambda_2, 1]$. The REM T_λ is renormalizable, i.e.,*

$$\widehat{T_M}|_Y = \phi^{-1} \circ T_M \circ \phi$$

where $\phi : X \to Y$ is the affine map

$$\phi : (x, y) \mapsto \left(\frac{x + \lambda_1 - 1}{\lambda_1}, \frac{y + \lambda_2 - 1}{\lambda_2} \right).$$

We next prove that multistage REMs are minimal and have a renormalization scheme with multiple steps.

Theorem 3.1.8. *Multistage REMs are minimal.*

Theorem 3.1.9. *Let $W = M_{n_L} \cdots M_{n_2} M_{n_1} \in \mathcal{M}_R$ and define $W_k = M_{n_k} \cdots M_{n_2} M_{n_1}$ for $1 \leq k \leq L$. The associated multistage REM is renormalizable, i.e., for each k there exists $Y_k \subset X$ and an affine map $\phi_k : Y_k \to X$ such that*

$$\widehat{T}_{W_{k+1}}|_{Y_{k+1}} = \phi_k^{-1} \circ T_{W_k} \circ \phi_k.$$

Each affine map has the form

$$\phi_k : (x, y) \mapsto \left(\frac{x + x_k - 1}{x_k}, \frac{y + y_k - 1}{y_k} \right)$$

where x_k and y_k are the dimensions of the tile in the partition corresponding to the rectangle $[1 - x_k, 1] \times [1 - y_k, 1]$.

We conjecture that the closure of the set of renormalizable multistage REMs is topologically a Cantor set.

3.1.2 Background

A DEM is an example of a discrete dynamical system which is a piecewise affine isometry. These systems have applications to the study of substitutive dynamical systems, outer billiards, and digital filters. Originally J. Moser proposed studying outer billiards as a toy model for celestial dynamics. In much the same manner, DEMs provide a toy problem for the study of Hamiltonian dynamical systems with nonzero field. See [Goe03] for a nice survey including many open questions related to 2-dimensional piecewise isometries.

Although the maps we study are locally translations, the sharp discontinuities produce a dynamical system with extremely rich long-term behavior. This complexity can even be seen in the 1-dimensional case of interval exchange transformations (IETs). We wish to classify points in the domain by the long-term behavior of their orbits. The domain of an affine isometry is subdivided into tiles on which the map is locally constant. Each point in a piecewise isometry can be classified by the sequence of tiles visited by the forward orbit of a point. The most basic question is to give an encoding for each point in terms of this sequence. While this problem is particularly challenging, there has been some success in classifying points into sets of points whose orbits are eventually periodic and those whose orbits are not periodic. Such a classification has been carried out successfully in a few particular cases, [AKT01], [Goe03], [LKV04], [AH13], [Hoo13] and [Sch14].

In each case the authors used the principle of *renormalization* to study the dynamical system. Renormalization provides a way to understand the long-term behavior of a discrete dynamical system. Unfortunately for piecewise isometries in dimension 2 or higher there are no general methods for developing a renormalization scheme for a dynamical system. In the 1-dimensional case of the IET, G. Rauzy developed a general technique known as *Rauzy induction* for finding a renormalization scheme for an IET [Rau79]. His method does not generalize to higher dimensions.

REMs were first studied by Haller who gave a minimality condition [Hal81]. Unfortunately this condition is extremely difficult to check in practice. Finding a recurrent REM was included as question #19 in a list of open problems in combinatorics at the *Visions in Mathematics* conference [Gow00]. Hooper developed the first renormalization scheme for a family of REMs parametrized by the square [Hoo13]. In [Sch14] Schwartz used multigraphs to construct polytope exchange transformations (PETs) in every dimension. He developed a renormalization scheme for the simplest case in which the corresponding multigraphs are bigons. The renormalization map is a piecewise Möbius map.

The topological entropy of a dynamical system gives a numerical measure of its complexity. For a dynamical system defined on a compact topological space the topological entropy is an upper bound for the exponential growth rate of points whose orbits which remain a distance ϵ apart as $\epsilon \to 0$ [Thu14]. The topological entropy gives an upper bound on the metric entropy of the dynamical system. In [Buz01] J. Buzzi proved that the topological entropy is zero for piecewise isometries defined on a finite union of polytopes in $\mathbb{R}^d$ which are actual isometries on the interior of each polytope. The REMs we study in this paper are examples of such systems and as a consequence have zero topological entropy. However when the domain is not a union of polytopes the techniques in [Buz01] must be modified. We expect that our technique for constructing domain exchange maps produces dynamical systems with zero topological entropy but have not proved this.

Throughout this paper we make extensive use of the connection between non-negative integer matrices and *Perron numbers*. A Perron number is a positive real algebraic integer λ which is strictly larger than the absolute value of any of its Galois conjugates. In [Lin84] it was proven that for every Perron number λ there exists a non-negative integer matrix M which is *irreducible* (i.e. M^k is positive for some power k) and has λ as a leading eigenvalue.

In this paper we use algebraic properties of a subset of Perron numbers known as *Pisot-Vijayaraghavan numbers* or *PV numbers* to find REMs which are renormalizable. A PV number is a positive real algebraic integer whose Galois conjugates lie in the interior of the unit disk. We use cut-and-project sets associated to PV numbers to produce DEMs. Cut-and-project sets were introduced in [Mey95] and further studied in [Lag96].

Our proof of the renormalization schemes in this paper rely on algebraic properties of PV numbers. In two recent works monoids of matrices were discovered whose leading eigenvalues are PV numbers ([AI01] and [AD15]). The authors called these matrices *Pisot matrices*. We find a new monoid of Pisot matrices with an infinite generating set.

The techniques we use in this paper are influenced by [Ken92] and [**?**]. These works focused on self-similar tilings of the plane whose expansion constant is a complex Perron number. Unlike the tiles in our DEMs, the tiles in [**?**] have a fractal boundary. Our construction of DEMs also share similarities with the Rauzy fractal [Rau82].

3.2 Constructing minimal DEMs with cut-and-project sets

Let X be a smooth Jordan domain in $\mathbb{R}^2$ and L a lattice in $\mathbb{R}^3$ such that $\Lambda = \Lambda(X, L)$ is a cut-and-project set: $\Lambda = \{p \in L | \ \pi_{xy}(p) \in X\}$. We construct a DEM on X by projecting a dynamical system on Λ onto the window X. Projection onto the z-coordinate gives an ordering of the points in Λ. Order the points in Λ by increasing z-coordinate: $\Lambda = \{\dots, \mathbf{x}_{-1}, \mathbf{x}_0, \mathbf{x}_1, \dots\}$. Let $\widetilde{T} : \Lambda \to \Lambda$ be the dynamical system defined by

$$\widetilde{T}(\mathbf{x}_i) = \mathbf{x}_{i+1}.$$

Consider the set of steps in the lattice walk

$$\mathcal{E} = \{\widetilde{T}(\mathbf{x}) - \mathbf{x} : \mathbf{x} \in \Lambda\}.$$

Since L is a lattice, $\mathcal{E}$ is a finite set. Suppose there are $N + 1$ vectors in $\mathcal{E}$ and label them by $\mathcal{E} = \{\eta_0, \eta_1, \dots, \eta_N\}$. Projection onto the z-coordinate induces an order on $\mathcal{E}$. We assume that $\mathcal{E}$ is indexed so that

$$\pi_z(\eta_0) < \pi_z(\eta_1) < \cdots < \pi_z(\eta_N).$$

Define $V = \{v_i = \pi_{xy}(\eta) \ : \ \eta \in \mathcal{E}\}$. The DEM $T : X \to X$ is defined by

$$T(p) = p + v_i \text{ with } i = \min\{0, \dots, N \ : \ v_j \in V \text{ and } p + v_j \in X\}$$

for $p \in X$. Note that T is well-defined and bijective on X. The map T is a piecewise translation on X.

The DEM induces a partition of X into subdomains $\{A_k\}_{i=0}^{N}$ for which $T(p) = p + v_i$ for all $p \in A_k$. Likewise T^{-1} induces a partition $\{B_k\}_{i=0}^{n}$ for which $T^{-1}(p) = p - v_i$ for all $p \in B_k$. Note that

$$X = \bigcup_{k=0}^{N} A_k = \bigcup_{k=0}^{N} B_k$$

and $A_k = B_k + v_i$, verifying that T is a DEM. The subdomains are not necessarily connected. However, each connected component of a subdomain is bounded by a smooth Jordan curve as long as X is a smooth Jordan domain.

In Figure 3.3 we show both the lattice walk $\widetilde{T}$ and the resulting DEM T.

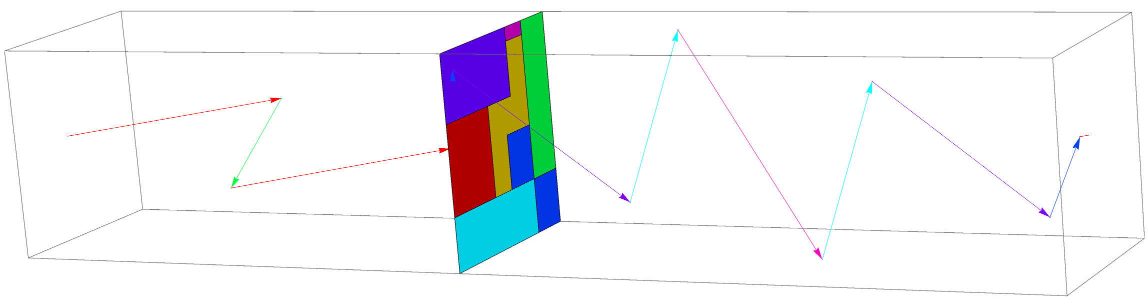

Figure 3.3: Lattice walk in $\Lambda(X, L)$ and the partition associated to the DEM on X. Each colored region in the partition is translated by the projection of the step in the lattice walk, with the same color, onto the xy-plane.

For a dynamical system $T : X \to X$, the *orbit* of p is the set $O(p) = \{T^j(p) \mid j \in \mathbb{Z}\}$. We also define $O^{k+}(p) = \{T^j(p) | \ j \in \mathbb{Z}, 0 \leq j \leq k\}$ the k-th *forward orbit* of p, and $O^+(p) = \{T^j(p) \mid j \geq 0\}$ the forward orbit.

Proof of Theorem 3.1.3. Let $p, q \in X$ with $p \neq q$. We show that there exists a subsequence of points in $O^+(p)$ that converge to q. By assumption $\pi_{xy}(\Lambda(X, L))$ is dense in X. Define a subsequence $\{\mathbf{x}_n\}_{n \in \mathbb{N}}$ of the forward orbit of $\mathbf{x}_0$ under $\widetilde{T}$ with

$\mathbf{x}_0 \in \Lambda(X, L)$ such that

$$\lim_{n\to\infty} \pi_{xy}(\mathbf{x}_n) = p.$$

When a point p' is close to p their respective orbits will stay close for some time. More precisely, we define

$$\partial_k = \partial A_k \text{ and } \partial = \bigcup_{k=0}^{n} A_k.$$

and the forward orbits of the points in the boundaries

$$D^t = \bigcup_{r\in\partial} O^{t+}(r).$$

The complement $X \setminus D^t$ can be written as a finite union of m connected open sets

$$X \setminus D^t = \bigcup_{k=0}^{m} C_k^t.$$

The set D^5 is illustrated in figure 3.4. All points in C_k^t have the same sequence of translation vectors for t steps. If two points $p, p' \in C_k^t$ then

$$T^n(p) - T^{n-1}(p) = T^n(p') - T^{n-1}(p') \quad \forall n = 0, 1, 2 \ldots, t-1. \tag{3.2.1}$$

Since $\pi_{xy}(O^+(\mathbf{x}_n))$ is dense in X there exists a sequence

$$\mathbf{x}_n, \widetilde{T}^{m_1}(\mathbf{x}_n), \widetilde{T}^{m_2}(\mathbf{x}_n), \ldots$$

such that

$$\lim_{m_i\to\infty} \pi_{xy} \circ \widetilde{T}^{m_i}(\mathbf{x}_n) = q.$$

For $p \in X$, there exists $N \in \mathbb{N}$ such that for all $n \geq N$, we have $\|\pi_{xy}(\mathbf{x}_n) - p\| < \epsilon$ for every $\epsilon > 0$. Moreover, for each $\mathbf{x}_n$ with $n > N$, there exists a large integer $M > 0$ such that $\|\pi_{xy} \circ \widetilde{T}^{m_i}(\mathbf{x}_n) - q\| < \epsilon$ for all $m_i > M$. Thus there must exist an $\mathbf{x}_n \in \mathbf{x}$ with $n > N$ such that $\mathbf{x}_n \in C_k^{m_i}(p)$ for some $m_i > M$. Then we have

$$\begin{aligned}
\|T^{m_i}(p) - q\| &\leq \|T^{m_i}(p) - \pi_{xy} \circ \widetilde{T}^{m_i}(\mathbf{x}_n)\| + \|\pi_{xy} \circ \widetilde{T}^{m_i}(\mathbf{x}_n) - q\| \\
&\leq \|T^{m_i}(p) - \pi_{xy} \circ \widetilde{T}^{m_i}(\mathbf{x}_n)\| + \epsilon \\
&= \|(p + \sum_{j=1}^{m_i}(T^j(p) - T^{j-1}(p)) \\
&- \left(\pi_{xy}(\mathbf{x}_n) + \sum_{j=1}^{m_i}(\pi_{xy} \circ \tilde{T}^j(\mathbf{x}_n) - \pi_{xy} \circ \tilde{T}^{j-1}(\mathbf{x}_n))\right) \| + \epsilon \\
&= \|\pi_{xy}(x_n) - p\| + \epsilon \\
&\leq 2\epsilon.
\end{aligned}$$

Between lines 3 and 4 we applied the property in equation 3.2.1.

□

3.2.1 PV REMs

We explain here the details of the REM construction when $X = [0,1] \times [0,1]$ and L is the Galois embedding of $\mathbb{Z}[\lambda]$ where λ is a certain family of PV numbers. Define for each $n \geq 6$ a polynomial

$$q_n(x) = x^3 - (n+1)x^2 + nx - 1.$$

Lemma 3.2.2. *The polynomial q_n has three real roots, λ_1, λ_2 and λ_3, which satisfy*

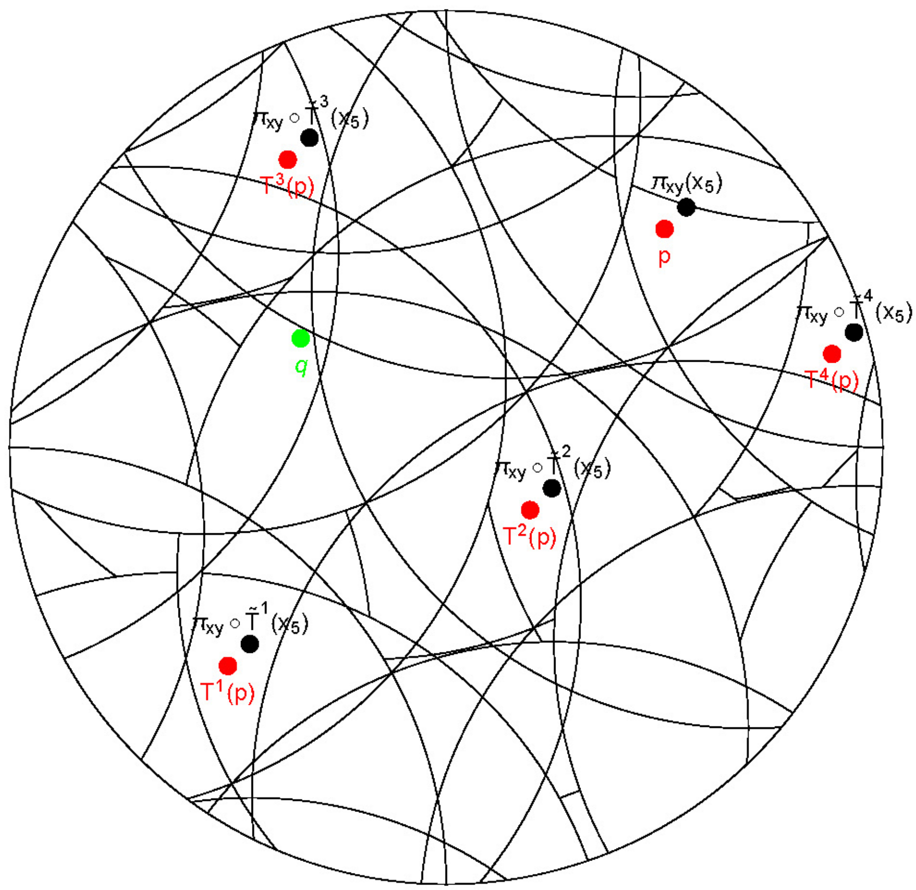

Figure 3.4: Forward Orbit of Boundaries after 5 steps

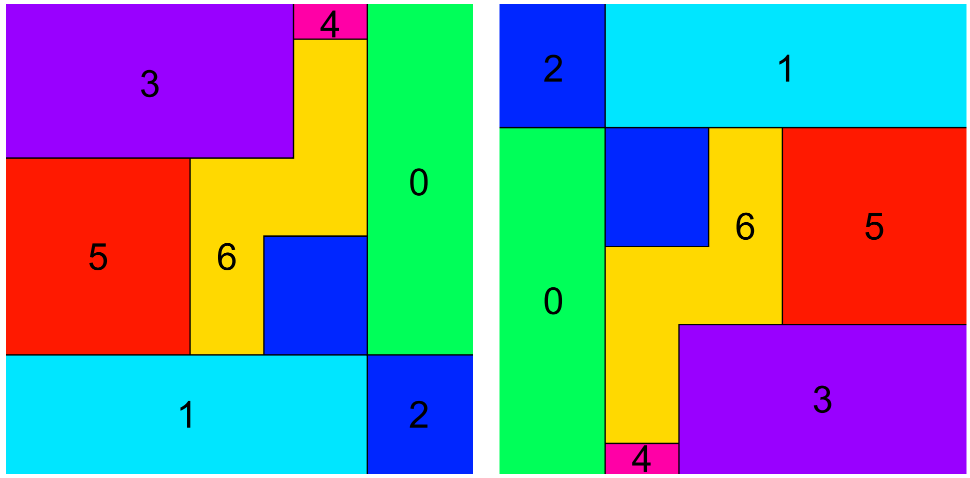

Figure 3.5: The two partitions associated to the REM T_{M_6}

the inequalities $0 < \lambda_1 < \lambda_2 < 1 < \lambda_3$.

Proof. The discriminant of q_n is

$$D(n) = n^4 - 6n^3 + 7n^2 + 6n - 31.$$

It has two real roots $n = 1/2(3 + \sqrt{13 + 16\sqrt{2}})$ and $1/2(3 - \sqrt{13 + 16\sqrt{2}})$. Thus for $n \geq 6$ the discriminant is strictly positive and we find q_n has three distinct real roots.

Since

$$\lambda_1 \lambda_2 \lambda_3 = 1 \quad \text{and} \quad \lambda_1 + \lambda_2 + \lambda_3 = n + 1$$

it follows that $\lambda_3 > 1$ and $\lambda_1 < 1$. However, $\lambda_3 < n + 1$ and so $\lambda_1 + \lambda_2 > 0$. This implies $\lambda_2 > 0$. The product of the three roots is one which implies that $\lambda_1 > 0$.

It remains to show that $\lambda_2 < 1$. Evaluating q_n and its derivative at 0 and 1 gives

$$q_n(0) = -1, \quad q_n'(0) = n, \quad q_n(1) = -1 \quad \text{and} \quad q_n'(1) = 1 - n.$$

We find that $q_n(x)$ has two roots between 0 and 1 and conclude that $0 < \lambda_1 < \lambda_2 < 1$. □

Note that q_n is the characteristic polynomial of the matrix

$$M_n = \begin{bmatrix} 0 & 1 & 0 \\ 0 & 0 & 1 \\ 1 & -n & n+1 \end{bmatrix}.$$

Let $T_{M_n} : X \to X$ be the PV REM associated to the Galois embedding of the roots of q_n. The two partitions associated to the REM T_{M_6} are shown in figure 3.5. When L has this form there are seven possible steps in the lattice walk $\mathcal{E}_n$. It is convenient to identify points in L by their representation in $\mathbb{Z}^3$, i.e., if $(a, b, c) \in \mathbb{Z}^3$ then

$$\pi_{xy}(a, b, c) = (a + b\lambda_1 + c\lambda_1^2, a + b\lambda_2 + c\lambda_2^2) \text{ and } \pi_z(a, b, c) = a + b\lambda_3 + c\lambda_3^2.$$

Using this representation the vectors in $\mathcal{E}_n$ are

$$\begin{aligned} &\eta_0 = (-1, 1, 0), \quad \eta_1 = (0, 1, 0), \quad \eta_2 = \eta_0 + \eta_1 = (-1, 2, 0) \\ &\eta_3 = (1, -3, 1), \quad \eta_4 = \eta_0 + \eta_3 = (0, -2, 1), \\ &\eta_5 = \eta_1 + \eta_3 = (1, -2, 1), \quad \text{and} \quad \eta_6 = \eta_0 + \eta_1 + \eta_3 = (0, -1, 1). \end{aligned} \tag{3.2.3}$$

Theorem 3.4.1 establishes that the steps in the lattice walk are independent of n and as a consequence we set $\mathcal{E}_n = \mathcal{E}$.

The partition associated to the REM T_{M_n} is constructed as follows. A visual depiction of the construction is shown in figure 3.6. Define the projections onto the

xy-plane of the translation vectors in $\mathcal{E}$ by

$$V_n = \{v_i = \pi_{xy}(\eta_i), \text{ for } i = 0, 1, \dots 6\}.$$

Note that V_n depends on n since the projection π_{xy} is a function of the roots of q_n.

For a vector $v \in \mathbb{R}^2$ let f_v be the translation $f_v(x) = x + v$ for $x \in \mathbb{R}^2$. We define the partition $\mathcal{A} = \{A_k\}_{k=0}^{N}$ of X associated to T_{M_n} inductively as follows:

$$A_0 = f_{v_0}^{-1}(X) \cap X \quad \text{and} \quad A_k = (f_{v_k}^{-1}(X) \cap X) \setminus \bigcup_{j=0}^{k-1} A_j \quad \text{for} \quad k > 0. \tag{3.2.4}$$

For a point x in the interior of a tile in the partition A_k the dynamical system is defined by

$$T_{M_n}|_{A_k^\circ}(x) = f_{v_k}(x) = x + v_k.$$

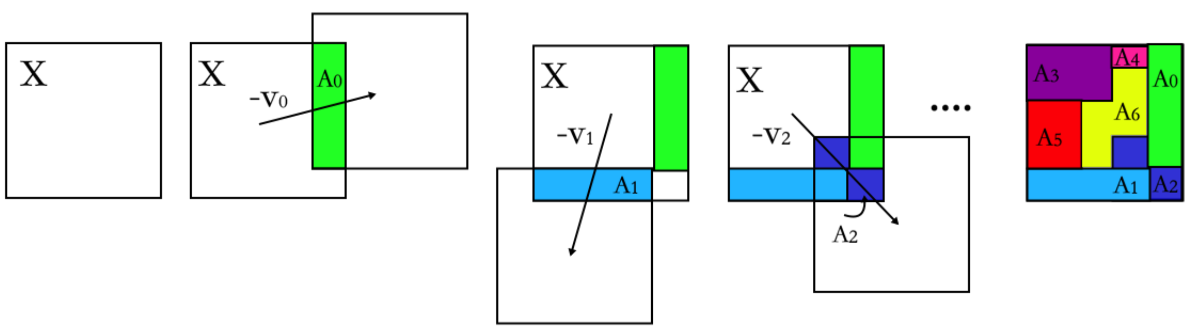

Figure 3.6: The steps in the construction of the partition $\mathcal{A}$ associated to the REM T_{M_n} and the resulting partition.

Each tile in the partition $\mathcal{A}$ is a rectilinear polygon (refer to the example in Figure 3.5) and can be written as a disjoint union of rectangles. We use the standard notation for a rectangle

$$[a, b] \times [c, d] = \{(x, y) \in \mathbb{R}^2 : a \leq x \leq b \text{ and } c \leq y \leq d\}.$$

Recall that λ_1 and λ_2 are roots of the polynomial $q_n(x)$ with $0 < \lambda_1 < \lambda_2 < 1$. The tiles are as follows

$$
\begin{aligned}
A_0 &= [1-\lambda_1, 1] \times [1-\lambda_2, 1] \\
A_1 &= [0, 1-\lambda_1] \times [0, 1-\lambda_2] \\
A_2 &= ([1-2\lambda_1, 1-\lambda_1] \times [1-\lambda_2, 2-2\lambda_2]) \cup ([1-\lambda_1, 1] \times [0, 1-\lambda_2]) \\
A_3 &= [0, 3\lambda_1 - \lambda_1^2] \times [-1+3\lambda_2 - \lambda_2^2, 1] \\
A_4 &= [3\lambda_1 - \lambda_1^2, 1-\lambda_1] \times [2\lambda_2 - \lambda_2^2, 1] \\
A_5 &= [0, 2\lambda_1 - \lambda_1^2] \times [1-\lambda_2, -1+3\lambda_2 - \lambda_2^2] \\
A_6 &= \big([1-2\lambda_1, 3\lambda_1 - \lambda_1^2] \times [2-2\lambda_2, -1+3\lambda_2 - \lambda_2^2]\big) \\
&\quad \cup \big([2\lambda_1 - \lambda_1^2, 1-2\lambda_1] \times [1-\lambda_2, -1+3\lambda_2 - \lambda_2^2]\big) \\
&\quad \cup \big([3\lambda_1 - \lambda_1^2, 1-\lambda_1] \times [2-2\lambda_2, 2\lambda_2 - \lambda_2^2]\big).
\end{aligned}
\tag{3.2.5}
$$

3.3 Analysis of the PV REM T_{M_6} and its Renormalization

Before analyzing the general case, we give a detailed description of the PV REM T_{M_6} in which the Galois lattice L_λ is determined by the polynomial $q_6(x) = x^3 - 7x^2 + 6x - 1$.

Let $V = \{v_i\}_{i=0}^6$ be the set of translation vectors of the REM T_{M_6} where $v_i = \pi_{xy}(\eta_i)$ for $\eta_i \in \mathcal{E}$ listed in Lemma 3.3.1. We obtain the REM $T_{M_6} : X \to X$ defined on the partition $\{A_i\}_{i=0}^6$ as shown in Figure 3.5.

Lemma 3.3.1. *Let $\mathcal{E} = \{\eta_i\}_0^6$ where the η_i are defined in (3.2.3). The set of translation vectors of T_{M_n} are $\{\pi_{xy}(\eta_i)\}_{i=1}^6$ for $n = 6$.*

Proof. The characteristic polynomial of the matrix

$$M_6 = \begin{bmatrix} 0 & 1 & 0 \\ 0 & 0 & 1 \\ 1 & -6 & 7 \end{bmatrix}.$$

is $q_6(x) = x^3 - 7x^2 + 6x - 1$. By Lemma 3.2.2, the polynomial $q_n(x)$ has three roots λ_1, λ_2 and λ_3 with $0 < \lambda_1 < \lambda_2 < 1 < \lambda_3$. The eigenvector ξ_i of M_6 associated to λ_i is $(1, \lambda_i, \lambda_i^2)$ for $i = 1, 2$ and 3.

By direct computation, we find that the seven vectors $\eta_0, \eta_1, \ldots, \eta_6$ are the seven solutions for vectors in $\mathbb{Z}^3$ of the following inequalities

$$-1 < v \cdot \xi_1 < 1$$
$$-1 < v \cdot \xi_2 < 1$$
$$0 < v \cdot \xi_3 < 31.$$

The first two equations ensure that the projection of each step of the lattice walk in $\mathbb{Z}^3$ is a translation vector in the REM. The third equation ensures that these are the first seven vectors in $\mathcal{E}$ which define a partition of the unit square. The set of real solutions to the above inequalities is a convex polytope in $\mathbb{R}^3$ which contains exactly seven integer points. Each solution corresponds to a permissible step in the lattice walk on Λ_X. □

Theorem 3.3.2. *Let $Y = A_0$. The first return map $\hat{T}_{M_6}|_Y$ to the set Y is conjugate to T_{M_6} by the affine map $\psi : Y \to X$ given by*

$$\phi_n(x, y) = \left(\frac{x + \lambda_1 - 1}{\lambda_1}, \frac{y + \lambda_2 - 1}{\lambda_2} \right).$$

where $0 < \lambda_1 < \lambda_2 < 1$ *are the smaller eigenvalues of the matrix* M_6*.*

Theorem 3.3.2 is a particular case of Theorem 3.1.7 whose proof is given in Section 3.4.2. In the Appendix we give a computational proof of Theorem 3.3.2 and a symbolic encoding of the partition of Y induced by the first return map $\hat{T}_{M_6}|_Y$.

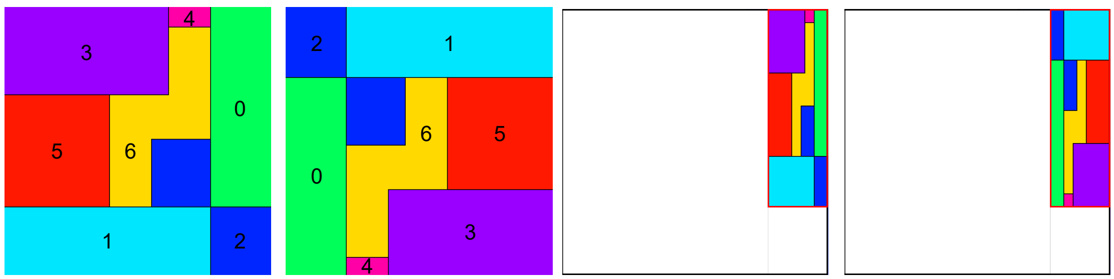

Figure 3.7: The REM T_{M_6} and the partition induced by the first return map $\hat{T}_{M_6}|_Y$ to $Y = A_0$.

3.4 The renormalization scheme for PV REMs

3.4.1 Analyzing the lattice walk for $M_n \in \S$

Let T_{M_n} be the PV REM constructed from a matrix $M_n \in \mathcal{S}$ using the method outlined in section 3.2.1. Let $L = L_\lambda$ be the associated Galois lattice. In this section, we analyze the dynamical system $\widetilde{T}$ on L and prove

Theorem 3.4.1. *Lemma 3.3.1 holds for all* $n \geq 6$*.*

There are a number of steps in the proof. The first step is proving a more refined version of Lemma 3.2.2.

Lemma 3.4.2. *Label the roots of* q_n $\lambda_1^n, \lambda_2^n, \lambda_3^n$ *with* $0 < \lambda_1^n < \lambda_2^n < 1 < \lambda_3^n$*. Then* λ_2^n *and* λ_3^n *are monotonically increasing functions of* n *while* λ_1^n *is monotonically* *decreasing as a function of n. Moreover we have the following inequalities*

$$\begin{gathered} n < \lambda_3^n < n+1 \\ 1 - \frac{1}{n-3} < \lambda_2^n < 1 - \frac{1}{n-2} \\ \frac{1}{n-1} < \lambda_1^n < \frac{1}{n-2}. \end{gathered}$$

Proof. The polynomial is cubic and therefore changes sign at most three times. We find three disjoint intervals in which q_n changes sign. Since the polynomial is cubic each root must lie in one of these intervals.

$$\begin{aligned} q_n(n) = -1 < 0 \qquad &\text{and} \qquad q_n(n+1) = n^2 + n - 1 > 0, \\ q_n\left(1 - \frac{1}{n-2}\right) = -\frac{1}{(n-2)^3} < 0 \qquad &\text{and} \qquad q_n\left(1 - \frac{1}{n-3}\right) = \frac{11 - 7n + n^2}{(n-3)^3} > 0, \\ q_n\left(\frac{1}{n-1}\right) = \frac{3-2n}{(n-1)^3} < 0 \qquad &\text{and} \qquad q_n\left(\frac{1}{n-2}\right) = \frac{11 - 7n + n^2}{(n-2)^3} > 0. \end{aligned}$$

This establishes the desired inequalities. The monotonicity of the roots can be verified from the inequalities by inspection. □

Recall the definitions of η_0, η_1, η_3 from (3.2.3). Since η_0, η_1 and η_3 are independent over $\mathbb{Z}$, every element $\omega \in \mathbb{Z}^3$ can be written as

$$\omega = a\eta_0 + b\eta_1 + c\eta_3, \qquad \text{for } a, b, \text{ and } c \in \mathbb{Z}.$$

The following lemma is an important step in the proof of Theorem 3.4.1.

Lemma 3.4.3. *Each element of $\mathcal{E}_n$ is a nonnegative linear combination of η_0, η_1, η_3.*

Proof. Note that $\pi_z(\eta_i) > 0$ for $i = 0, \ldots, 3$ and $\eta_2 = \eta_0 + \eta_1$. Here we discuss all possible cases of $\omega \in \mathbb{Z}^3$ such that

1. $\pi_{xy}(\omega) \in (-1,1)^2$ which ensures that $\pi_{xy}(\omega)$ is a translation vector on X.

2. $0 < \pi_z(\omega) < \pi_z(\eta_i)$ for some $i = 0, 1$ and 3.

Case 1: $\omega = a\eta_0 - b\eta_1$ for positive integers a and b. Suppose that the vector

$$\omega = a\eta_0 - b\eta_1 = (-a, a-b, 0)$$

has $\pi_z(\omega) > 0$ and $\pi_{xy}(\omega) \in (-1,1)^2$. The y-component of the projection $\pi_{xy}(\omega)$ is

$$-a + (a-b)\lambda_2$$

where λ_2 is the second largest eigenvalue of matrix M_n for some n. By assumption, we have

$$-1 < -a + (a-b)\lambda_2 < 1.$$

It follows that

$$\frac{-1+a}{\lambda_2} < a-b < \frac{1+a}{\lambda_2}.$$

By Lemma 3.4.2 and $\frac{2}{3} < \lambda_2 < 1$

$$-1+a < \frac{-1+a}{\lambda_2} < a-b < \frac{1+a}{\lambda_2} < \frac{3}{2}(1+a).$$

Then, we can conclude that

$$-2 < b < 1$$

which contradicts to the assumption that $a, b \geq 1$.

This argument also shows that if $\omega = a\eta_0 - b\eta_1$ with $a, b \in \mathbb{Z}^2$ positive, $\pi_{xy}(-\omega) \notin (-1,1)^2$.

Case 2: $\omega = c\eta_3 - b\eta_1$ for positive integers b and c. Note that

$$\omega = c\eta_3 - b\eta_1 = c(1, -3, 1) - b(0, 1, 0) = (c, -3c - b, c).$$

Consider the y-component of $\pi_{xy}(\omega)$: we have

$$\begin{aligned} c - (3c + b)\lambda_2 + c\lambda_2^2 &\leq c(1 + \lambda_2^2) - (3c + 1)\lambda_2 \\ &\leq 2c - \frac{3}{4}(3c + 1) \\ &\leq -\frac{1}{4}c - \frac{3}{4} \leq -1. \end{aligned}$$

It follows that $\pi_{xy}(\omega) \notin (-1, 1)^2$ for all $c\eta_3 - b\eta_1$ with $v, t \in \mathbb{Z}_+$. Similarly, $\pi_{xy}(\omega) \notin (-1, 1)^2$ for all $\omega = b\eta_1 - c\eta_3$ with positive integers b and c.

Case 3: $\omega = c\eta_3 - a\eta_0$ for positive integers a and c. Note that

$$c\eta_3 - a\eta_0 = c(1, -3, 1) - a(-1, 1, 0) = (a + c, -3c - a, c).$$

Consider the x-coordinate of the projection $\pi_{xy}(\omega)$. By Lemma 3.4.2, $\lambda_1 \leq 1/4$ and we have

$$\begin{aligned} (a + c) - (3c + a)\lambda_1 + c\lambda_1^2 &\geq (a + c) - (3c + a)\frac{1}{4} + c\lambda_1^2 \\ &\geq \frac{1}{4}c + \frac{3}{4}a + c\lambda_1^2 \geq 1. \end{aligned}$$

Therefore, $\pi_{xy}(\omega) \notin (-1, 1)^2$ for all $\omega = c\eta_3 - a\eta_0$ with integers $a, c \geq 1$. Similarly, if $\omega = a\eta_0 - c\eta_3$ with positive coefficients a, c, then the x-coordinate of $\pi_{xy}(\omega)$ is less than -1.

Case 4: $\omega = c\eta_3 + a\eta_0 - b\eta_1$ with positive integers a, b and c. Consider the y-component of $\pi_{xy}(\omega)$

$$\pi_{xy}(c\eta_3 + a\eta_0 - b\eta_1)_y = \pi_{xy}(c\eta_3 - b\eta_1)_y + a\pi_{xy}(\eta_0)_y$$

By Case 2, $\pi_{xy}(c\eta_3 - b\eta_1)_y \leq -1$ for all $b, c \in \mathbb{Z}_+$. Moreover, $\pi_{xy}(\eta_0)_y < 0$. Thus, there is no possible $\omega = c\eta_3 + a\eta_0 - b\eta_1$ with $\pi_{xy}(\omega) \in (-1,1)^2$. For the same reason, $\pi_{xy}(-\omega) \notin (-1,1)^2$.

Case 5: $\omega = c\eta_3 - a\eta_0 + b\eta_1$ for $a, b, c \in \mathbb{Z}_+$. Consider the x-component $\pi_{xy}(\omega)_x$ of the projection $\pi_{xy}(\omega)$ given as

$$\pi_{xy}(c\eta_3 - a\eta_0 + b\eta_1)_x = \pi_{xy}(c\eta_3 - a\eta_0)_x + b\pi_{xy}(\eta_1)_x.$$

In Case 3, we show that $\pi_{xy}(c\eta_3 - a\eta_0)_x \geq 1$ for all positive integers a and c. Since

$$\pi_{xy}(\eta_1)_x > 0$$

we have $\pi_{xy}(\pm\omega) \notin (-1,1)^2$.

Case 6: $\omega = c\eta_3 - a\eta_0 - b\eta_1$ for positive integers a, b, c. Since $\omega = (a+c, -3c-a-b, c)$

$$\pi_{xy}(\omega) = (a + c - (3c + a + b)\lambda_1 + c\lambda_1^2,\ a + c - (3c + a + b)\lambda_2 + c\lambda_2^2).$$

We consider the difference $|\pi_{xy}(\omega)_y - \pi_{xy}(\omega)_x|$ which is

$$\begin{aligned}|\pi_{xy}(\omega)_y - \pi_{xy}(\omega)_x| &= |-(3c+a+b)(\lambda_2-\lambda_1) + c(\lambda_2^2-\lambda_1^2)| \\ &= |(\lambda_2-\lambda_1)[c(\lambda_1+\lambda_2-3)-a-b]|\end{aligned}$$

By Lemma 3.4.2, we have $0 \leq \lambda_1 \leq 1/5$ and $3/4 \leq \lambda_2 \leq 1$ where λ_2 is the second largest eigenvalue for matrix M_n with $n \geq 7$. Therefore,

$$\begin{aligned}|\pi_{xy}(\omega)_y - \pi_{xy}(\omega)_x| &\geq \frac{1}{2}\ |c(\lambda_1+\lambda_2-3)-a-b| \\ &\geq \frac{1}{2}\ |-2c-a-b|.\end{aligned}$$

Since $a, b, c \geq 1$ are integers, it means that $|\pi_{xy}(\omega)_y - \pi_{xy}(\omega)_x| \geq 2$. It follows that $\pi_{xy}(\omega)_x$ and $\pi_{xy}(\omega)_y$ cannot be in the interval $(-1, 1)$ at the same time. It follows that $\pi_{xy}(\omega) \notin (-1,1)^2$ for any positive integer a, b, c. Moreover, $\pi_{xy}(-\omega) \notin (-1,1)^2$.

Case 7. $\omega = a\eta_0 + b\eta_1$ for non-negative integers a and b with $a \geq 2$ or $b \geq 2$. We compute the case when $a = 2$. Then $\omega = 2\eta_0 = (-2, 2, 0)$ which implies that the x-coordinate of $\pi_{xy}(\omega) \notin (-1, 1)$ by Lemma 3.4.2. Similarly, when $b = 2$ we compute $\omega = 2\eta_1 = (0, 2, 0)$ and the y-coordinate of the projection $\pi_{xy}(\omega)$ is not in the interval $(-1, 1)$.

Therefore, we remain to check the case when $a + b \geq 3$ for non-negative integers a and b. We have the vector $\omega = a\eta_0 + a\eta_1 = (-a, a+b, 0)$. Therefore

$$-a + \frac{a+b}{n-1} \leq \pi_{xy}(\omega)_x \leq -a + \frac{a+b}{n-2}$$

$$b - \frac{a+b}{n-3} \leq \pi_{xy}(\omega)_y \leq b - \frac{a+b}{n-2}$$

so that

$$\begin{aligned} \pi_{xy}(v)_y - \pi_{xy}(v)_x &\geq (a+b)(1 - \frac{1}{n-3} - \frac{1}{n-2}) \\ &\geq 3(1 - \frac{2}{n-3}) \geq 2 \quad \text{for } n \geq 9. \end{aligned}$$

When $n = 7$,

$$-a + \frac{1}{2} \leq \pi_{xy}(\omega)_x \leq -a + \frac{3}{5}$$

so that if $\pi_{xy}(\omega)_x \in (-1, 1)$, then a must be 0 or 1. It means that $b = 3$ or $b = 2$ respectively. However,

$$b - \frac{3}{4} \leq \pi_{xy}(\omega)_y \leq b - \frac{3}{5}.$$

For either case, $\pi_{xy}(\omega)_y > 1$. The proof of the case $n = 8$ is the same. □

Proof of Theorem 3.4.1. Recall that $\mathcal{E}_n$ is defined to be a set of steps in the lattice walk $\widetilde{T} : \Lambda(X, L) \to \Lambda(X, L)$. By Lemma 3.4.3 every vector in $\mathcal{E}_n$ is a non-negative linear combination of η_0, η_1 and η_3. We show that the seven vectors in $\mathcal{E}_n$ with the smallest projections under π_z are sufficient to describe all steps in the lattice walk $\widetilde{T}$. Moreover, Lemma 3.4.3 establishes that the seven vectors in Equation 3.2.3 are exactly the seven shortest vectors in $\mathcal{E}_n$.

In Equation 3.2.5 we construct the partition $\mathcal{A} = \{A_i\}_{i=0}^{6}$ with translation vectors $v_i = \pi_{xy}(\eta_i)$. Applying the inequalities from Lemma 3.4.2 one can verify that $\mathcal{A}$ gives a partition of X into seven rectilinear polygons with disjoint interiors. Let $p \in \Lambda(X, L)$ and A_i the tile with $\pi_{xy}(p) \in A_i$. Then $\pi_{xy}(p) + v_i \in X$ since X overlaps with $X + v_i$ for each $i = 0, 1, \ldots, 6$. It follows that $p + \eta_i \in \Lambda(X, L)$ and therefore η_i is a valid step in the lattice walk. Since p is an arbitrary point in $\Lambda(X, L)$ we conclude that the vectors in $\mathcal{E}_n = \{\eta_i\}_{i=0}^{6}$ are sufficient to define all of the steps in the lattice walk in $\Lambda(X, L)$. $\square$

3.4.2 Proof of Theorem 3.1.7

Fix $n \geq 6$ and consider the REM $T_{M_n} : X \to X$. Let Y be the rectangle $A_0 \in \mathcal{A}$. It is sufficient to compute the first return map for the lattice walk $\widetilde{T}$ because the lattice is dense in X and points which are sufficiently close in X have the same sequence of translation of vectors for finite time.

Define

$$\Lambda_X = \Lambda(X, L) \text{ and } \Lambda_Y = \{(x, y, z) \in \mathbb{Z}^3 \mid \pi_{xy}(x, y, z) \in Y\}.$$

Since $Y \subset X$, we have $\Lambda_Y \subset \Lambda_X$. Let (a, b, c) be a lattice point in Λ_X. Consider the map Ψ defined by

$$\Psi : \begin{bmatrix} a \\ b \\ c \end{bmatrix} \mapsto (M_n)^t \begin{bmatrix} a \\ b \\ c \end{bmatrix} + \begin{bmatrix} 1 \\ -1 \\ 0 \end{bmatrix}.$$

We show that Ψ maps Λ_X to Λ_Y. Then

$$\pi_{xy} \circ \Psi \left(\begin{bmatrix} a \\ b \\ c \end{bmatrix} \right)$$

has the i-th coordinate

$$(c + 1) + \lambda_i(a - nc - 1) + \lambda_i^2(b + (n + 1)c)$$

for $i = 1$ and 2. Since λ_i is a root of the characteristic polynomial

$$q_n(x) = x^3 - (n+1)x^2 + nx - 1$$

we have

$$\begin{aligned}
&(c+1) + \lambda_i(a - nc - 1) + \lambda_i^2(b + (n+1)c) \\
&= \lambda_i(a + \lambda_i b) + [(n+1)\lambda_i^2 - n\lambda_i + 1]c + 1 - \lambda_i \\
&= \lambda_i(a + b\lambda_i + c\lambda_i^2) + (1 - \lambda_i).
\end{aligned}$$

It follows that for element $(a, b, c) \in \Lambda_X$, we have

$$\pi_{xy} \circ \Psi \left(\begin{bmatrix} a \\ b \\ c \end{bmatrix} \right) \in Y \quad \text{and} \quad \Psi \begin{bmatrix} a \\ b \\ c \end{bmatrix} \in \Lambda_Y.$$

In addition, the map $\Psi : \Lambda_X \to \Lambda_Y$ is a bijection with the inverse

$$\Psi^{-1} \left(\begin{bmatrix} a \\ b \\ c \end{bmatrix} \right) = \begin{bmatrix} n & 1 & 0 \\ -(n+1) & 0 & 1 \\ 1 & 0 & 0 \end{bmatrix} \left(\begin{bmatrix} a \\ b \\ c \end{bmatrix} - \begin{bmatrix} 1 \\ -1 \\ 0 \end{bmatrix} \right).$$

Lemma 3.4.4. *The map Ψ preserves the ordering of the lattice walk $\{\omega_0, \omega_1, \omega_2 \cdots\}$ corresponding to the orbits $\{p, T(p), T^2(p), \cdots\}$, i.e.*

$$\pi_z(\omega_i) < \pi_z(\omega_j) \quad \textit{if and only if} \quad \pi_z \circ \Psi(\omega_i) < \pi_z \circ \Psi(\omega_j).$$

Proof. The proof follows directly from the calculation

$$\pi_z \circ \Psi \left(\begin{bmatrix} a \\ b \\ c \end{bmatrix} \right) = \lambda_3(a + b\lambda_3 + c\lambda_3^2) + (1 - \lambda_3) = \lambda_3\, \pi_z \left(\begin{bmatrix} a \\ b \\ c \end{bmatrix} \right) + (1 - \lambda_3)$$

where $\lambda_3 > 1$ is a root of the polynomial $q_n(x)$.

□

Suppose $\omega_1 \in \Lambda(Y, L)$ and $q = \pi_{xy}(\omega_1)$. Consider the sequence $\{\omega_1, \omega_2, \cdots\}$ of consecutive points of the lattice walk in Λ_Y. Let $\omega_1' = \Psi^{-1}(\omega_1)$ and $\{\omega_1', \omega_2', \cdots\}$ be the lattice walk in Λ_X starting at ω_1'. We claim that

$$\omega_2 = \omega_1 + \Psi(\omega_2' - \omega_1').$$

To see this, note that Ψ is bijective and

$$\Psi^{-1}(\omega_1 + \Psi(\omega_2' - \omega_1')) = \omega_1' + \omega_2' - \omega_1' = \omega_2' \in \Lambda_X.$$

Also note that ω_2' is the point in $\Lambda(X, L)$ of smallest z-coordinate after ω_1'.

□

3.5 Multi-stage REMs

3.5.1 Construction

Recall that for $n \geq 6$ there is a PV REM T_{M_n} associated to a matrix

$$M_n = \begin{bmatrix} 0 & 1 & 0 \\ 0 & 0 & 1 \\ 1 & -n & n+1 \end{bmatrix}.$$

Let $\{v_i'\}_{i=0}^{6}$ be the translation vectors of T_{M_n} constructed as in section 3.2.1. Certain products of the matrices in $\mathcal{S}$ define REMs with the same combinatorics as T_{M_n} (recall that the family of REMs defined by single matrices in $\mathcal{S}$ all have the same combinatorics).

Let $W \in \mathcal{M}$ and define the normalized eigenvectors of W associated to λ_1, λ_2 to be

$$\xi_1 = (1, x, x') \quad \text{and} \quad \xi_2 = (1, y, y'),$$

scaled so that the first coordinate is 1. Lemma 3.1.4 establishes that W has real and positive eigenvalues. Since W is an integer matrix the eigenvectors are also real and we can define the projection $\pi_{xy} : \mathbb{Z}^3 \to \mathbb{R}^2$ by

$$\pi_{xy} : \mathbf{x} \mapsto (\mathbf{x} \cdot \xi_1,\ \mathbf{x} \cdot \xi_2).$$

There is a dynamical system induced by W whose translation vectors are

$$V = \{v_i = \pi_{xy}(\eta_i),\ \text{for } i = 0, 1, \ldots 6\}$$

where $\mathcal{E} = \{\eta_i\}_{i=0}^{6}$ are

$$\eta_0 = (-1, 1, 0), \quad \eta_1 = (0, 1, 0), \quad \eta_2 = \eta_0 + \eta_1 = (-1, 2, 0)$$
$$\eta_3 = (1, -3, 1), \quad \eta_4 = \eta_0 + \eta_3 = (0, -2, 1),$$
$$\eta_5 = \eta_1 + \eta_3 = (1, -2, 1), \quad \text{and} \quad \eta_6 = \eta_0 + \eta_1 + \eta_3 = (0, -1, 1)$$

(their representations in $\mathbb{Z}^3$ are the same as in (3.2.3)).

Definition 3.5.1. We say that W is an ***admissible*** matrix when $\xi_1, \xi_2 \in \mathbb{R}^3_{>0}$ and the following two conditions are satisfied for each $i = 0, 1 \ldots, 6$:

1. $v_i \in (-1, 1)^2$
2. v_i and v_i' lie in the same quadrant of $\mathbb{R}^2$.

We let T_W be the REM constructed with these translation vectors whose partition is constructed using the method in section 3.2.1; we call it an **admissible REM**. Let $\mathcal{M}_A \subset \mathcal{M}$ be the subset of admissible matrices.

The tiles in the partition $\mathcal{A} = \{A_0, \ldots, A_6\}$ associated to T_W are

0. $A_0 = [1 - x, 1] \times [1 - y, 1]$
1. $A_1 = [0, 1 - x] \times [0, 1 - y]$
2. $A_2 = ([1 - 2x, 1 - x] \times [1 - y, 2 - 2y]) \cup ([1 - x, 1] \times [0, 1 - y])$
3. $A_3 = [0, 3x - x'] \times [-1 + 3y - y', 1]$
4. $A_4 = [3x - x', 1 - x] \times [2y - y', 1]$
5. $A_5 = [0, 2x - x'] \times [1 - y, -1 + 3y - y']$

6. $A_6 = \big([1-2x, 3x-x'] \times [2-2y, -1+3y-y']\big)$
   $\cup \big([2x-x', 1-2x] \times [1-y, -1+3y-y']\big)$
   $\cup \big([3x-x', 1-x] \times [2-2y, 2y-y']\big)$.

Within $\mathcal{M}_A$ there is a subset $\mathcal{M}_R$ of matrices whose resulting REMs are renormalizable. Suppose $W \in \mathcal{M}_A$ written in terms of generators as $W = M_{n_L} M_{n_{L-1}} \cdots M_{n_1}$ with each $M_{n_i} \in \mathcal{S}$. We develop an L-step renormalization scheme for the multistage REM T_W.

To simplify the exposition, we introduce a notation for partial matrix products. Let $W_1 = M_{n_1}$ and set

$$W_k = M_{n_k} \cdots M_{n_1}, \qquad \text{for } k = 1, 2, \ldots L$$

with $W = W_L$. For $k = 1, 2, \cdots, L$, define the vectors $\xi_1^k = (1, x_k, x'_k)$ and $\xi_2^k = (1, y_k, y'_k)$ to be scalings of

$$W_k \xi_1 \quad \text{and} \quad W_k \xi_2$$

normalized so that the first coordinate is 1. Define the projection $\pi_{xy}^k : \mathbb{Z}^3 \to \mathbb{R}^2$ by the formula

$$\pi_{xy}^k : \mathbf{x} \mapsto (\mathbf{x} \cdot \xi_1^k,\ \mathbf{x} \cdot \xi_2^k).$$

At the k-th stage the translation vectors

$$V_k = \{v_i^k = \pi_{xy}^k(\eta_i),\ \text{for } i = 0, 1, \ldots 6\}$$

define a REM T_{W_k} with partition $\mathcal{A}_k = \{A_0, \ldots A_6\}$ where $x = x_k$,$x' = x'_k$, $y = y_k$ and $y' = y'_k$.

Definition 3.5.2. An admissible REM T_W is a ***multi-stage REM*** when the two conditions:

1. $v_i^k \in (-1,1)^2$
2. v_i^k and v_i' lie in the same quadrant of $\mathbb{R}^2$

are satisfied for all $i = 0, 1 \ldots, 6$ and all $k = 1, 2 \ldots, L$.

At every stage i the REM T_{W_i} has the same combinatorics as T_W. We prove that a multistage REM associated to a word W decomposed into a product of L generating elements $\mathcal{S}$ has a L-step renormalization scheme.

Theorem (Detailed statement of Theorem 3.1.9)**.** *Let $W = M_{n_L} M_{n_{L-1}} \cdots M_{n_1} \in \mathcal{M}_R$ and $T_{W_k} : X \to X$ be the k-th stage of the multistage REM T_W. For each stage k let $Y_k = A_0^k$ be the rectangle of width x_k and height y_k whose upper left vertex is (1,1). Then*

$$\widehat{T}_{W_k}|_{Y_k} = \phi_k^{-1} \circ T_{W_{k+1}} \circ \phi_k$$

where $\phi_k : Y_k \to X$ is defined by

$$\phi_k : (x, y) \mapsto \left(\frac{x + x_k - 1}{x_k}, \frac{y + y_k - 1}{y_k} \right).$$

Figure 3.8 shows the sequence of partitions in the renormalization scheme for a multistage REM with four stages.

Proof of theorem 3.1.8. Let $W \in \mathcal{M}_A$ with eigenvalues $\lambda_1, \lambda_2, \lambda_3$ and associated eigenvectors ξ_1, ξ_2, and ξ_3 normalized so that the first coordinate is one. The multi-

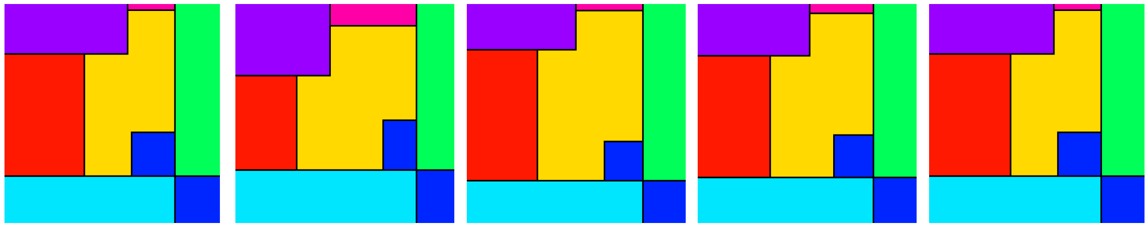

Figure 3.8: The multi-stage REM T_W and associated REMs $T_{W_1}, T_{W_2}, T_{W_3}$ and $T_{W_4} = T_W$ with $W = M_7 M_7 M_8 M_6$.

stage REM T_W can be constructed using cut-and-project sets with

$$\Lambda(X, L) = \{\mathbf{x} \in \mathbb{Z}^3 : \ \pi_{xy}(\mathbf{x}) \in X\}$$

where the projection π_{xy} is defined as above. Therefore the same method as used in the proof of Theorem 3.1.3 can be used to show that multistage REMs are minimal. However it remains to show that $\pi_{xy}(\Lambda(X, L))$ is dense in X. This follows from irreducibility: by admissibility, ± 1 are not eigenvalues of W, so the characteristic polynomial of W is irreducible over $\mathbb{Q}$. This implies that W cannot have a proper $\mathbb{Q}$-invariant subspace, and thus the projection $\pi_{xy}(\Lambda(X, L))$ is dense. $\square$

3.5.2 $\mathcal{M}$ is a monoid of Pisot matrices

We prove Lemma 3.1.4 establishing that $\mathcal{M}$ is a monoid of Pisot matrices.

Proof of lemma 3.1.4. For a 3×3 matrix M label its eigenvalues $\lambda_1(M), \lambda_2(M)$, and $\lambda_3(M)$ and assume that they are ordered by increasing modulus. Let $W = M_{n_0} \cdots M_{n_{L-1}}$ where each $M_{n_i} \in \mathcal{S}$.

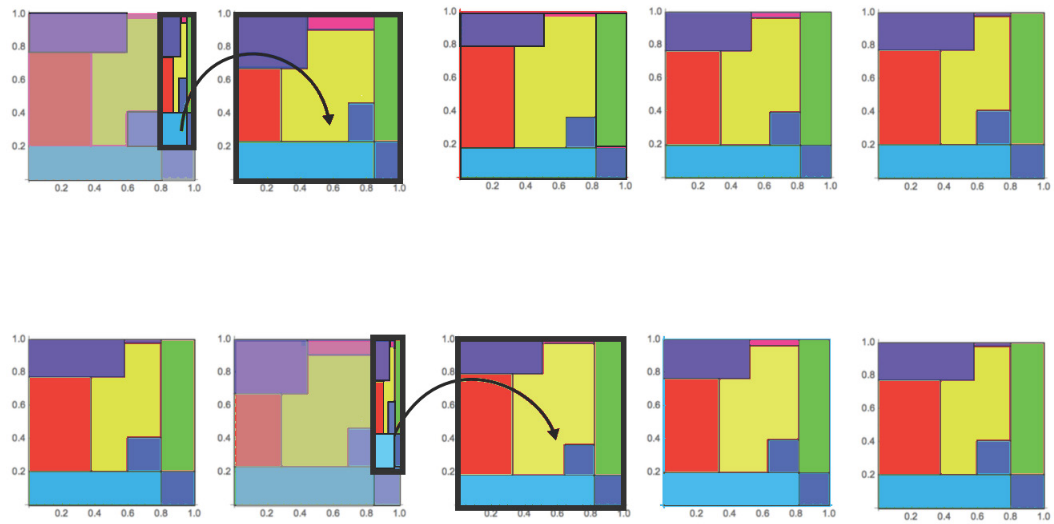

Figure 3.9: Detailed view of the renormalization scheme shown in Figure 3.8. The first row shows the first return set Y_0 bordered in black with the partition induced by the first return map overlayed. An arrow points to the REM in the sequence to which the first return map is affinely conjugate. The second row shows the same for Y_1.

By a change of basis we have

$$P_n = S^{-1}M_nS = \begin{bmatrix} 0 & 1 & 0 \\ 0 & 1 & 1 \\ 1 & 0 & n \end{bmatrix} \quad \textit{where} \quad S = \begin{bmatrix} 1 & 0 & 0 \\ 0 & 1 & 0 \\ 0 & 1 & 1 \end{bmatrix}.$$

The matrix P_n is primitive (has a strictly positive power) because

$$P_n^3 = \begin{bmatrix} 1 & 1 & 1+n \\ 1+n & 2 & 1+n+n^2 \\ n^2 & 1+n & 1+n^3 \end{bmatrix}$$

therefore by the Perron-Frobenius theorem $\lambda_3(P_n) > 1$. It follows that that the leading eigenvalue of the product $P = P_{n_0} \cdots P_{n_L} \cdots P_{n_2}P_{n_1}$ is real and larger than 1 since it is a finite product of primitive matrices and therefore primitive. Note that the products $P = P_{n_0} \cdots P_{n_{L-1}}$ and $W = M_{n_0} \cdots M_{n_{L-1}}$ have the same eigenvalues. Thus, we conclude that the leading eigenvalue $\lambda_3(W)$ is real and larger than 1.

Arguing similarly as in the previous paragraph, we can use the Perron-Frobenius theorem to show $\lambda_1(M_n) > 0$: by a change of basis of M_n^{-1} we have

$$Q_n = A^{-1} M_n^{-1} A = \begin{bmatrix} 0 & 1 & 0 \\ 0 & 2 & 1 \\ 1 & -5+n & -2+n \end{bmatrix} \quad \textit{where} \quad A = \begin{bmatrix} 0 & 2 & 1 \\ 0 & 1 & 0 \\ 1 & 0 & 0 \end{bmatrix}.$$

Note that Q_n is primitive because

$$Q_n^3 = \begin{bmatrix} 1 & -1+n & n \\ n & -1+(-3+n)n & -1+(-1+n)n \\ -1+(-3+n)n & 5+(-5+n)(-1+n)n & 3+(-4+n)n^2 \end{bmatrix}$$

which is positive for $n \geq 6$. By the Perron-Frobenius this implies $1/\lambda_1(Q_n) > 1$ and thus $\lambda_1(Q_n)$ is real, positive, and less than 1. Using the same argument as above, the product $Q = Q_{n_1} Q_{n_2} \cdots Q_{n_L} = A^{-1}(M_{n_L} \cdots M_{n_2} M_{n_1})^{-1} A$ is primitive and therefore its leading eigenvalue is real and larger than one. Thus we find $0 < \lambda_1(W) < 1$.

It remains to show $\lambda_2(W) < 1$. For simplicity we show this for the conjugated matrices P_n. The characteristic polynomial q_P of the matrix P has the form

$$\begin{aligned} q_P(x) &= x^3 - \mathrm{Tr}(P)x^2 + b(P)x - 1 \\ &= x^3 - (P_{1,1} + P_{2,2} + P_{3,3})x^2 + ([P]_{1,1} + [P]_{2,2} + [P]_{3,3})x - 1 \end{aligned}$$

where $P_{i,j}$ denotes the entry of the matrix in the i-th column and j-th row and $[P]_{i,j}$ denotes the minor of P obtained by deleting the i-th row and j-th column (i.e., the determinant of the submatrix obtained by deleting row i and column j). Evaluating q_P and its derivatives at -1 and 1 we find

$$q_P(-1) = -1, \quad q_P'(0) = b(P), \quad q_n(1) = -\operatorname{Tr}(P)+b(P) \quad \text{and} \quad q_n'(1) = 3-2\operatorname{Tr}(P)+b(P).$$

Since $\lambda_1 > 0$ we find that $\lambda_2 < 1$ as long as $b(P) < \operatorname{Tr}(P)$.

In order to prove that $b(P) < \operatorname{Tr}(P)$ we need one fact about the signs of the minors of P. We claim that P^{-1} can be written as

$$P^{-1} = \begin{bmatrix} a_{11} & -a_{12} & a_{13} \\ a_{21} & -a_{22} & a_{33} \\ -a_{31} & a_{32} & -a_{33} \end{bmatrix}$$

where a_{ij} are non-negative integers for $i, j = 1, 2$ and 3. The proof of this fact is postponed until after our main argument in which we prove $b(P) < \operatorname{Tr}(P)$. For an arbitrary 3×3 matrix A, the inverse can be calculated in terms of the minors of A

$$A^{-1} = \begin{bmatrix} a & b & c \\ d & e & f \\ g & h & i \end{bmatrix}^{-1} = \frac{1}{\det(A)} \begin{bmatrix} [A]_{1,1} & -[A]_{1,2} & [A]_{1,3} \\ -[A]_{2,1} & [A]_{2,2} & -[A]_{2,3} \\ [A]_{3,1} & -[A]_{3,2} & [A]_{3,3} \end{bmatrix}.$$

Since $[P]_{2,2} \leq 0$ and $[P]_{3,3} \leq 0$, we have

$$b(P) = [P]_{1,1} + [P]_{2,2} + [P]_{3,3} \leq [P]_{1,1}$$

Thus $[P]_{1,1} \leq \operatorname{Tr}(P)$ implies that $b(P) \leq \operatorname{Tr}(P)$. We use induction on the length of the product P to prove that $[P]_{1,1} \leq P_{3,3}$. Since P has non-negative entries this will imply $[P]_{1,1} \leq \operatorname{Tr}(P)$.

In the base case, $P = P_{n_0}$, and we have

$$[P_{n_0}]_{1,1} = n_0 \leq n_0 + 1 = P_{3,3}.$$

For the inductive step assume that $[P]_{1,1} < \mathrm{Tr}(P)$ for any P a product of $L-1$ matrices. Let P' be a product of L matrices. We can write $P' = PP_{n_L}$ where

$$P = P_{n_0} \cdots P_{n_{L-1}} = \begin{bmatrix} x_{11} & x_{12} & x_{13} \\ x_{21} & x_{22} & x_{23} \\ x_{31} & x_{32} & x_{33} \end{bmatrix}.$$

The matrix P' has the form

$$P' = PP_{n_L} = \begin{bmatrix} x_{13} & x_{11} + x_{12} & x_{12} + n_L x_{13} \\ x_{23} & x_{21} + x_{22} & x_{22} + n_L x_{23} \\ x_{33} & x_{31} + x_{32} & x_{32} + n_L x_{33} \end{bmatrix}.$$

Now we have

$$\begin{aligned} [P']_{1,1} &= x_{21}x_{32} - x_{22}x_{31} + n_L(x_{22}x_{33} - x_{23}x_{32}) + n_L(x_{21}x_{33} - x_{23}x_{31}) \\ &= [P]_{3,1} - [P]_{2,1}n_L + [P]_{1,1}n_L \\ &\leq [P]_{1,1}n_L \\ &\leq x_{33}n_L \\ &\leq x_{32} + x_{33}n_L = P'_{3,3}. \end{aligned}$$

Between lines three and four we applied the inductive hypothesis and between lines four and five we used the fact that the matrix has non-negative entries.

Next we prove the fact about the signs of the entries of P^{-1}. Label the entries of P^{-1} as

$$P^{-1} = \begin{bmatrix} a_{11} & -a_{12} & a_{13} \\ a_{21} & -a_{22} & a_{33} \\ -a_{31} & a_{32} & -a_{33} \end{bmatrix}$$

where $a_{ij} \geq 0$. First we use induction on the length of the matrix product to show the following six inequalities

$$a_{1j} > 3a_{2j} \text{ for } j = 1, 2, \text{ or } 3$$
$$a_{1j} > 3a_{3j} \text{ for } j = 1, 2, \text{ or } 3.$$

In the base case we have

$$P_{n_1}^{-1} = \begin{bmatrix} n_1 & -n_1 & 1 \\ 1 & 0 & 0 \\ -1 & 1 & 0 \end{bmatrix}.$$

Since $n \geq 6$ the inequalities hold by inspection. For the inductive step let $P' = PP_{n_L}$ be a product of $L+1$ matrices. Then we have

$$P'^{-1} = P_{n_L}^{-1} P^{-1} = \begin{bmatrix} -a_{31} + n_L(a_{11} - a_{21}) & a_{32} + n_L(a_{22} - a_{12}) & -a_{33} + n_L(a_{13} - a_{23}) \\ a_{11} & -a_{12} & a_{13} \\ a_{21} - a_{11} & a_{12} - a_{22} & a_{23} - a_{13} \end{bmatrix}.$$

Using the inductive hypothesis we have

$$(a_{11} - a_{21})n_L - a_{31} > a_{11}(n_L - \frac{1}{3}n_L - \frac{1}{3}) > 3a_{11}$$

since $n_L \geq 6$. This shows $a_{11} > 3a_{21}$. For P', again using the inductive hypothesis

$$\begin{aligned}(a_{11} - a_{21})n_L - a_{31} &> a_{11}(n_L - \frac{1}{3}) - a_{21}n_L > (n_L - 1)(a_{11} - a_{21}) - a_{21} + \frac{2}{3}a_{11} \\ &> (n_L - 1)(a_{11} - a_{21})\end{aligned}$$

and $n_L \geq 6$ from which we deduce that $a_{11} > 3a_{31}$. The calculations in the proofs of the remaining four inequalities are identical.

Finally we complete the proof of the signs of the entries of P^{-1}. Once again we induct on the length of the matrix product. The base case holds by inspection. In the inductive step we compute the signs of the entries of the first column of P'^{-1}. We have

$$-a_{31} + n_L(a_{11} - a_{21}) > a_{11}(n_L - 1/3 - 1/3) > 0$$

and

$$a_{21} - a_{11} < a_{11}(1 - 1/3) < 0.$$

Similar calculations show that the signs of the other entries are as stated. □

3.5.3 Proof of Theorem 3.1.9

Let $W = M_{n_L} \cdots M_{n_1}$ be a matrix in $\mathcal{M}_R$ (Section 3.5.1) and λ_1, λ_2, λ_3 be the eigenvalues of W such that $0 < \lambda_1 < \lambda_2 < 1 < \lambda_3$ (Lemma 3.1.4). Let $\xi_1 = (1, x_0, x_0')$ and $\xi_2 = (1, y_0, y_0')$ be eigenvectors of W with respective eigenvalues λ_1 and λ_2. Define the product $W_k = M_{n_k} \cdots M_{n_1}$ and $\xi_1^k = (1, x_k, x_k')$ as a scaling of $W_k\xi_1$.

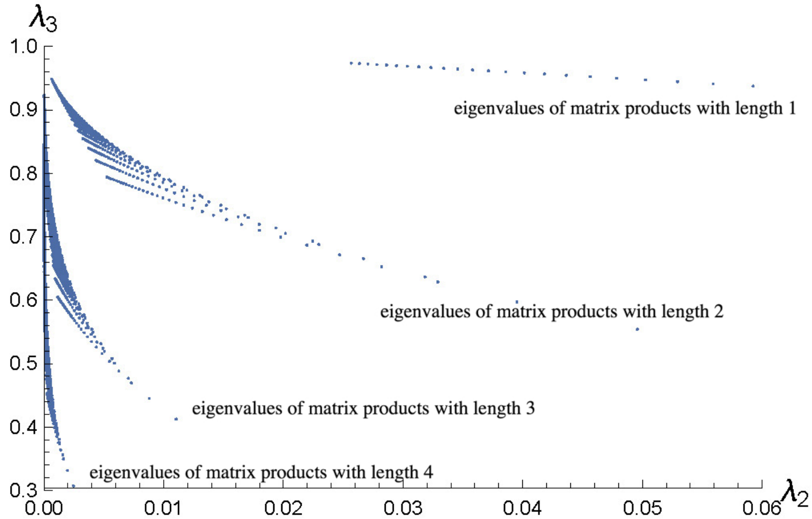

Figure 3.10: Two of the three eigenvalues for matrices in the monoid. Each cluster of points corresponds to matrix products with the same length.

Although the ξ_i are not eigenvectors they do satisfy the important property

$$M_{n_{k+1}}\xi_1^k = x_k\xi_1^{k+1}$$

because

$$\begin{aligned}
\begin{bmatrix} 0 & 1 & 0 \\ 0 & 0 & 1 \\ 1 & -n_{k+1} & n_{k+1}+1 \end{bmatrix}\begin{bmatrix} 1 \\ x_k \\ x'_k \end{bmatrix} &= \begin{bmatrix} x_k \\ x'_k \\ 1 - x_k n_{k+1} + x'_k(n_{k+1}+1) \end{bmatrix} \\
&= x_k \begin{bmatrix} 1 \\ x'_k/x_k \\ \left(1 - x_k n_{k+1} + x'_k(n_{k+1}+1)\right)/x_k \end{bmatrix} \\
&= x_k\xi_1^{k+1}.
\end{aligned}$$

Similarly we define $\xi_2^k = (1, y_k, y'_k)$ be a scaling of $W_k\xi_2$. Recall the projection

π_{xy}^k at stage k where $1 \leq k \leq L$ is defined by the formula

$$\pi_{xy}^k(\mathbf{x}) = (\xi_1^k \cdot \mathbf{x},\ \xi_2^k \cdot \mathbf{x})$$

Let Y_k be the set A_0^k of the multistage REM T_W associated to W. More precisely, Y_k is a rectangle of width x_k and height y_k and the upper right vertex of Y_k is $(1,1)$. Define

$$\Lambda_{X_k} = \{\mathbf{x} \in \mathbb{Z}^3 |\ \pi_c^k(\mathbf{x}) \in X\} \quad \text{and} \quad \Lambda_{Y_k} = \{\mathbf{x} \in \mathbb{Z}^3 |\ \pi_c^k(\mathbf{x}) \in Y_k\}.$$

Define the affine map

$$\Psi_k : \begin{bmatrix} a \\ b \\ c \end{bmatrix} \mapsto (M_{n_{k+1}})^T \begin{bmatrix} a \\ b \\ c \end{bmatrix} + \begin{bmatrix} 1 \\ -1 \\ 0 \end{bmatrix}.$$

We claim that $\Psi_k : \Lambda_{X_{k+1}} \to \Lambda_{Y_k}$ is a bijection. To prove the statement, we first show that $\Psi_k(\mathbf{x}) \in \Lambda_{Y_k}$ for $\mathbf{x} \in \Lambda_{X_{k+1}}$, i.e.

$$\pi_{xy}^k \circ \Psi_k(\omega) = (\xi_1^k \cdot \Psi_k(\omega),\ \xi_2^k \cdot \Psi_k(\omega)) \in (1 - x_k, 1) \times (1 - y_k, 1).$$

We compute the x-component of the projection $\pi_{xy}^k \circ \Psi_k(\omega)$

$$\begin{aligned} \xi_1^k \cdot \Psi_k(\omega) &= \xi_1^k \cdot \left(M_{n_{k+1}}^T \omega + \begin{bmatrix} 1 \\ -1 \\ 0 \end{bmatrix} \right) \\ &= M_{n_{k+1}} \xi_1^k \cdot \omega + \xi_1^k \cdot (1, -1, 0) \\ &= x_k\ \xi_1^{k+1} \cdot \omega + 1 - x_k \end{aligned}$$

By the assumption $\omega \in \Lambda_{X_{k+1}}$, we have $\xi_1^{k+1} \cdot \omega \in (0,1)$. Therefore we conclude that

$$\xi_1^k \cdot \Psi_k(\omega) \in (1 - x_k, 1).$$

Using the same argument, we can show that the y-component of $\pi_{xy} \circ \Psi_k(\omega) \in (1 - y_1, 1)$. Moreover, the inverse Ψ^{-1} is given by

$$\Psi_k^{-1} : \omega \mapsto (M_{n_{k+1}}^T)^{-1} \left(\omega - \begin{bmatrix} 1 \\ -1 \\ 0 \end{bmatrix} \right).$$

Thus, the map $\Psi_k : \Lambda_{X_{k+1}} \to \Lambda_{Y_k}$ is a bijection.

We apply the same argument as in Section 3.4.2 to show the renormalization of multistage REMs. Here we show that Ψ_k corresponds to a return map of the multistage REM T_{W_k}. Let $\omega_0 \in \Lambda_{Y_k}$ and $q_0 = \pi_{xy}^k(\omega_0) \in Y_k$. Define $\omega_0' = \Psi_k^{-1}(\omega_0) \in \Lambda_{X_{k+1}}$ and $q_0' = \pi_{xy}^{k+1}(\omega_0')$. Let $\{\omega_0', \omega_1', \cdots\}$ be a sequence of consequence points of the lattice walk in $\Lambda_{X_{k+1}}$ where $\omega_1' \in \Lambda_{X_{k+1}}$ and

$$\pi_c^{k+1}(\omega_j') = T_{W_{k+1}}^j(q).$$

We have

$$q_1 = q_0 + \pi_c^k \circ \Psi_k(\omega_1' - \omega_0') \in Y_k$$

since

$$\begin{aligned} q_1 = q_0 + \pi_c^k \circ \Psi_k(\omega_1' - \omega_0') &= \pi_{xy}^k(\omega_0) + \pi_{xy}^k \circ \Psi_k(\omega_1' - \omega_0') \\ &= \pi_{xy}^k(\omega_0 + \Psi_k(\omega_1') - \Psi_k(\omega_0')) \\ &= \pi_{xy}^k(\omega_0 - \omega_0 + \Psi_k(\omega_1')) \\ &= \pi_{xy}^k \circ \Psi_k(\omega_1') \in Y_k. \end{aligned}$$

Moreover, because the map Ψ_k is bijective, the point q_1 must be the image of the first return map $\hat{T}_{W_k}(q_0)|_{Y_k} = q_1$. It means that

$$\hat{T}_{W_k}|_{Y_k} = \phi_k^{-1} \circ T_{W_{k+1}} \circ \phi_k$$

where the affine map ϕ_k maps Y_k to the unit square $X = X_k$.

3.6 Parameter space of multistage REMs

The space of multistage REMs is a subset of $\mathbb{R}^4$. It can be naturally parametrized by the two eigenvectors associated to a matrix in $\mathcal{M}_R$ whose associated eigenvalues are less than one. Let λ_1, λ_2 and λ_3 denote the eigenvalues of a matrix in $\mathcal{M}_R$ ordered by increasing magnitude. Scale the eigenvectors of $\mathcal{M}_R$ so that the first coordinate is 1. Let $(1, x, x')$ denote the eigenvector associated to the eigenvalue λ_1 and let $(1, y, y')$ denote the eigenvector associated to the eigenvalue λ_2. In Figure 3.11 we plot points in the parameter space with (x, x', y)-coordinates colored by their y'-coordinate.

Conjecture 3.6.1. *The closure of the parameter space of all renormalizable multistage REMs is a Cantor set in* $\mathbb{R}^4$.

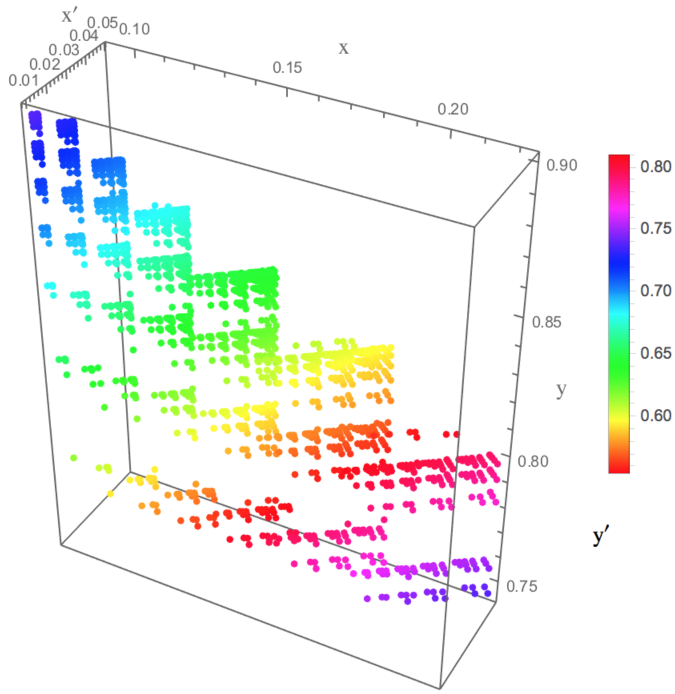

Figure 3.11: The 4-dimensional parameter space of multi-stage REMs. Each point in coordinates (x, x', y, y') corresponds to a pair of eigenvectors $(1, x, x')$ and $(1, y, y')$ of a matrix determining a multi-stage REM. Points are colored by the coordinate y'.

3.7 Appendix

We give a computational proof of Theorem 3.1.7 when $n = 6$.

Proof. Note that $Y = \phi_n^{-1}(X)$ and we consider the first return map $\hat{T}_{M_6}|_Y$ restricting to each element $\hat{A}_k = \phi_n^{-1}(A_k)$ for $k = 0, 1, \cdots, 6$. Let $\rho : X \to X$ be the map given by $(x, y) \mapsto (\lambda_1 x,\ \lambda_2 y)$. Let v_k be the translation vector on the set $A_k \in \mathcal{A}$. We show that the map $\hat{T}_{M_6}|_Y$ consists of translations by vectors $\rho(v_k)$ on each $\hat{A}_k^\circ$.

For each point in $\hat{A}_k$, we associate a symbolic sequence tracking its orbit until it returns to the set Y. More precisely, let $\Omega = \{0, 1, \cdots, 6\}^{\mathbb{Z}^+}$ be the set of sequences in $\{0,1,\cdots,6\}$, and define $\iota : X \to \Omega$ to be the coding

$$\iota(p) = \alpha_0\ \alpha_1 \cdots\ \alpha_m, \quad \text{for } \alpha_j \in \{0,1,\cdots,6\} \text{ and } T^m(p) \in Y,$$

where A_{α_j} is the tile containing $T^j(p)$. Define $\mathcal{R}_{\iota(p)} = \{q \in Y |\ \iota(q) = \iota(p)\}$ the maximal set of points with the same coding associated to $\iota(p)$. The first return map $\hat{T}|_Y$ restricting to $\mathcal{R}_{\iota(p)}$ is the translation given by

$$p \mapsto p + \pi_{xy}(\sum_{i=0}^{m-1} \eta_i).$$

By computation, we obtain that $\hat{A}_0 = \mathcal{R}_{05} \cup \mathcal{R}_{013} \cup \mathcal{R}_{031}$. The first return map restricting on $\hat{A}_0$ is the translation by the vector $v_i' = \pi_{xy}(\eta_0')$ where

$$\eta_0' = (0,-1,1) = \eta_0 + \eta_5 = \eta_0 + \eta_1 + \eta_3 = \eta_0 + \eta_3 + \eta_1.$$

Then we have

$$\pi_{xy}(\eta_0') = (-\lambda_1 + \lambda_1^2, -\lambda_2 + \lambda_2^2) = (\lambda_1(-1+\lambda_1),\ \lambda_2(-1+\lambda_2)).$$

Since $\eta_0 = (-1,1,0)$ we have $v_0' = \pi_{xy}(\eta_0') = \rho(\pi_{xy}(\eta_0)) = \rho(v_0)$.

The element $\hat{A}_1 = \mathcal{R}_{0131}$ so that the map $\hat{T}_{M_6}|_Y$ translates $\hat{A}_1$ by vector $\pi_{xy}(\eta_1')$ where

$$\eta_1' = \eta_0 + \eta_1 + \eta_3 + \eta_1 = \eta_0 + 2\eta_1 + \eta_3 = (0,0,1).$$

Therefore,

$$\pi_{xy}(\eta_1') = (\lambda_1^2,\ \lambda_2^2) = \rho \circ \pi_{xy}(\eta_1).$$

Since $\hat{A}_2 = \mathcal{R}_{05231} \cup \mathcal{R}_{013231} \cup \mathcal{R}_{01325}$ and $\eta_5 = \eta_1 + \eta_3$, we have $\hat{T}_{M_6}|_Y : p \mapsto p + \pi_{xy}(\eta_2')$ where

$$\eta_2' = \eta_0 + \eta_5 + \eta_2 + \eta_5 = 2\eta_0 + 3\eta_1 + 2\eta_3 = (0, -1, 2).$$

It follows that

$$\pi_{xy}(\eta_2') = (-\lambda_1 + 2\lambda_1^2,\ -\lambda_2 + \lambda_2^2) = (\lambda_1(-1 + 2\lambda_1), \lambda_2(-1 + 2\lambda_2)) = \rho \circ \pi_{xy}(\eta_2).$$

The set $\hat{A}_3$ is the disjoint union of seven subsets

$$\hat{A}_3 = \mathcal{R}_{0313265} \cup \mathcal{R}_{031665} \cup \mathcal{R}_{053265} \cup \mathcal{R}_{05665} \cup \mathcal{R}_{056235} \cup \mathcal{R}_{056613} \cup \mathcal{R}_{0562313}.$$

Since

$$\eta_5 = \eta_1 + \eta_3 \quad \text{and} \quad \eta_6 = \eta_0 + \eta_1 + \eta_3,$$

the map $\hat{T}_{M_6}|_Y$ translates every well-defined point in $\hat{A}_3$ by the vector $\pi_{xy}(\eta_3')$ for

$$\eta_3' = 3\eta_0 + 4\eta_1 + 4\eta_3 = (1, -5, 4).$$

Then we compute

$$\begin{aligned}
\pi_{xy}(\eta_3') &= (1 - 5\lambda_1 + 4\lambda_1^2,\ 1 - 5\lambda_2 + 4\lambda_2^2) \\
&= (\lambda_1^3 - 3\lambda_1^2 + \lambda_1, \lambda_2^3 - 3\lambda_2^2 + \lambda_2) \\
&= (\lambda_1(1 - 3\lambda_1 + \lambda_1^2),\ \lambda_2(1 - 3\lambda_2 + \lambda_2^2)) \\
&= \rho \circ \pi_{xy}(\eta_3).
\end{aligned}$$

The element $\hat{A}_4 = \mathcal{R}_{03166613}$ with translation vector $\pi_{xy}(\eta_4')$ under the first return map $\hat{T}_{M_6}|_Y$ where

$$\eta_4' = 4\eta_0 + 5\eta_1 + 5\eta_3 = \eta_0' + \eta_3' = (1, -6, 5).$$

We have shown that for each $j = 0, 1$ and 3, we have $\pi_{xy}(\eta_j') = \rho \circ \pi_{xy}(\eta_j)$. Therefore,

$$\begin{aligned}
\pi_{xy}(\eta_4') &= \pi_{xy}(\eta_0' + \eta_3') \\
&= \pi_{xy}(\eta_0') + \pi_{xy}(\eta_3') \\
&= \rho \circ \pi_{xy}(\eta_1) + \rho \circ \pi_{xy}(\eta_3) \\
&= \rho \circ \pi_{xy}(\eta_1 + \eta_3) = \rho \circ \pi_{xy}(\eta_4).
\end{aligned}$$

The set $\hat{A}_5$ is the union of seven disjoint subsets

$$\mathcal{R}_{056613231} \cup \mathcal{R}_{0523613231} \cup \mathcal{R}_{052361325} \cup \mathcal{R}_{0523141325} \cup \mathcal{R}_{052316325} \cup \mathcal{R}_{0132316325} \cup \mathcal{R}_{013231665}.$$

The vector

$$\eta_5' = 4\eta_0 + 6\eta_1 + 5\eta_3 = (1, -5, 5).$$

On the other hand,

$$\eta_5' = \eta_1' + \eta_3'.$$

By the same argument as above, we have

$$\pi_{xy}(\eta_5') = \rho \circ \pi_{xy}(\eta_5).$$

The element $\hat{A}_6$ is partitioned into 19 subsets which are listed here

$$\mathcal{R}_{03166613231},\ \mathcal{R}_{0566613231},\ \mathcal{R}_{05623613231},\ \mathcal{R}_{0562361325},\ \mathcal{R}_{05623141325},\ \mathcal{R}_{0566132325},$$
$$\mathcal{R}_{05623132325}, \mathcal{R}_{0562316325}, \mathcal{R}_{05236132325}, \mathcal{R}_{052323132325}, \mathcal{R}_{05232316325}, \mathcal{R}_{0132316665},$$
$$\mathcal{R}_{0523613265}, \mathcal{R}_{05232313265}, \mathcal{R}_{0523231665}, \mathcal{R}_{05231413265}, \mathcal{R}_{0523163265}, \mathcal{R}_{01323163265}, \mathcal{R}_{01323166613}.$$

Then

$$\eta_6' = 5\eta_0 + 7\eta_1 + 6\eta_3 = \eta_0' + \eta_1' + \eta_3'.$$

The translation vector for the map $\hat{T}_{M_6}|_Y$ on $\hat{A}_6$ satisfies the equality

$$\pi_{xy}(\eta_6') = \pi_{xy}(\eta_0' + \eta_1' + \eta_3') = \rho \circ \pi_{xy}(\eta_0 + \eta_1 + \eta_3) = \rho \circ \pi_{xy}(\eta_6)$$

. $\square$

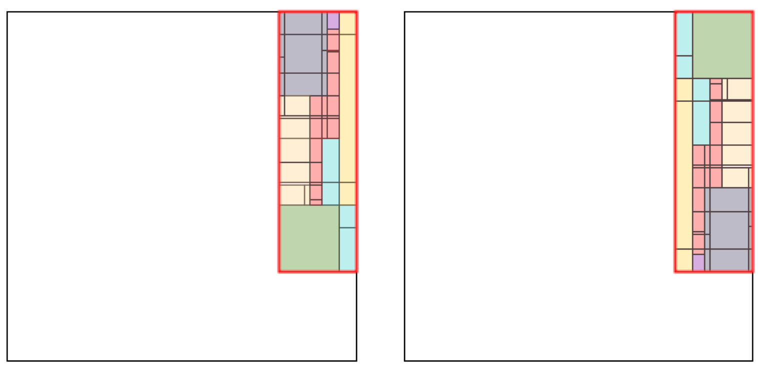

Figure 3.12: The first return set Y partitioned into tiles with the same symbolic codings

Acknowledgments

The authors would like to thank Richard Schwartz and Patrick Hooper for many helpful conversations. I. Alevy is supported by the NSF grant DMS-1713033. R. Kenyon is supported by the NSF grant DMS-1713033 and the Simons Foundation award 327929.

Chapter Four

Domain Exchange Maps Associated to 4-Dimensional Lattices and a Geometric Construction of a DEM on a Disk

This chapter discusses joint work with Richard Kenyon and Ren Yi.

4.1 Introduction

In [AKY18] we introduced a method for constructing domain exchange maps (DEMs) on a Jordan domain X using cut-and-project sets associated to lattices in $\mathbb{R}^3$ whose projection onto a 2-dimensional subspace is dense. The translation vectors of a DEM were defined by projecting steps in a single bi-infinite lattice walk onto the plane containing X. In this section we generalize this construction to cut-and-project sets associated to lattices in $\mathbb{R}^4$ whose projection onto a 2-dimensional subspace is dense. Since the projection onto the orthogonal subspace is a discrete set of points in $\mathbb{R}^2$, multiple non-intersecting lattice walks can be defined on it. We can create DEMs with exotic behavior by modifying these lattice walks.

4.2 Construction

Let X be a smooth Jordan domain in the x_1x_2-plane in $\mathbb{R}^4$. Let π_X be the projection onto the subspace containing X and $\pi_\perp$ be the projection onto the perpendicular subspace. Let $p(x)$ be a non-constant degree 4 polynomial, irreducible over $\mathbb{Z}$ whose roots are all real. Let λ be a root of $p(x)$. Then $\mathbb{Z}[\lambda]$ has four embeddings into $\mathbb{R}^4$ and we can identify $\mathbb{R}^4$ with the product of these four embeddings. Let $\{\lambda\}_{i=1}^4$ be the roots of $p(x)$ ordered by magnitude. Define the vectors $\{\xi_i\}_{i=1}^4$ with $\xi_i = (1, \lambda_i, \lambda_i^2, \lambda_i^3)$.

Then $\mathbb{Z}[\lambda]$ is a lattice in $\mathbb{R}^4$ with

$$\pi_X(a + b\lambda + c\lambda^2 + d\lambda^3) = ((a, b, c, d) \cdot \xi_1, (a, b, c, d) \cdot \xi_2)$$
$$\pi_\perp(a + b\lambda + c\lambda^2 + d\lambda^3) = ((a, b, c, d) \cdot \xi_3, (a, b, c, d) \cdot \xi_4).$$

We call a lattice constructed in this manner the *Galois embedding* of an algebraic integer.

A *Perron number* is a positive (real) algebraic integer which is an upper bound for the absolute values of each of its Galois conjugates. Let λ be a degree four Perron number whose Galois conjugates are all real. The Galois embedding of $\mathbb{Z}[\lambda]$ denoted L is a lattice in $\mathbb{R}^4$. Consider the set of points in the "window" $\Lambda(X, L) = \{\mathbf{x} \in L : \pi_X(x) \in X\}$. Since λ is irreducible over $\mathbb{Q}$, the projection $\pi_X(\Lambda(X, L)$ will be dense in X.

We define a dynamical system $T : X \to X$ by first defining a dynamical system on $\widetilde{T} : \Lambda(X, L) \to \Lambda(X, L)$ and then projecting it onto X under π_X. This defines T on a dense set of points in X. A standard argument allows us to extend the dynamical system to all of X. Our construction of the dynamical system $\widetilde{T}$ is quite involved and we must introduce some background material first.

The point set $\pi_\perp(\Lambda(X, L))$ is a discrete set of points in $\mathbb{R}^2$. To fix notation, let $G = (V, E)$ be a graph with vertices V and edges E. We introduce some basic graph theory terminology. A *tree* is an undirected graph in which any two vertices are connected by exactly one path. A *spanning tree* is a subgraph of G which contains every vertex in G. A connected component of a graph is a subgraph in which any two vertices are connected by a path. A *forest* is an undirected graph in which every connected component is a tree. A *spanning forest* is a subgraph of the graph G which contains all of the vertices of G and for which every connected component is a tree.

Let $G = (V, E)$ be the graph whose vertices V are the points in $\pi_\perp(\Lambda(X, L))$ and which has edges E connecting every pair of points in V. The dynamical system $\widetilde{T}$ is defined most naturally by defining a directed spanning forest on G. Let $S \subset E$ of this graph which define a spanning forest on V. Denote this graph by G_S.

For each connected component of G_S one can associated a directed graph on this component in which every vertex has exactly one ingoing edge and one outgoing edge. Note that the connected components of G_S are infinite. Consider a finite subgraph G_S^n in which each connected component of G_S^n has n vertices. One can put an orientation on the graph to form the graph $\tilde{G}_S^n$ for which every connected component has two exceptional vertices, a *source* which has one outgoing edge and no ingoing edges and a *sink* which has one ingoing edge and no outgoing edges. Note that $\tilde{G}_S^n$ converges to $\tilde{G}_S$ in the usual graph topology on $\tilde{G}_S$.

Each $\mathbf{x} \in \Lambda(X, L)$ has a successor $\mathbf{y}$ induced by the ordering on $\tilde{G}_s^n$. We define

$$\widetilde{T}(\mathbf{x}) = \mathbf{y}.$$

The dynamical system $T : X \to X$ is defined by projecting a dynamical system $\widetilde{T} : \Lambda(X, L) \to \Lambda(X, L)$ onto X.

The construction can be modified when the roots of $p(x)$ are not all real. If the roots are not real then they come in complex conjugate pairs. Suppose λ_1 and λ_2 are the roots with nonzero imaginary roots and are complex conjugates. Then define

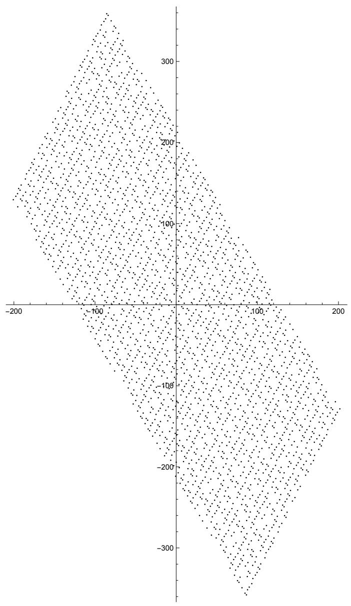

(a) $\pi_\perp(\Lambda(X,L))$

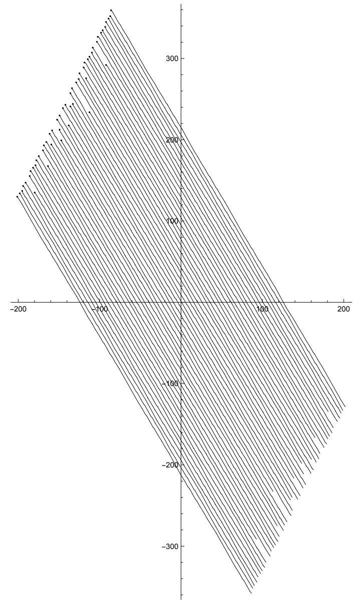

(b) Spanning forest on $\pi_\perp(\Lambda(X,L))$

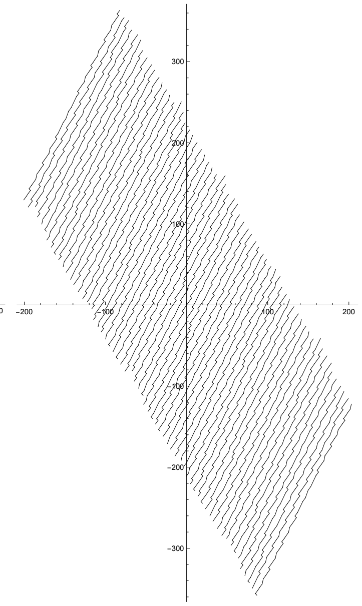

(c) A second spanning forest on $\pi_\perp(\Lambda(X,L))$

Figure 4.1: $x^4 - 4x^2 + x + 1$

the projection by $\xi_{1r} = (1, \Re\lambda_1, \Re\lambda_1^2, \Re\lambda_1^3)$ and $\xi_{1i} = (1, \Im\lambda_1, \Im\lambda_1^2, \Im\lambda_1^3)$

$$\pi_\parallel(a + b\lambda + c\lambda^2 + d\lambda^3) = ((a,b,c,d)\cdot\xi_{1r}, (a,b,c,d)\cdot\xi_{1i})$$

$$\pi_\perp(a + b\lambda + c\lambda^2 + d\lambda^3) = ((a,b,c,d)\cdot\xi_3, (a,b,c,d)\cdot\xi_4)$$

Likewise the construction can be modified if λ_3 and λ_4 are a complex conjugate pair.

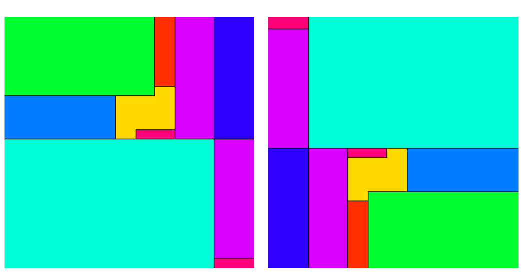

(a) REM induced by figure 4.1b

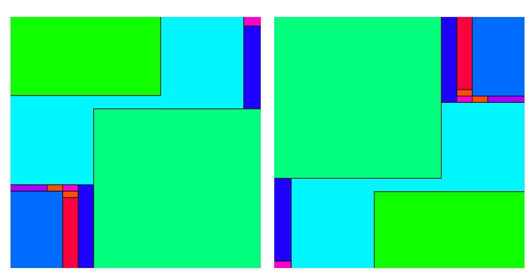

(b) REM induced by figure 4.1c

Figure 4.2: Two REMs associated to $x^4 - 4x^2 + x + 1$

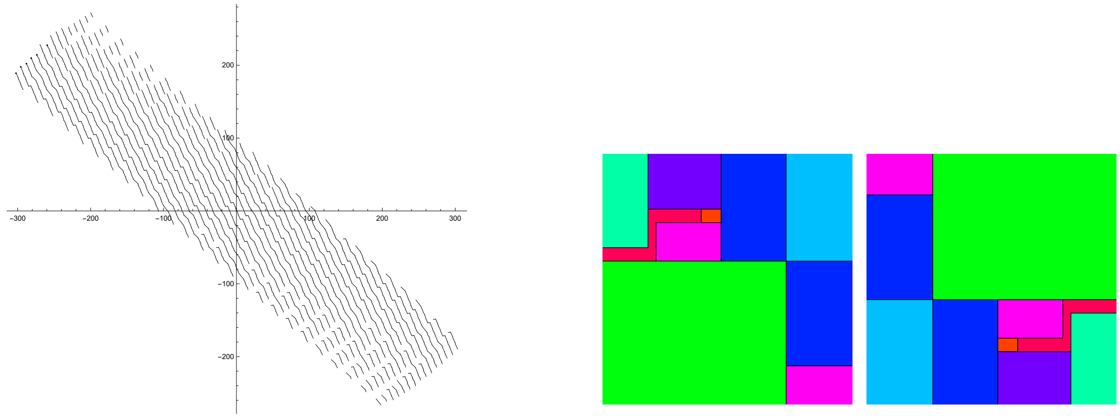

(a) Spanning Forest (b) REM

Figure 4.3: Spanning forest and REM associated to $x^4 + x^3 + 8x^2 - 6x + 1$

4.3 Geometric construction of a DEM on a disk

In this section we give a geometric construction which produces the same *domain exchange map* (DEM) on the unit circle as the one constructed using the cut-and-project set associated to the lattice $\mathbb{Z}[\lambda]$ where λ is the largest root (in modulus) of the polynomial $q(x) = x^3 - 6x^2 + 5x - 1$. Crucially, λ is a PV number. Let λ_1, λ_2 be the Galois conjugates of λ_3. For this polynomial they satisfy the inequality $0 < \lambda_1 < \lambda_2 < 1$.

As previously, let π_{xy} be projection onto the xy-plane and π_z be the projection onto the z-axis in $\mathbb{R}^3$. Let X be the unit disk centered at the origin. Let L be the Galois embedding of $\mathbb{Z}[\lambda]$ and set

$$\Lambda(X, L) = \{\mathbf{x} \in L : \pi_{xy}(\mathbf{x}) \in X\}.$$

The PV DEM $T : X \to X$ produced by our cut-and-project method is defined in terms of the map $\widetilde{T} : \Lambda(X, L) \to \Lambda(X, L)$ whose translation vectors are

$$\mathcal{E} = \{1, 1 - 5\lambda + 1, -3 + 6\lambda - \lambda^2, 2 - 5\lambda + \lambda^2, -2 + 6\lambda - \lambda^2, -1 + \lambda, \lambda\}.$$

The resulting translation vectors of the PV DEM T are

$$V = \{v_i = \pi_{xy}(\eta) : \eta \in \mathcal{E}\}$$

where as before

$$\pi_{xy}(a + b\lambda + c\lambda^2) = (a + b\lambda_1 + c\lambda_1^2, a + b\lambda_2 + c\lambda_2^2).$$

The two partitions associated to T are shown in figure 4.4a.

We give an alternate geometric construction of T which doesn't rely on the existence of a lattice. Let T' be the DEM constructed as follows. The seven different regions in the partition are as follows

$$\begin{aligned}
D_{\text{green}} &= D_1(z_1) \cap X \\
D_{\text{light blue}} &= D_1(z_1) \cap X \\
D_{\text{dark blue}} &= D_1(z_2) \cap X \\
D_{\text{purple}} &= (D_1(z_1 + z_3) \cap X) \setminus (D_{\text{light blue}} \cup D_{\text{green}}) \\
D_{\text{red}} &= (D_1(z_1 + z_2) \cap X) \setminus (D_{\text{dark blue}} \cup D_{\text{green}}) \\
D_{\text{yellow}} &= D_1(z_1 + z_2 + z_3) \setminus (D_{\text{light blue}} \cup D_{\text{dark blue}} \cup D_{\text{red}}) \\
D_{\text{white}} &= X \setminus (D_{\text{green}} \cup D_{\text{light blue}} \cup D_{\text{dark blue}} \cup D_{\text{purple}} \cup D_{\text{red}} \cup D_{\text{yellow}})
\end{aligned}$$

where $D_r(p)$ denotes the closed disk of radius r centered at p. The DEM $T' : X \to X$

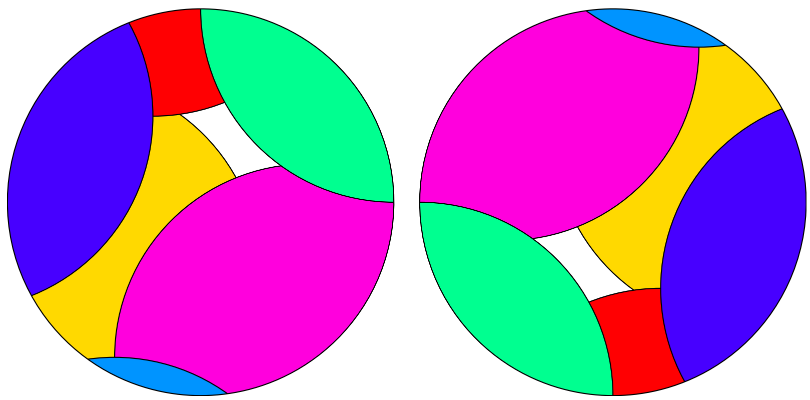

(a) PV DEM associated to $x^3 - 6x^2 + 5x - 1$

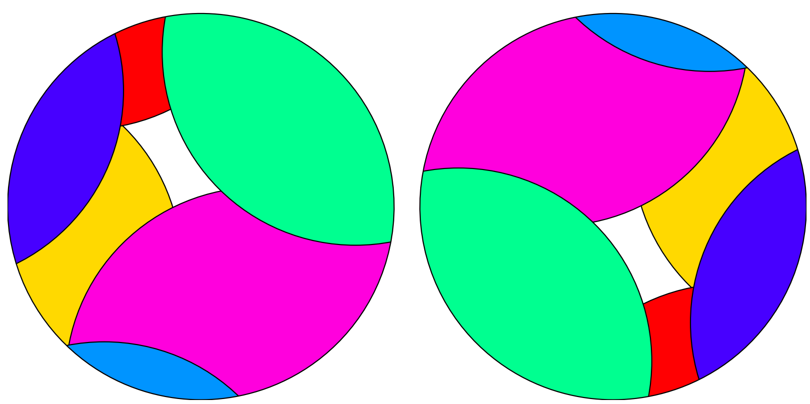

(b) DEM constructed geometrically using the points in equation 4.3.1

Figure 4.4: Two DEMs on the disk

is defined by

$$T'(p) = p - z.$$

where p is in a region formed by intersecting the disk $D_1(z)$ with X and removing certain portions of other overlapping disks.

To see that T and T' define the same dynamical system note that each piece, except for the white piece, in figure 4.4a is constructed greedily by first translating a disk of radius one centered at the origin, then intersecting it with X, and finally removing some portions of the region. Let z_4 denote the center of the purple disk that is translated to form the purple region. After applying the map T, the relative positions of the light blue and green regions swap places. Therefore it must be rotationally symmetric with respect to rotation by π radians about the midpoint of the centers of the light blue and green disks. This point is located at $(z_1+z_3)/2$. Since the part of the boundary of the purple region corresponding to the disk centered at z_4 goes to the boundary of X under T it must be located at the point obtained by rotating the origin by π radians about $(z_1 + z_3)/2)$. Therefore $z_4 = z_1 + z_3$. Similar calculations show that the red region is formed by translating a disk centered at $z_1 + z_2$. Since the yellow region neighbors the dark blue, purple, and light blue regions it must be rotationally symmetric about the midpoint of the centers of these four circles, which is at $(z_1 + z_2 + z_3)/2$.

This establishes that the DEM associated to the polynomial $x^3 - 6x^2 + 5x - 1$ lies in a family of DEMs with the same combinatorics determined by three points $z_1, z_2, z_3 \in \mathbb{R}^2$. In figure 4.4b we show the DEM associated to the points

$$z_1 = (0.8, 0.8),\ z_2 = (-0.5, -1.7),\ \text{and}\ z_3 = (-1.4, 0.6) \tag{4.3.1}$$

while in figure 4.4a we show the DEM constructed using the cut-and-project scheme. This DEM can also be constructed in a geometric manner using the three points

$$z_1 = 1 = (1,1),\ z_2 = 1 - 5\lambda + 1 \approx (-0.44, -1.80) \text{ and } z_3 = -3 + 6\lambda - 1 \approx (-1.25, 0.45).$$

4.4 Open questions

Does an algorithm exist for constructing the dynamical system $\widetilde{T}$ on every 4-dimensional lattice which is the Galois embedding of a degree 4 Perron number? Do any of the induced DEMs have periodic orbits? Are any of them renormalizable? Does a DEM exist with periodic orbits whose periods are arbitrarily long?

Acknowledgments

I thank Richard Kenyon and Ren Yi for many helpful conversations. The existence of the geometric construction for the DEM in figure 4.4a was first noticed by W. Patrick Hooper.

Chapter Five

Random Regular Polygon Surfaces

5.1 Introduction

We study a model for random surfaces using the framework of *regular polygon surfaces* (RPSs) introduced in [Ale18]. Recall that a RPS is defined by both a *surface graph* and a *geometric realization*. Sometimes the combinatorics of the surface graph imposes too many constraints on the geometric realization and one can prove rigidity theorems about these RPSs. However, there are certain surfaces graphs which support a family of geometric realizations. We find two examples of surface graphs which support a family of different geometric realizations. These examples are inspired by [Ken15] in which Kenyon studies random geometric structures in $\mathbb{H}^2$.

5.2 Measures on (4)-RPSs

We find two examples of (4)-RPSs which support a space of geometric realizations. In the first example every vertex has degree 5. Figure 5.1 shows a portion of such a surface. In the second example the surface graph is defined by gluing in rings of squares along each cycle in the honeycomb lattice.

5.2.1 (4)-RPSs with only degree 5 vertices

Consider a vertex v and let $\phi_1, \ldots, \phi_5$ denote the dihedral angles in the geometric realization of this RPS made by edges incident to v. Any two incident dihedral angles determine the other three and we have the formulas

$$\cos \phi_i = -\sin \phi_{i+2} \sin \phi_{i+3} \tag{5.2.1}$$

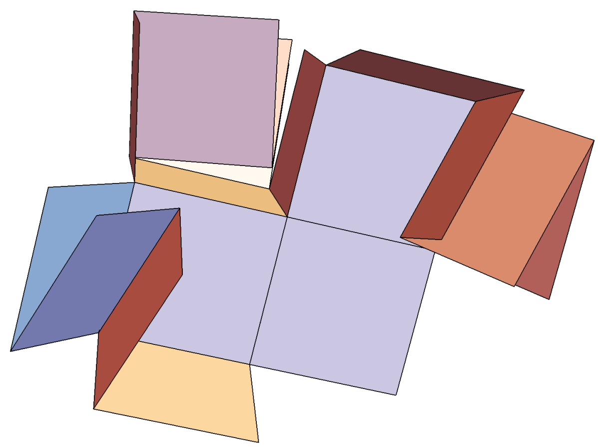

Figure 5.1: Part of a (4)-RPS in which every vertex has degree 5

for $i = 1, 2, \ldots, 5$ with indices determined modulo 5. There are no other feasibility conditions on the possible dihedral angles besides the above formulas.

Equation 5.2.1 can be proven as follows. Place a sphere of unit radius at a vertex. The edges incident to the vertex form great circle segments with length $\pi/2$. The condition that the five faces form a circuit implies a relation on a product of rotation matrices and the solution is given as above. We also have the formulas

$$\begin{aligned}
\sin\phi_1 &= -\frac{\cos\phi_4}{\sqrt{1-\sin^2\phi_4\sin^2\phi_5}} \\
\sin\phi_2 &= \sqrt{1-\sin^2\phi_4\sin^2\phi_5} \\
\sin\phi_3 &= -\frac{\cos\phi_5}{\sqrt{1-\sin^2\phi_4\sin^2\phi_5}}.
\end{aligned}$$

If ϕ_4 and ϕ_5 are chosen with respect to the measure on $[0,\pi/2]$ with density

$$f(\phi_4,\phi_5)d\phi_4 d\phi_5 = \frac{C\ d\phi_4\phi_5}{\sqrt{1-\sin^2\phi_4\sin^2\phi_5}} = \frac{C d\phi_4\phi_5}{\sin\phi_2}$$

where $C = K(1/\sqrt{2})^2$ is the complete elliptic integral of the first kind, then any other two consecutive dihedral angles at the same vertex will also have this distribution. This is proven by computing the Jacobian of the mapping from (ϕ_4,ϕ_5) to (ϕ_1,ϕ_2).

If we set $a = e^{i\phi_4}$ and $b = e^{i\phi_5}$ then the density is

$$\begin{aligned}
f(a,b)dadb &= \frac{C}{\sqrt{1-\frac{1}{16}\left(-2+a^{-2}+a^2\right)\left(-2+b^{-2}+b^2\right)}}\frac{da}{ia}\frac{db}{ib} \\
&= -\frac{4Cdadb}{\sqrt{-(ab+a+b-1)(ab-a+b+1)(ab+a-b-1)(ab-a-b-1)}}.
\end{aligned}$$

5.2.2 (4)-RPSs with boundary

We study a second example of a (4)-RPS which supports a family of geometric realizations. In this case the surface has boundary. The surface graph is formed by gluing rings of 6 degree 4 four faces together along their edges with the combinatorics of the triangular lattice. The surface has vertices of degree 6 at which 6 degree 4 faces meet and boundary vertices at which only 2 degree 4 faces meet.

Let v be a vertex at which 6 degree four faces meet and label the incident dihedral angles $\phi_1, \ldots, \phi_6$ in consecutive order. If 3 non-consecutive dihedral angles are known then the other three can be determined by the formulas

$$\cos\phi_1 = -\frac{\cos\phi_2\cos\phi_4 + \cos\phi_6}{\sin\phi_2\sin\phi_4} \tag{5.2.2}$$

$$\cos\phi_3 = -\frac{\cos\phi_2\cos\phi_6 + \cos\phi_4}{\sin\phi_2\sin\phi_6} \tag{5.2.3}$$

$$\cos\phi_5 = -\frac{\cos\phi_4\cos\phi_6 + \cos\phi_2}{\sin\phi_4\sin\phi_6}. \tag{5.2.4}$$

Equivalently these equations can be written in terms of exponentials. Define

$$a = e^{i\phi_2} \qquad b = e^{i\phi_6} \qquad c = e^{i\phi_4}$$

$$C = e^{i\phi_1} \qquad B = e^{i\phi_3} \qquad A = e^{i\phi_5}$$

then the equations are

$$\frac{A+1}{A-1} = \sqrt{\frac{(1+abc)(a+bc)}{(b+ac)(c+ab)}}$$

$$\frac{B+1}{B-1} = \sqrt{\frac{(1+abc)(b+ac)}{(a+bc)(c+ab)}}$$

$$\frac{C+1}{C-1} = \sqrt{\frac{(1+abc)(c+ab)}{(a+bc)(b+ac)}}$$

Note that

$$\frac{A+1}{A-1} = i\cot(\phi_5/2)$$

These formulas are strikingly similar to the coordinate transformation in the Ising model known as the $Y-\Delta$-transformation [KP16]. Unlike in the Ising model our weights are complex.

Consider the equation for ϕ_1. Applying the product-to-sum identity for cosine we find

$$\cos\phi_1 = -\frac{\cos(\phi_2-\phi_4)+\cos(\phi_2+\phi_4)+2\cos\phi_6}{\cos(\phi_2-\phi_4)-\cos(\phi_2+\phi_4)}.$$

In order for the degree 6 to be geometrically realizable the right-hand side must be less than or equal to one in absolute value and so

$$|\cos(\phi_2-\phi_4)+\cos(\phi_2+\phi_4)+2\cos\phi_6| \leq |\cos(\phi_2-\phi_4)-\cos(\phi_2+\phi_4)|$$

and two more equations for ϕ_3 and ϕ_5

$$|\cos(\phi_2-\phi_6)+\cos(\phi_2+\phi_6)+2\cos\phi_4| \leq |\cos(\phi_2-\phi_6)-\cos(\phi_2+\phi_6)|$$
$$|\cos(\phi_4-\phi_6)+\cos(\phi_4+\phi_6)+2\cos\phi_2| \leq |\cos(\phi_4-\phi_6)-\cos(\phi_4+\phi_6)|\,.$$

Assume that the denominators in eqs. 5.2.2, 5.2.3 and 5.2.4 are all positive (one way to achieve this is to choose $\phi_2, \phi_4\phi_6 \in (0,\pi)$). The first inequality simplifies to

$$-\cos(\phi_2-\phi_4)+\cos(\phi_2+\phi_4) \leq \cos(\phi_2-\phi_4)+\cos(\phi_2+\phi_4)+2\cos(\phi_6) \leq \cos(\phi_2-\phi_4)-\cos(\phi_2+$$

which can be further simplified to

$$
\begin{aligned}
-\cos(\phi_2-\phi_4) \le \cos(\phi_2-\phi_4)+2\cos(\phi_6) &\le \cos(\phi_2-\phi_4)-2\cos(\phi_2+\phi_4)\\
0 \le 2\cos(\phi_2-\phi_4)+2\cos(\phi_6) &\le 2\cos(\phi_2-\phi_4)-2\cos(\phi_2+\phi_4)\\
0 \le \cos(\phi_2-\phi_4)+\cos(\phi_6) &\le \cos(\phi_2-\phi_4)-\cos(\phi_2+\phi_4)\\
-\cos(\phi_2-\phi_4) \le \cos(\phi_6) &\le -\cos(\phi_2+\phi_4).
\end{aligned}
$$

The function $\arccos(x)$ is monotonically decreasing on the domain $(-1, 1)$ and so the inequality simplifies to

$$\pi - (\phi_2+\phi_4) \le \phi_6 \le \pi - (\phi_2-\phi_4)$$

which can be further simplified as follows

$$
\begin{aligned}
-\phi_2-\phi_4 \le \phi_6-\pi &\le -\phi_2+\phi_4\\
-\phi_4 \le \phi_2+\phi_6-\pi &\le \phi_4.
\end{aligned}
$$

Now the three equations on ϕ_2, ϕ_4 and ϕ_6 that guarantee that the dihedral angles are permissible for a vertex of degree six are

$$
\begin{aligned}
|\phi_4+\phi_6-\pi| &< \phi_2\\
|\phi_2+\phi_6-\pi| &< \phi_4\\
|\phi_2+\phi_4-\pi| &< \phi_6.
\end{aligned}
$$

Note that the dihedral angles cannot be zero or π and so the inequalities must be strict in order for the solution to be feasible. Let D be the region in $\mathbb{R}^3$ in which the three above equations are satisfied. It has volume

$$\mathrm{vol}(D) = \frac{\pi^3}{3}.$$

The cube $c = [3\pi/8, 5\pi/8]$ is contained within D.

If ϕ_2, ϕ_4 and ϕ_6 are chosen independently with measure μ_0 whose density is

$$f(\phi)d\phi = \frac{C}{\sin^{1/3}(\phi)}$$

where

$$C = \frac{\sqrt{3}\Gamma(2/3)\Gamma(5/6)}{2\pi^{3/2}}$$

then ϕ_1, ϕ_3, ϕ_5 will also be independent with distribution μ_0.

In terms of $u = \cos(\phi)$ the density is

$$f(u) = \frac{A}{(1-u^2)^{2/3}}$$

where $u = \cos(\phi)$ and

$$A = \frac{\Gamma(5/6)}{\sqrt{\pi}\Gamma(1/3)}.$$

Bibliography

[AB14] J. Ambjrn and T. Budd, *Geodesic distances in Liouville quantum gravity*, Nucl. Phys. **B889**, 676–691 (2014), 1405.3424.

[AD15] A. Avila and V. Delecroix, *Some monoids of Pisot matrices*, ArXiv e-prints (June 2015), 1506.03692.

[AH13] S. Akiyama and E. Harriss, *Pentagonal domain exchange*, Discrete Contin. Dyn. Syst. **33**(10), 4375–4400 (2013).

[AI01] P. Arnoux and S. Ito, *Pisot substitutions and Rauzy fractals*, Bull. Belg. Math. Soc. Simon Stevin **8**(2), 181–207 (2001), Journées Montoises d'Informatique Théorique (Marne-la-Vallée, 2000).

[AKT01] R. Adler, B. Kitchens and C. Tresser, *Dynamics of non-ergodic piecewise affine maps of the torus*, Ergodic Theory Dynam. Systems **21**(4), 959–999 (2001).

[AKY18] I. Alevy, R. Kenyon and R. Yi, *A Family of Minimal and Renormalizable Rectangle Exchange Maps*, ArXiv e-prints (March 2018), 1803.06369.

[Ale05] A. D. Alexandrov, *Convex polyhedra*, Springer Monographs in Mathematics, Springer-Verlag, Berlin, 2005, Translated from the 1950 Russian edition by N. S. Dairbekov, S. S. Kutateladze and A. B. Sossinsky, With comments and bibliography by V. A. Zalgaller and appendices by L. A. Shor and Yu. A. Volkov.

[Ale18] I. M. Alevy, *Regular Polygon Surfaces*, ArXiv e-prints (April 2018), 1804.05452.

[AT16] I. Alevy and E. Tsukerman, *Polygonal bicycle paths and the Darboux transformation*, Involve **9**(1), 57–66 (2016).

[BCD+02] T. Biedl, T. M. Chan, E. D. Demaine, M. L. Demaine, P. Nijjar, R. Uehara and M. wei Wang, Tighter bounds on the genus of nonorthogonal polyhedra built from rectangles, in *in: Proceedings of the 14th Canadian Conference on Computational Geometry, 2002*, pages 105–108, 2002.

[BdT11] C. Boutillier and B. de Tilière, *The critical Z-invariant Ising model via dimers: locality property*, Comm. Math. Phys. **301**(2), 473–516 (2011).

[Buz01] J. Buzzi, *Piecewise isometries have zero topological entropy*, Ergodic Theory Dynam. Systems **21**(5), 1371–1377 (2001).

[CK62] D. L. Caspar and A. Klug, Physical principles in the construction of regular viruses, in *Cold Spring Harbor symposia on quantitative biology*, volume 27, pages 1–24, Cold Spring Harbor Laboratory Press, 1962.

[Cox63] H. S. M. Coxeter, *Regular polytopes*, Second edition, The Macmillan Co., New York; Collier-Macmillan Ltd., London, 1963.

[Dav92] F. David, Simplicial quantum gravity and random lattices, in *Gravitation and quantizations. Proceedings, 57th Session of the Les Houches Summer School in Theoretical Physics, NATO Advanced Study Institute, Les Houches, France, July 5 - August 1, 1992*, pages 0679–750, 1992.

[DO01] M. Donoso and J. O'Rourke, *Nonorthogonal Polyhedra Built from Rectangles*, eprint arXiv:cs/0110059 (October 2001), cs/0110059.

[GM63] B. Grünbaum and T. S. Motzkin, *The number of hexagons and the simplicity of geodesics on certain polyhedra*, Canad. J. Math. **15**, 744–751 (1963).

[Goe03] A. Goetz, Piecewise isometries—an emerging area of dynamical systems, in *Fractals in Graz 2001*, Trends Math., pages 135–144, Birkhäuser, Basel, 2003.

[Gol37] M. Goldberg, *A class of multi-symmetric polyhedra*, Tohoku Math. J **43**, 104–108 (1937).

[Gow00] W. T. Gowers, *Rough structure and classification*, Geom. Funct. Anal. (Special Volume, Part I), 79–117 (2000), GAFA 2000 (Tel Aviv, 1999).

[Gru03a] B. Grunbaum, Are your polyhedra the same as my polyhedra?, in *Discrete and computational geometry*, volume 25 of *Algorithms Combin.*, pages 461–488, Springer, Berlin, 2003.

[Gru03b] B. Grunbaum, *Convex polytopes*, volume 221 of *Graduate Texts in Mathematics*, Springer-Verlag, New York, second edition, 2003, Prepared and with a preface by Volker Kaibel, Victor Klee and Gunter M. Ziegler.

[Gru09] B. Grunbaum, *An enduring error*, Elem. Math. **64**(3), 89–101 (2009).

[GS09] B. Grünbaum and L. Szilassi, *Geometric realizations of special toroidal complexes*, Contrib. Discrete Math. **4**(1), 21–39 (2009).

[GSW14] G. Gévay, E. Schulte and J. M. Wills, *The regular Grünbaum polyhedron of genus 5*, Adv. Geom. **14**(3), 465–482 (2014).

[Hal81] H. Haller, *Rectangle exchange transformations*, Monatsh. Math. **91**(3), 215–232 (1981).

[Hoo13] W. P. Hooper, *Renormalization of polygon exchange maps arising from corner percolation*, Invent. Math. **191**(2), 255–320 (2013).

[JA68] W. Jamnitzer and J. Amman, *Perspectiva corporum regularium*, Vienna, 1568, Available at `http://digital.slub-dresden.de/werkansicht/dlf/12830/45/`.

[Kea75] M. Keane, *Interval exchange transformations*, Math. Z. **141**, 25–31 (1975).

[Ken92] R. Kenyon, Self-replicating tilings, in *Symbolic dynamics and its applications (New Haven, CT, 1991)*, volume 135 of *Contemp. Math.*, pages 239–263, Amer. Math. Soc., Providence, RI, 1992.

[Ken96] R. Kenyon, *A note on tiling with integer-sided rectangles*, J. Combin. Theory Ser. A **74**(2), 321–332 (1996).

[Ken09] R. Kenyon, *Lectures on Dimers*, ArXiv e-prints (October 2009), 0910.3129.

[Ken15] R. Kenyon, *Right-angled hexagon tilings of the hyperbolic plane*, ArXiv e-prints (March 2015), 1503.05510.

[KO06] R. Kenyon and A. Okounkov, *Planar dimers and Harnack curves*, Duke Math. J. **131**(3), 499–524 (2006).

[KP16] R. Kenyon and R. Pemantle, *Double-dimers, the Ising model and the hexahedron recurrence*, J. Combin. Theory Ser. A **137**, 27–63 (2016).

[Lag96] J. C. Lagarias, *Meyer's concept of quasicrystal and quasiregular sets*, Comm. Math. Phys. **179**(2), 365–376 (1996).

[LGM12] J.-F. Le Gall and G. Miermont, Scaling limits of random trees and planar maps, in *Probability and statistical physics in two and more dimensions*, volume 15 of *Clay Math. Proc.*, pages 155–211, Amer. Math. Soc., Providence, RI, 2012.

[Li14] Z. Li, *Spectral curves of periodic Fisher graphs*, J. Math. Phys. **55**(12), 123301, 25 (2014).

[Lin84] D. A. Lind, *The entropies of topological Markov shifts and a related class of algebraic integers*, Ergodic Theory Dynam. Systems **4**(2), 283–300 (1984).

[LKV04] J. H. Lowenstein, K. L. Kouptsov and F. Vivaldi, *Recursive tiling and geometry of piecewise rotations by* $\pi/7$, Nonlinearity **17**(2), 371–395 (2004).

[Mas82] H. Masur, *Interval exchange transformations and measured foliations*, Ann. of Math. (2) **115**(1), 169–200 (1982).

[Mey95] Y. Meyer, Quasicrystals, Diophantine approximation and algebraic numbers, in *Beyond quasicrystals (Les Houches, 1994)*, pages 3–16, Springer, Berlin, 1995.

[NSAD14] T. Nagylaki, L. Su, I. Alevy and T. F. Dupont, *Clines with partial panmixia in an environmental pocket*, Theoretical Population Biology **95**, 24 – 32 (2014).

[OWHB17] J. T. Overvelde, J. C. Weaver, C. Hoberman and K. Bertoldi, *Rational design of reconfigurable prismatic architected materials*, Nature **541**, 347–352 (2017).

[Poi17] H. Poincaré, *The three-body problem and the equations of dynamics*, volume 443 of *Astrophysics and Space Science Library*, Springer, Cham, 2017, Poincaré's foundational work on dynamical systems theory, Translated from the 1890 French original and with a preface by Bruce D. Popp.

[Rau79] G. Rauzy, *Échanges d'intervalles et transformations induites*, Acta Arith. **34**(4), 315–328 (1979).

[Rau82] G. Rauzy, *Nombres algébriques et substitutions*, Bull. Soc. Math. France **110**(2), 147–178 (1982).

[Riv96] I. Rivin, *A characterization of ideal polyhedra in hyperbolic* 3*-space*, Ann. of Math. (2) **143**(1), 51–70 (1996).

[Sch11] R. E. Schwartz, *Mostly surfaces*, volume 60 of *Student Mathematical Library*, American Mathematical Society, Providence, RI, 2011.

[Sch14] R. E. Schwartz, *The octogonal PETs*, volume 197 of *Mathematical Surveys and Monographs*, American Mathematical Society, Providence, RI, 2014.

[Sch15] R. E. Schwartz, *Notes on Shapes of Polyhedra*, ArXiv e-prints (June 2015), 1506.07252.

[Sch18] R. E. Schwartz, *Square turning maps and their compactifications*, Geom. Dedicata **192**, 295–325 (2018).

[Thu98] W. P. Thurston, Shapes of polyhedra and triangulations of the sphere, in *The Epstein birthday schrift*, volume 1 of *Geom. Topol. Monogr.*, pages 511–549, Geom. Topol. Publ., Coventry, 1998.

[Thu14] W. P. Thurston, Entropy in dimension one, in *Frontiers in complex dynamics*, volume 51 of *Princeton Math. Ser.*, pages 339–384, Princeton Univ. Press, Princeton, NJ, 2014.

[TPQ17] G. Tikhomirov, P. Petersen and L. Qian, *Fractal assembly of micrometre-scale DNA origami arrays with arbitrary patterns*, Nature **552**(7683), 67 (2017).

[Vee82] W. A. Veech, *Gauss measures for transformations on the space of interval exchange maps*, Ann. of Math. (2) **115**(1), 201–242 (1982).